ABSTRACT

CAI, CHANGJIE. Performance Evaluation and Testing of New Particle Formation and Growth Parameterizations Using Two Regional Online-Coupled Meteorology-Chemistry Models. (Under the direction of Dr. Yang Zhang).

New particle formation (NPF) is usually considered as an important source of aerosol particles and cloud condensation nuclei (CCN), which may result in an enhanced cloud droplet number concentration (CDNC) and cloud shortwave albedo. In this work, East Asia is selected for studying the new particle formation and its impacts on aerosol-cloud interactions by applying two online-coupled meteorology-chemistry models: (1) the Weather Research and Forecasting model coupled with chemistry (WRF/Chem), and (2) the WRF with the physics and chemistry package from Community Atmosphere Model version 5 (WRF-CAM5). For WRF/Chem, two simulation periods are selected with different purposes (1) July in 2008, and (2) four representative months (January, April, July and October), one for each season in 2001. For WRF-CAM5, the summer 2008 is selected for testing and evaluating the new model. WRF/Chem simulations are performed with the Model for Simulating Aerosol Interactions and Chemistry (MOSAIC) using default 8-bin (39 nm – 10 µm), modified 8-bin (22 nm - 10 µm) and 12-bin (1 nm - 10 µm). The default 8-bin structure used in MOSAIC is insufficient to the accurate representation of the nucleation mode (1 nm – 20 nm). Thus, in this study, the default 8-bin size structure is first modified, then extended to the 12-bin structure with the first 4 bins for ultrafine particles (with the diameters of 1 - 20 nm) to accurately simulate the formation and early growth of the ultrafine particles.

Various nucleation schemes (including binary, ternary, power law, and ion-mediated nucleation schemes) have been tested using WRF/Chem. The simulations identify an optimal nucleation parameterization that combines nucleation parameterizations over urban and non-

urban areas and within and above planetary boundary layer (PBL) heights (referred to as COMB hereafter). Compared with that simulations with the modified 8-bin, WRF/Chem with 12-bin and the COMB nucleation parameterization improves the simulated particle size distribution and reproduces better the reported NPF events in Beijing during July 2008. However, the model overpredicts the concentrations of H_2SO_4, a key precursor of NPF, and underpredicts the condensation sink, growth rate, and PM concentrations. Major uncertainties in reproducing the NPF include the atmospheric oxidation capability, precipitation, background PM concentrations, and particle early growth. In addition, the simulation results with 12-bin indicate that the anthropogenic aerosols can increase aerosol optical depth, cloud droplet number concentration, cloud optical thickness, and liquid water path during the four months in 2001. The simulated precipitation increases or decreases at various locations, but shows a net decrease on domain-average. In addition, anthropogenic aerosols can reduce surface net shortwave radiation, 2 meter temperature, and PBL height.

The COMB nucleation parameterization is incorporated into WRF-CAM5 for its further evaluation during three months (July, August, and September) in 2008. The results show that the wind speed has been greatly improved (changing the NMB from 49.1% to -5.6%) by updating the surface drag parameterization. 2-meter temperature and water vapor mixing ratios, and pressure are simulated reasonably well (with NMBs of -6.9% to 3.0%) and R values of 0.57 to 0.94. However, the precipitation is poorly simulated with a NMB of -16% and a R value of 0.05. PM_{10} concentrations are underpredicted due in part to underestimate in dust emissions and $PM_{2.5}$ concentrations. All those column variables (CO, NO_2, O_3, and SO_2) are simulated reasonably well with NMBs of -37.8% to 13.8% and R values of 0.54 to 0.72. Cloud fraction is reasonably well predicted, but the aerosol optical depth, cloud condensation nuclei, and cloud optical thickness are significantly underpredicted with NMBs of -74.8% to -65.9%. In addition, the simulation with the COMB nucleation generates more Aitken mode particles compared with the default one used in WRF-CAM5. Overall, WRF-CAM5 demonstrates reasonably good skills in capturing most meteorological variables and chemical concentrations in East Asia.

Performance Evaluation and Testing of New Particle Formation and Growth
Parameterizations Using Two Regional Online-Coupled
Meteorology-Chemistry Models

by
Changjie Cai

A thesis submitted to the Graduate Faculty of
North Carolina State University
in partial fulfillment of the
requirements for the degree of
Master of Science

Marine, Earth, and Atmospheric Sciences

Raleigh, North Carolina

2013

APPROVED BY:

Dr. Yang Zhang
Committee Chair

Dr. Shaocai Yu

Dr. Anantha R. Aiyyer

BIOGRAPHY

Changjie Cai was born (1988) and raised in Yichun, a small and beautiful city, which is located in Jiangxi province, China. Upon graduating from high school in 2005, he entered Nanjing University of Information Science and Technology to pursue a Bachelor's degree in Atmospheric Science (Weather Modification). He graduated from Nanjing University of Information Science and Technology in June 2009 with a Bachelor of Science degree in Atmospheric Science (Weather Modification). Changjie worked for Laboratory of Atmospheric Chemistry in Shanghai Meteorological Bureau as an assistant engineer for two years before continuing his Master's degree. He was accepted to North Carolina State University's Marine, Earth, and Atmospheric Science Graduate Program in April 2011 and began working with Dr. Yang Zhang in August 2011.

ACKNOWLEDGMENTS

I would first like to thank my committee members, Drs. Yang Zhang, Shaocai Yu, and Anantha R. Aiyyer. I am extremely grateful to Dr. Zhang's patience. I am extremely grateful to Dr. Zhang for giving me the opportunity to work on this project and for giving me numerous opportunities for academic growth throughout the entire process. I also greatly appreciate the scientific knowledge and guidance provided by Drs. Shaocai Yu, Anantha R. Aiyyer, and Markus Petters, who helped to take my M.S. research to its full potential.

I also appreciate the Pacific Northwest National Laboratory (PNNL) collaborators, Drs. Jiwen Fan, L. Ruby Leung, and Kyo-Sun Lim, for developing the WRF-CAM5 model, Dr. Litao Wang for providing the emissions for 2001. Thanks are also due to the following people for their scientific contributions: Xin Zhang, Dr. Kai Wang, Wei Wang, Jian He, and Yaosheng Chen. I also appreciate all other AQFL members.

I want to thank the following two programs for supporting this research: DOE climate modeling program (DE-SC000695) and NSF EaSM program (AGS-1049200).

Finally, enormous thanks are due to my wife Dan Li, I would not be where I am today without your support and encouragements. To my parents, Wenguang Cai and Xiuchun Hua. You have been behind me through everything and have given me never ending support and encouragement. All of you have given me the strength and motivation that I need for my career growth.

TABLE OF CONTENTS

Page

LIST OF TABLES

LIST OF FIGURES

LIST OF ABBREVIATIONS

Acronym	Definition
A	Activation coefficient
AOD	Aerosol optical depth
API	Air pollution index
AQMN	Air Quality Monitoring Network
ASTEM	Adaptive Step Time-Split Euler Method
BC	Boundary condition
BO08	Boy et al., 2008
BO08_ACTI	BO08 with activation theory
BO08_KINE	BO08 with kinetic theory
C_{cir,H_2SO_4}	Critical concentration in µg m^{-3}
C_{NH_3}	Volume mixing ratio of NH_3
CAM5	Community Atmosphere Model version 5
CAREBeijing 2008	Campaigns of Air Quality Research in Beijing and Surrounding Region 2008
CBMZ	Carbon-Bond Mechanism version Z
CCN	Cloud condensation nuclei
CDNC	Cloud droplet number concentration
CER	Cloud effective radius
CF	Cloud fraction

CO	Carbon monoxide
CoagS	Coagulation sink
COMB	A combination of three nucleation schemes
CONUS	Continental U.S.
COT	Cloud optical thickness
CS	Condensation sink
CWP	Cloud water path
DEAD	Dust Entrainment and Deposition
EPD	Environmental Protection Department
FR	Formation rate
FTUV	Fast Tropospheric Ultraviolet-Visible
GCMs	Global Climate Models
GEOS-Chem	Global Chemical Transport Model with chemistry
GOME	Global Ozone Monitoring
GR	Growth rate
H_2O	Water
H_2SO_4	Sulfuric acid
IC	Initial condition
INTEX-B	Intercontinental Chemical Transport Experiment-Phase B
IPCC	Intergovernmental Panel on Climate Change
J	Formation rate

K	Kinetic coefficient
KK02	Kerminen and Kulamala, 2002
LE07	Lehtinen et al., 2007
LH	Latent heat
LWP	Liquid water path
MAM	Modal aerosol module
MAM3	Modal aerosol module with three lognormal modes
MCM	Maximum concentration method
ME09	Merikanto et al., 2009
MEGAN	Model of Emissions of Gases and Aerosols from Nature
MEP	Ministry of Environmental Protection of China
MESA-MTEM	Multicomponent Equilibrium Solver for Aerosols-Multicomponent Taylor Expansion Method
MFM	Mode fitting method
MODIS	Moderate-resolution Imaging Spectroradiometer
MOPITT	Measurements of Pollution in the Troposphere
MOSAIC	Model for Simulating Aerosol Interactions and Chemistry
N_{sulf}	Number concentrations of H_2SO_4, cm^{-3}
N-PSD	Number particle size distribution
NASA	National Atmospheric and Space Adiministration
NCAR	National Center for Atmospheric Research

NCDC	National Climatic Data Center
NCL	National Center for Atmospheric Research Command Language
NCEP	National Centers for Environmental Prediction
NIES	National Institute of Environmental Studies
NMB	Normalized mean bias
NME	Normalized mean error
NO	Nitrogen monoxide
NO_2	Nitrogen dioxide
NO_NUCL	No nucleation
NOAA	National Oceanic and Atmospheric Adiministration
NOAH	National Center for Environmental Prediction, Oregon State University, Air Force, and Hydrologic Research Lab's
NPF	New particle formation
O_2	Oxygen
O_3	Ozone
OH	Hydroxyl radical
OMI	Ozone Monitoring Instrument
P	Atmospheric pressure
PBL	Planetary boundary layer
PM	Particulate matter
PM_{10}	Particulate matter of diameter less than 10 µm

$PM_{2.5}$	Particulate matter of diameter less than 2.5 µm
PSD	Particle size distribution
PWV	Precipitable water vapor
Q	Ionization rate
Q2	Water vapor mixing ratios at 2 meters
RH	Relative humidity
RH2	Relative humidity at 2 meters
RRTM	Rapid radiative transfer model
RRTMG	Rapid radiative transfer model for GCMs
S	Surface area of pre-existing particles
SCIAMACHY	Scanning Imaging Absorption Spectrometer
SNSR	Surface net shortwave radiation
SO_2	Sulfuric dioxide
SOA	Secondary organic aerosols
T	Temperature
T2	Temperature at 2 meter
T_c	Thermodynamic coefficient
TOMS	Total Ozone Mapping Spectrometer
TEMI	Tropospheric Emission Monitoring Internet Service
TOL	Benzene, toluene, ethylbenzene, i-Propylbenzene, n-Propylbenzene

TRACE-P	Transport and Chemical Evolution over Pacific
USGS	U. S. Geological Survey
VOCs	Volatile organic compounds
WA08	Wang et al., 2008
WA09	Wang et al., 2009
WA11	Wang et al., 2011
WA11_ACTI	WA11 with activation theory
WA11_KINE	WA11 with kinetic theory
WA11_THER	WA11 with thermodynamic theory
WE94	Wexler et al., 1994
WD10	Wind directions at 10 meters
WS10	Wind speeds at 10 meters
XYL	m,p,o-xylene, styrene, 1,3,5-trimethylbenzene, 1,2,4-trimethylbenzene, 1,2,3-trimethylbenzene, p-ethyltoluene
YSU	Yonsei University
YU10	Yu, 2010
WRF/Chem	Weather Research and Forecasting model with chemistry
WRF-CAM5	WRF with the physics and chemistry packages from the Community Atmosphere Model version 5

1. INTRODUCTION

1.1 Background and Motivations

Aerosol particles are ubiquitous in the atmosphere. In recent years, increasing studies on aerosols have revealed their significant effects on the climate change, air quality, and human health in many ways (Intergovernmental Panel on Climate Change, IPCC 2007). New particle formation (NPF) is considered as an important source of aerosol particles and cloud condensation nuclei (CCN) on global scale (Yu, 2000; Spracklen et al., 2006, 2008; Merikanto et al., 2009a; Yu et al., 2008). An increased aerosol number concentration may result in an enhanced cloud droplet number concentration (CDNC) and cloud shortwave albedo (Twomey, 1977; Haywood and Boucher, 2000; Stier et al., 2007; Y. Zhang et al., 2012). Thus, the NPF has an important effect on climate through direct and indirect aerosol effects (Haywood and Boucher, 2000; Lohmann and Feichter, 2005; Wang and Penner, 2009; Kazil et al., 2010; Yu et al., 2012). Although significant progress achieved over the past several decades, there still exist large uncertainties in nucleation mechanisms (R. Zhang et al., 2012).

As early as 1897, Aitken (1897) provides some evidences on NPF in the atmosphere. However, until the 21st century, NPF has been observed worldwide due to the development of related instruments (McMurry, 2000; Kulmala et al., 2004). Measured aerosol size distributions usually show three or four peaks where a high number of particles can be found around a certain particle diameter. In most cases, each peak can be approximated by a log-normal distribution (Seinfeld and Pandis, 2006). Thus, four modes of aerosol are classified in atmospheric sciences: nucleation mode (0.003 ~ 0.02 μm, freshly nucleated particles), Aitken mode (0.02 ~ 0.1 μm, ultrafine particles), accumulation mode (0.1 ~ 2.5 μm, fine particles) and coarse mode (> 2.5 μm, coarse particles) (Whitby, 1978; Hussein et al., 2005; Young and Keeler, 2008). Figure 1.1 shows the idealized schematic of an atmospheric particle number size distribution, principle modes, sources, and particle formation and removal mechanisms (Hussein et al., 2005) indicating that nucleation mode particles are usually produced by the condensation of low volatility compounds to form the neutral or ion clusters and then followed by the subsequent condensation and coagulation (Kulmala, 2003; Seinfeld and Pandis, 2006; Zhang, 2010; Kulmala et al., 2013). In addition, the directly emitted hot vapor can also contribute to the increase of nucleation mode particles.

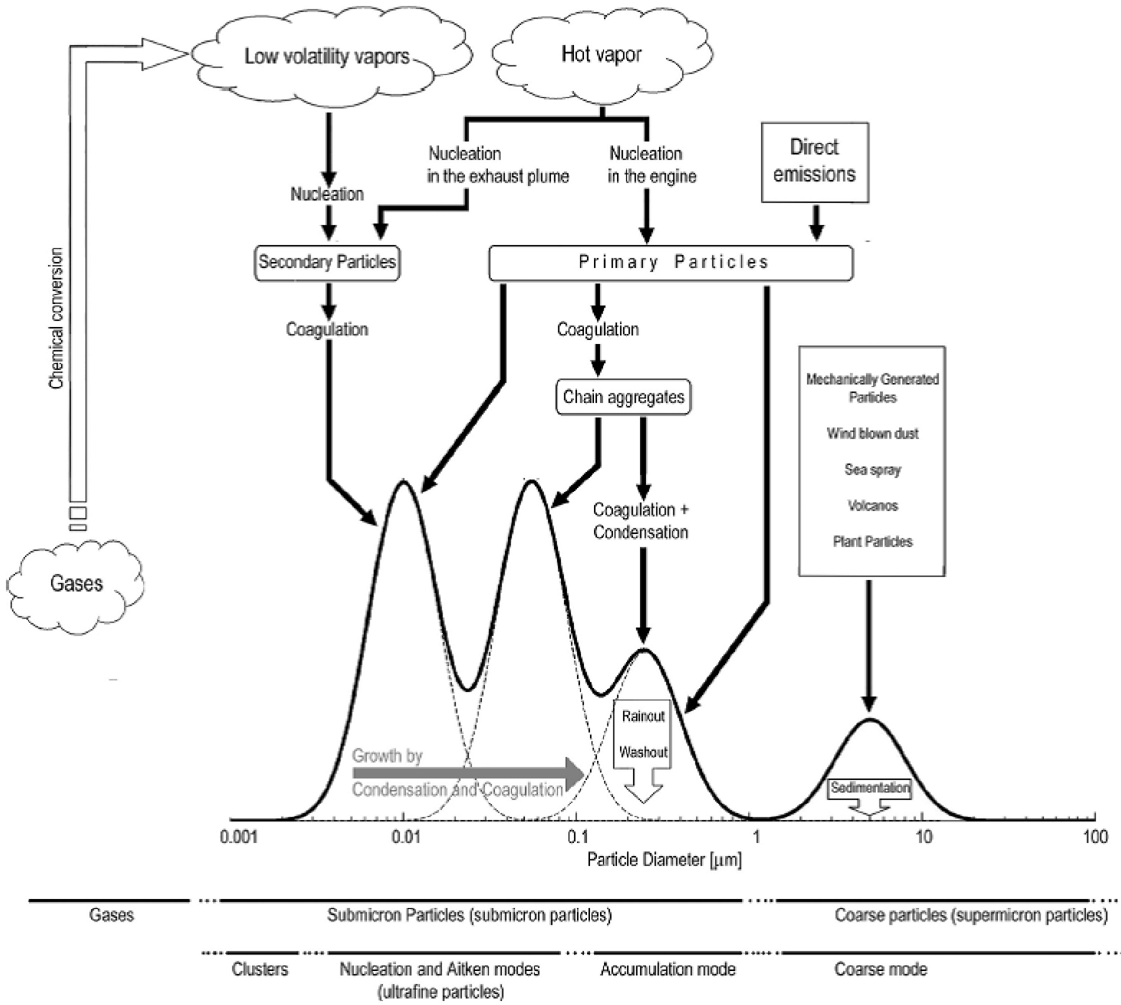

Figure 1.1 Idealized schematic of an atmospheric particle number size distribution. Principle modes, sources, and particle formation and removal mechanisms are indicated (Hussein et al., 2005).

NPF has been increasingly concerned by researchers for three main reasons: (1) it provides an important source of atmospheric aerosols, (2) it introduces uncertainties in climate predictions, and (3) it has large health effects. For reason 1, Merikanto et al. (2009) showed that the contributions of NPF on global aerosol number concentrations cannot be ignored, especially over ocean. Various nucleation mechanisms used in atmospheric models would give quite different results (Zhang et al., 2010a, b; Y. Zhang et al., 2012). Thus, it might not be appropriate to use just one mechanism over the whole domain. More details about this issue will be discussed in section 2. For reason 2, the effects of NPF on climate are mainly from their influences on CCN (Laaksonen et al., 2005). According to some measurement data, the NPF would increase CCN, especially in forest (Lihavainen et al., 2003) and coastal areas (O. Dowd, 2001; Kuwata et al., 2008). However, in some areas, the negative effects of NPF on CCN were shown from modeling studies, which might be due to the suppression effects of newly formed particles on the particle size and hygroscopicity (Matsui et al., 2011). For reason 3, many studies showed that ultrafine particles would greatly influence the human health due to their small size and large surface area ratio (Oberdorster et al., 2005). Thus, this study focuses on the first two aspects using two regional online-coupled meteorology-chemistry models.

1.2 Overall Approaches and Objectives

In this study, two regional online-coupled meteorology-chemistry models are applied to simulate meteorology, air quality, and their interactions over East Asia, one is the Weather Research and Forecasting model with chemistry (referred to as WRF/Chem) and the other is a variant of WRF/Chem with the physics and chemistry packages from the Community Atmosphere Model version 5 (CAM5) (referred to as WRF-CAM5). East Asia has been selected as a testbed for evaluating WRF/Chem and WRF-CAM5 and improving their performances. More details about the two models and testbed selection will be discussed in section 2.

The objectives for this research are to:

(1) improve the model's representation of the formation and fate of the ultrafine particles with diameters less than 20-nm (also referred to as the nucleation mode particles);

(2) evaluate the updated WRF/Chem's capability in simulating the ultrafine particles and also other meteorological and chemical variables;

(3) examine the sensitivity of the model predictions to different parameterizations for new particle formation and growth over East Asia using WRF/Chem and WRF-CAM5.

1.3 Literature Review

1.3.1 New Particle Formation and Particle Early Growth

Clusters form from molecules by nucleation (Kulmala, 2003). Figure 1.2 shows how particles form and grow. The continuous presence of a pool of numerous clusters in the sub-3 nm size range has been observed, showing that the nucleation occurs at any time (Kulmala et al., 2007).

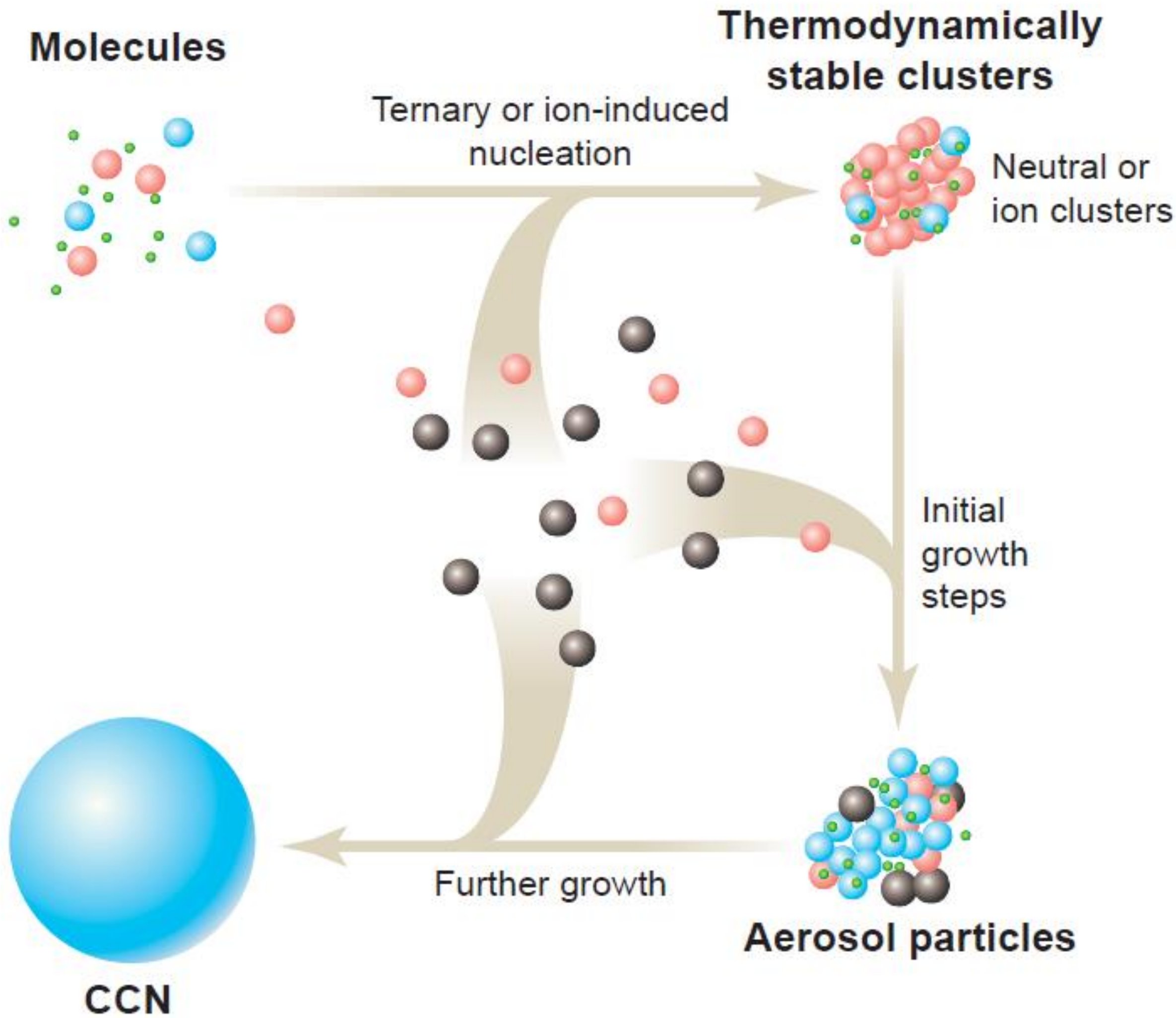

Figure 1.2 How particles form and grow (Kulmala, 2003).

Gaseous sulfuric acid (H_2SO_4) has been identified as a key component of the nucleation process (Lushnikov and Kulmala, 1998). Three power law nucleation theories have been reported based on the observed relationship between nucleation rates and ambient number concentrations of gaseous H_2SO_4 (N_{sulf}): (1) activation theory with with an exponent of 1 in N_{sulf} ($J = A \times N_{sulf}$); (2) kinetic theory with with an exponent of 2 in N_{sulf} ($J = K \times N_{sulf}^{2}$), and (3) thermodynamic theory with with an exponent of n in N_{sulf} ($J = K \times N_{sulf}^{n}$, (n > 2.5), where J is the formation rate (in of particles cm^{-3} s^{-1}), A is the activation coefficient (in s^{-1}), K is the kinetic coefficient (in cm^{3} s^{-1}), and T is the thermodynamic coefficient (in $cm^{(3n-3)}$ s^{-1}) (Lushnikov and Kulmala, 1998). However, H_2SO_4 alone may not always explain the observed high production rates of new particles. Since NH_3 is ubiquitous in the atmosphere and its presence can considerably decrease the vapor pressure of H_2SO_4 above the solution, NH_3 is expected to accelerate the nucleation rate of the binary nucleation rates (Scott and Cattell, 1979). In addition, recent modeling studies (e.g., Yu et al., 2008; Yu and Turco, 2011; Y. Zhang et al., 2012) and laboratory measurements (e.g., Enghoff et al., 2011; Kirkby et al., 2011) clearly showed that the ion-mediated nucleation is significant in the tropical upper troposphere, the entire middle latitude troposphere, and over Antarctica. In some regions (such as the coastal areas), the photooxidation of diiodomethane (CH_2I_2) may be another important mechanism for NPF events (Jimenez et al., 2003). Organic compounds may also be significant precursors for the nucleation process in some areas (Yu, 2000a; Zhang et al., 2004; Smith et al., 2008; Paasonen et al., 2010). The nucleation mechanisms can be grouped into five classes based on the compounds participated in the nucleation process: (1) H_2O+H_2SO_4 binary nucleation (Kulmala et al., 1998); (2) H_2O+H_2SO_4+NH_3 ternary nucleation (Merikanto et al., 2007, 2009); (3) H_2O+H_2SO_4+Ions ion-mediated nucleation (Yu et al., 2000b, 2010); (4) H_2O+H_2SO_4+IO_x Iodine-induced nucleation (Jimenez et al., 2003); (5) nucleation involving organic compounds (Zhang et al., 2004; Kulmala, 2013). Several nucleation schemes have been tested in both of 0-D and 3-D models by Zhang et al. (2010a, b). Although recent technical development makes it possible to measure the concentrations and size distributions of ions, molecular clusters, and nanoparticles in the 1~2 nm mobility diameter range, until now, only a few groups have taken comprehensive and simultaneous field measurements of charged and neutral clusters and their precursors (Kulmala et al., 2013). In most cases, atmospheric nucleation rates can be inferred indirectly by measuring the new particle formation rate of particles with a diameter of 3 nm and by extrapolating this down to the nuclei size. By analyzing the competition between nuclei growth and sink by background aerosols, Kerminen and Kulamala (2002) derived a simple expression (so-called K-K equation, KK02) to relate the nucleation rate (also called the “real” nucleation rate) and the new particle formation rate at larger size (also called the “apparent” nucleation rate). Lehtinen et al. (2007) (LE07) updated this K-K equation by using coagulation sink instead of condensation sink to overcome some limitations in KK02.

According to previous studies (Kulmala et al., 2004; Wang, 2012), nucleation mechanisms under different environments may be quite different which will lead to diversed formation rates of newly formed particles, especially in polluted urban areas (may vary by several orders of magnitude, see Figure 1.3).

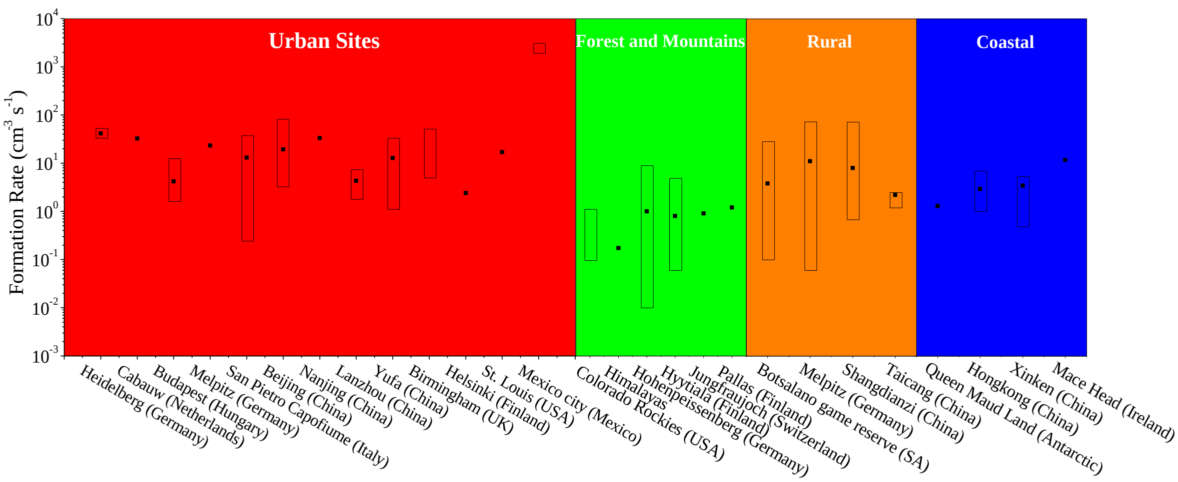

Figure 1.3 New particle formation rates reported at various sites worldwide (red represents urban sites, green for forest and mountain sites, orange for rural sites and blue for coastal sites; the dot represents the averaged values; and the bar represents the measurement range). The data were obtained from literatures (see Table 1.1).

Table 1.1 Summary of formation rates used in Figure 1.3.

Location	Lat[a] & Lon[b]	Type of location	Formation rate J (cm^{-3} s^{-1})			Time period	References
			Mean	Min[c]	Max[d]		
Heidelberg, Germany	49º23'N & 08º41'E	Urban	42.1	33.3	52.1	28, February – 3, April, 2004	Riipinen et al., 2007
Cabauw, Netherlands	51º57'N & 04º53'E	Urban	32.4	-	-	March, 2008 – May, 2009	Manninen et al., 2010
Budapest, Hungary	46º58'N & 19º35'E	Urban	4.2	1.7	12.5	March, 2008 – May, 2009	Manninen et al., 2010
Melpitz, Germany	51º32'N & 12º54'E	Urban	23.1	-	-	March, 2008 – May, 2009	Manninen et al., 2010
San Pietro Capofiume, Italy	44º39'N & 11º37'E	Urban	13.0	0.2	36.9	2002 - 2005	Hamed et al., 2007
Beijing, China	39º59'N & 116º18'E	Urban	19.3	3.3	81.4	March, 2004 – February, 2005	Wu et al., 2007
Nanjing, China	32º07'N & 118º57'E	Urban	33.2	-	-	18, November, 2011 – 31, March, 2012	Herrmann et al., 2013
Lanzhou, China	36º08'N & 103º41'E	Urban	4.3	1.8	7.1	25, June – 19, July, 2006	Gao et al., 2011
Yufa, China	39º31'N & 116º18'E	Urban	12.8	1.1	33.0	4 – 25, August, 2004; 10, August – 10, September, 2005 & 2006	Yue et al., 2009
Birmingham, United Kingdom	52º29'N & 01º53'W	Urban	-	5.0	50.0	28 – 30, October, 1998 & 9 – 19, February, 1999	Shi et al., 2001

Table 1 Continued

Helsinki, Finland	60º10'N & 24º56'E	Urban	2.4	-	-	May, 1997 – December, 2006	Hussein et al., 2008
St. Louis, USA	38º38'N & 90º12'W	Urban	17.0	-	-	1, April, 2001 – 31, May, 2003	Qian et al., 2007
Mexico city, Mexico	19º43'N & 98º58'W	Urban	-	1900.0	3000.0	15 – 31, March, 2006	Iida et al., 2008
Colorado Rockies, USA	39º59'N & 105º34'W	Forest and Mountains	-	0.1	1.0	September, 1993	Weber et al., 1997
Himalayas	30º38'N & 79º49'E	Forest and Mountains	0.2	-	-	2007	Venzac et al., 2008
Hohenpeissenberg, Germany	47º48'N & 11º00'E	Forest and Mountains	1.0	0.0	9.0	March, 2008 – May, 2009	Manninen et al., 2010
Hyytiala, Finland	61º51'N & 24º17'E	Forest and Mountains	0.8	0.1	5.0	5, April – 16, May, 2005	Riipinen et al., 2007
Jungfraujoch, Switzerland	46º32'N & 07º57'E	Forest and Mountains	0.9	-	-	March, 2008 – May, 2009	Manninen et al., 2010
Pallas, Finland	67º58'N & 24º07'E	Forest and Mountains	1.2	-	-	March, 2008 – May, 2009	Manninen et al., 2010
Botsalano game reserve, SA	25º54'N & 25º75'E	Rural	3.8	0.1	28.0	20, July, 2006 – 5, February, 2008	Vakkari et al., 2011
Melpitz, Germany	51º32'N& 12º54'E	Rural	11.1	0.1	74.0	March, 2008 – May, 2009	Manninen et al., 2010
Shangdianzi, China	40º39'N & 117º07'E	Rural	8.0	0.7	72.7	March, 2008 – August, 2009	Shen et al., 2011
Taicang, China	31º27'N & 121º08'E	Rural	2.2	1.2	2.5	5, May – 2, June, 2005	Gao et al., 2009

Table 1 Continued

Queen Maud Land, Antarctic	73º03’S& 13º25’W	Coastal	1.3	-	-	29, December – 29, January, 2006 & 2007	Asmi et al., 2010
Hongkong, China	22º15’N & 114º10’E	Coastal	2.9	1.0	6.9	25, October – 29, November, 2010	Guo et al., 2012
Xinken, China	22º37’N & 113º35’E	Coastal	3.4	0.5	5.2	3, October – 5, November, 2004	Liu et al., 2008a, b
Mace Head, Ireland	53º19’N& 09º53’E	Coastal	11.8	-	-	March, 2008 – May, 2009	Mannine n et al., 2010

[a]Lat – Latitude;
[b]Lon – Longtitude;
[c]Min – Minimum;
[d]Max – Maximum.

1.3.2 Aerosol-Cloud-Meteorology Interactions

Aerosols are liquid or solid particles suspended in the atmosphere. Their radiative effects can be divided into direct, semi-direct and indirect (Haywood and Boucher, 2000). The direct effect of atmospheric aerosols involves a combination of scattering and absorption of radiation by the aerosol particles themselves (Hind, 1999). According to the IPCC (2007) report, this effect is estimated to contribute a net radiative forcing of -0.5 ± 0.4 W m^{-2}. The troposphere would be heating when the aerosols absorb the shortwave (solar) radiation, that in turn changes the stability of the atmosphere and relative humidity, and this effect is called "semi-direct effect" (IPCC, 2007). The radiative balance can also be affected by the interactions between aerosols and clouds (aerosol indirect effects). The indirect effects are conventionally split into two main effects: (1) the first indirect effect (also known as "the cloud albedo effect" or "the Twomey effect"), and (2) the second indirect effect (also known as "the cloud lifetime effect"). In a cloud of constant liquid water content, increasing aerosol particles leads to a greater number of smaller cloud droplets, which results in an enhanced solar radiation reflection (because of the increased droplet surface areas), and therefore an enhancement of cloud albedo (Twomey, 1977; Haywood and Boucher, 2000). The second indirect effect is related to the cloud lifetime. An increase of aerosol number concentrations leads to many smaller cloud droplets and hence reduces the precipitation efficiency of the cloud due to the longer time of those small particles growing up to the precipitation size. Thus, the longer cloud lifetime would increase the reflectivity over time (Albrecht, 1989; Haywood and Boucher, 2000). The overall aerosol effects is illustrated in Figure 1.4.

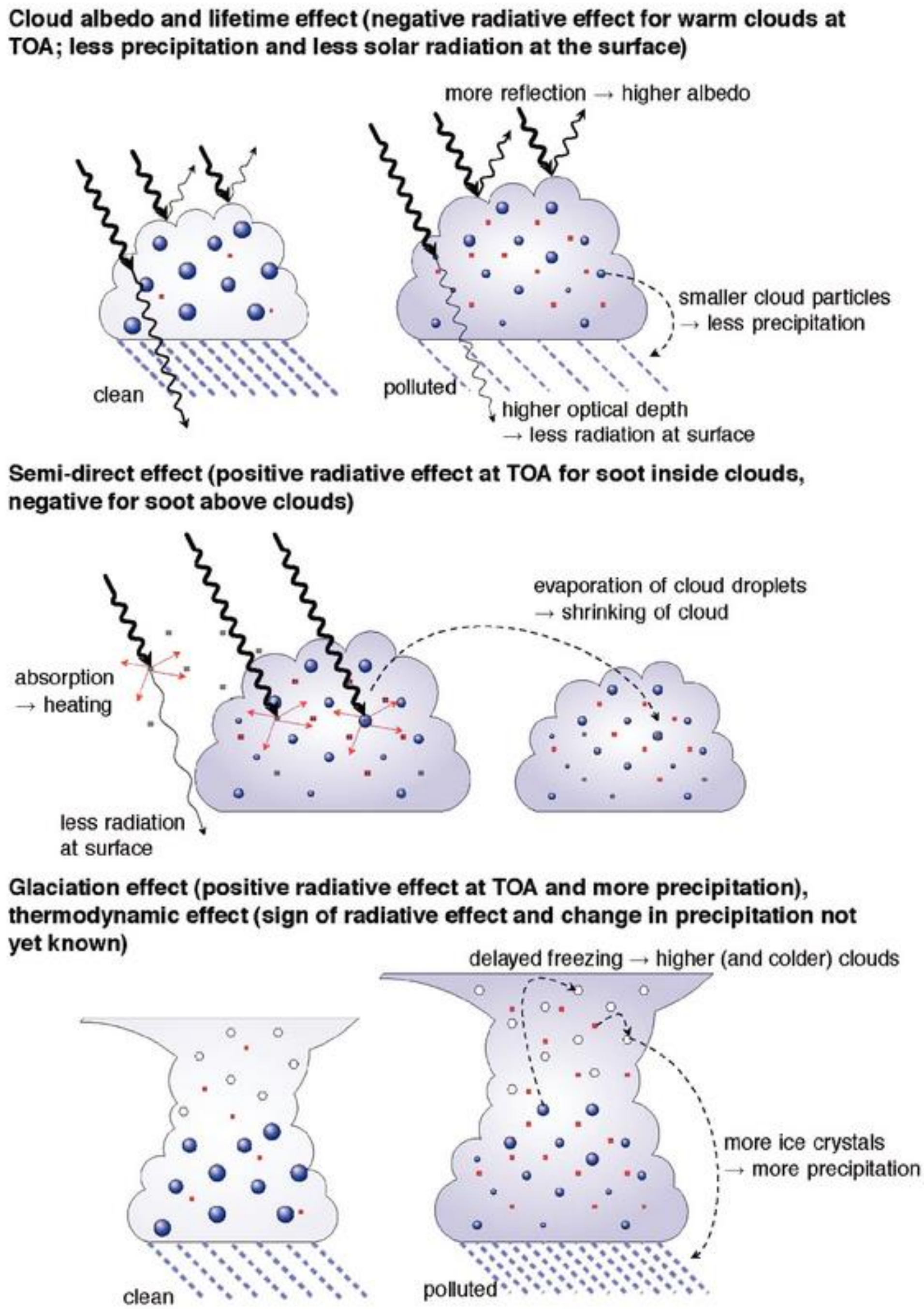

Figure 1.4 Schematic diagram of the aerosol effects (IPCC, 2007).

The processes that determine the number of CCN particles include emissions, photochemistry, nucleation, coagulation, condensation, and wet removal (Seinfeld and Pandis, 2006; Lamb and Verlinde, 2011). Atmospheric aerosols include primary particles from emissions (i.e., carbonaceous particles from open fires (Ito and Penner, 2005), sea-salt particles from the bubble-bursting process (Clarke et al., 2003) and dust particles from erosion of dry soils (Ginoux et al., 2001; Zender et al., 2003)) and secondary particles (Kulmala et al., 2007). Some of primary particles are large enough to serve as CCN, but some of them are not. For instant, some previous studies indicate that mineral dust particles are known to be efficient ice nuclei, but not very efficient CCN; however, recent in situ measurements showed that dust particles can get covered by sulfate from polluted areas during their transport (Levin et al., 1996; Trochkine et al., 2003), which may increase their effectiveness as CCN. In addition, some sea-salt particles are also large enough to act as CCN (Clarke et al., 2003). The secondary particles are mainly generated from nucleation of condensable gases (Kulmala et al., 2007). Some observations proved the capability of newly formed particles to grow to large enough to serve as CCN (Lihavainen et al., 2003; McNaughton et al., 2004).

The impact of aerosols on cloud (including both of macrophysical and microphysical) and precipitation has received extensive attention for over 50 years. According to previous studies, high CCN concentrations from anthropogenic sources can increase CDNC, thus reducing the size of cloud droplet, increasing the cloud stability and potentially reducing precipitation efficiency (Gunn and Phillips, 1957; Squires, 1958; Kauitman et al., 2002).

However, large uncertainties still exist about their effects on precipitation (Yin et al., 2000; Rosenfeld et al., 2008).

From the observational studies, the increase of CCN concentration from polluted areas has been widely observed (Twomey et al., 1978; Charlson et al., 1992). Radke and Hobbs (1976) concluded that the anthropogenic produced CCN might be comparable to the natural produced CCN. In addition, numerous observational evidences showed that, regardless of locations, increases in aerosol concentrations lead to increases in CDNC (see Figure 1.5) (Ramanathan et al., 2001). However, the relationship is not linear, and the trend appears to slow down as the increasing aerosol concentrations further increase. The CCN activation processes are related to many factors including the atmospheric temperature, updraft velocity, particle size distribution (PSD), chemical composition, mixing state, and surface coating (Abdul-Razzak and Ghan, 1998, 2000, 2002; McFiggans et al., 2006; Petters and Kreidenweis, 2007). Four types of clouds were divided by Andreae et al. (2004) in Amazon region: (1) “Blue Ocean”, which are developed over the ocean, and they have low CCN concentrations and few cloud drops (including a few large drops); (2) “Green Ocean”, which are developed inland in unpolluted conditions, and their CCN and CDNC are similar with the first one; (3) “Smoky Clouds”, which are characterized by high concentrations of CCN from smoke and high concentrations of cloud droplets, thus smaller sizes, which would reach higher altitudes and lower temperatures where ice could form; (4) “Pyro-Clouds”, which are directly fed with smoke and heat from biomass fires, and like the third one, the high concentrations of CCN produce large small droplet concentrations. In addition, the studies on the effects of particle transport from polluted and unpolluted sources (see Figure 1.6) indicated that the droplet concentrations from polluted air are higher than from clean air, however the cloud effective radius from polluted air is smaller (Garrett and Hobbs, 1995). As shown in the previous studies, aerosol impacts on cloud drop evolution are reasonably well understood, while large uncertainties still exist in ice particles, for example, measurements show large variations in ice concentrations in different types of clouds, even at the same temperature (Gultepe et al., 2001; Korolev et al., 2003; Field et al., 2005).

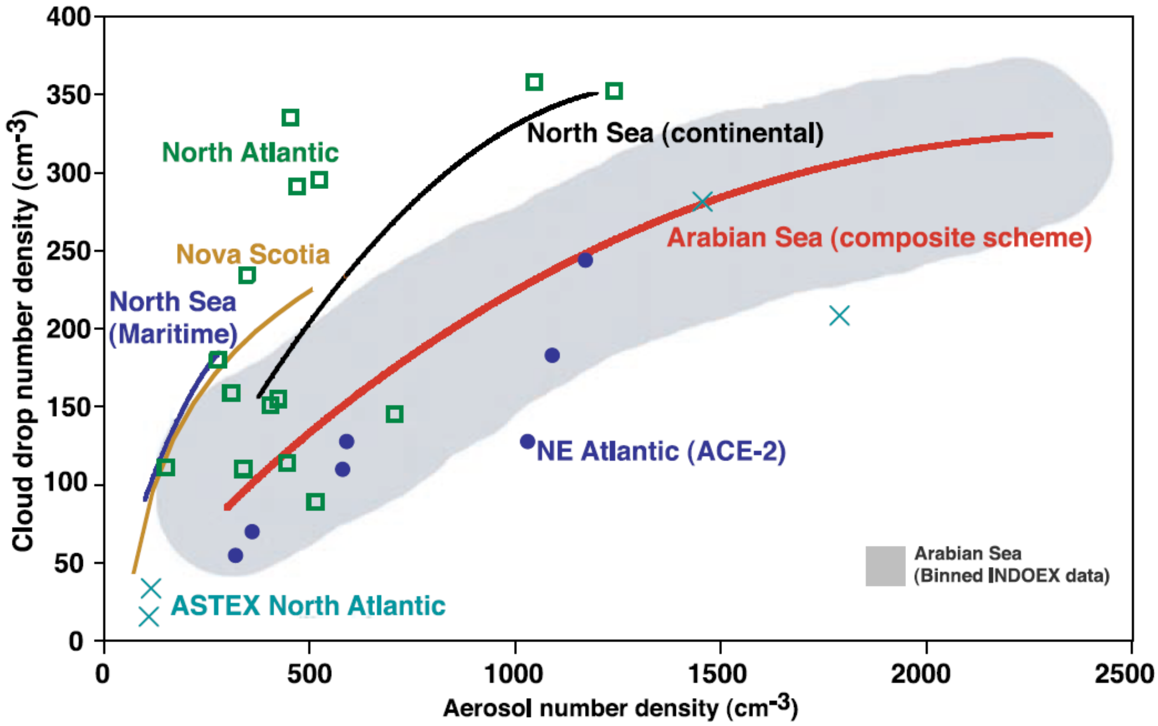

Figure 1.5 Aircraft data illustrating the increase in CDNC with aerosol number concentration (Ramanathan et al., 2001).

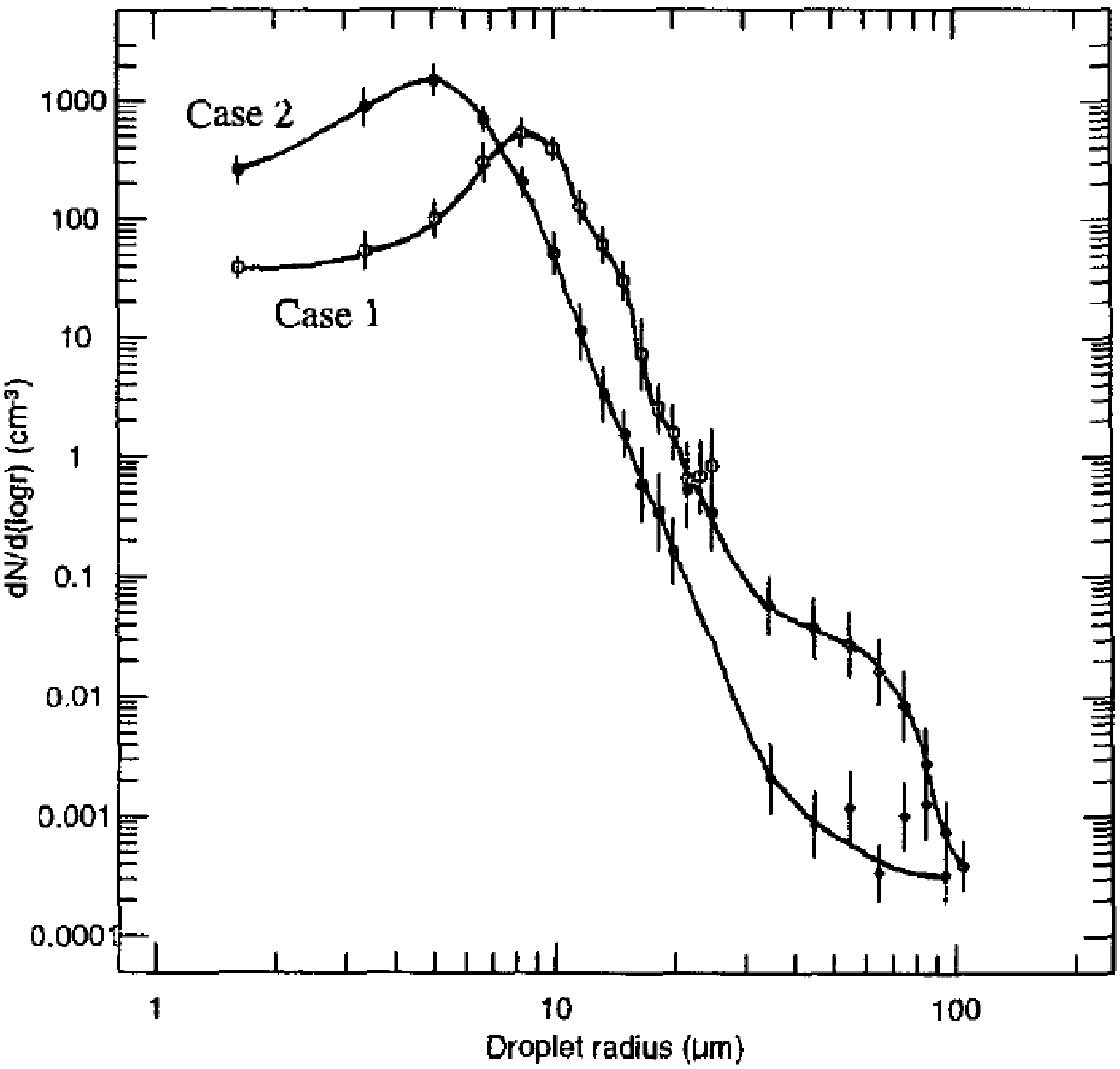

Figure 1.6 Cloud droplet number distribution measured in clean (case 1) and polluted (case 2) stratocumulus clouds over Azores (Garrett and Hobbs, 1995).

The numerical models are widely used for studying the atmospheric pollution issues due to their roles in understanding the formation mechanisms of atmospheric air pollutants, especially their chemical and physical processes. WRF/Chem has been recently developed as a new generation of regional air quality modeling system (Grell et al., 2005). It is an “online” coupled model in which its chemical and meteorological components are fully coupled with the same coordinates and physical parameterizations; it can simulate the interactions between meteorological and chemical processes (Chapman et al., 2009). WRF/Chem has been applied to examine aerosol-radiation-cloud-climate interactions in several studies (Fast et al., 2006; Chapman et al., 2009; Zhang et al., 2010c; Matsui et al., 2011). The Community Atmosphere Model (CAM) is another widely used global model for analyzing the issues of atmospheric gases/aerosols and aerosol-meteorology interactions (M. Wang et al., 2009; Wang and Penner, 2009; Liu et al., 2012; Yu et al., 2012). Based on the modeling results, M. Wang et al. (2009) and Yu et al. (2012) indicated that the nucleation may increase the aerosol number concentrations, thus leads to an enhancement of CCN, CDNC, cloud liquid water (CLW), and cloud cover (CF), but a reduction in precipitation. Due to the change of clouds, the radiative balance has also been affected. However, there are still large uncertainties using various nucleation schemes (M. Wang et al., 2009; Yu et al., 2012; R. Zhang et al., 2012; Y. Zhang et al., 2012).

2. DESCRIPTION OF MODELS, DATABASE, AND EVALUATION METHODOLOGY

2.1 Modeling System and Improvement

2.1.1 WRF/Chem

WRF/Chem version 3.3.1 released in September 2011 is applied in this study. WRF/Chem offers multiple physics and chemistry options to simulate a variety of atmospheric processes. The major physics and chemistry options are summarized in Table 2.1. The major physics options used include the modified Purdue Lin microphysics module (Lin et al., 1983; Rutledge and Hobbs, 1984), the Rapid Radiative Transfer Model (RRTM) long-wave radiation scheme (Mlawer et al., 1997), the Goddard short-wave radiation scheme (Chou and Max, 1994), the National Center for Environmental Prediction, Oregon State University, Air Force, and Hydrologic Research Lab's (NOAH) land-surface module (Tewari et al., 2004), the Yonsei University (YSU) Planetary Boundary Layer (PBL) scheme (Hong et al., 2006), the Grell-Devenyi cumulus parameterization (Grell and Devenyi, 2002), the Fast-J photolysis rate scheme (Wild et al., 2000). The gas-phase chemistry is based on the Carbon-Bond Mechanism version Z (CBMZ, Zaveri and Paters, 1999). The aerosol module is based on the Model for Simulating Aerosol Interactions and Chemistry (MOSAIC) (Zaveri et al., 2008). The nucleation scheme used in MOSAIC is from Wexler et al. (1994) (WE94), which calculates the critical concentration of H_2SO_4 based on temperature and relative humidity. This scheme only calculate the mass concentration, therefore, the number of particles produced by this is arbitrary (depending on the smallest size section). Aerosol coagulation is calculated using the algorithm of Jacobson et al. (1994) with a Brownian coagulation kernel. The new gas-particle partitioning module Adaptive Step Time-Split Euler Method (ASTEM) is used with the thermodynamic module Multicomponent Equilibrium Solver for Aerosols-Multicomponent Taylor Expansion Method (MESA-MTEM) to dynamically integrate the mass transfer equations. However, the MOSAIC in this version of WRF/Chem (3.3.1) does not treat secondary organic aerosols (SOA). More details about the MOSAIC treatments have been described by Zaveri et al. (2008). In the default WRF/Chem 8-bin structure of MOSAIC, the particle size distribution is simulated for eight size bins between 39-nm and 10-μm with six bins for $PM_{2.5}$ and two bins for $PM_{10-2.5}$ (Zaveri et al., 2008). More details about the chemistry, aerosol, and cloud treatments can be found in several studies (e.g., Fast et al., 2006; Gustafson et al., 2007; Chapman et al., 2009; and Zhang et al., 2010c).

Table 2.1 WRF/Chem model configurations

Attribute	Model Configuration
Simulation period	July, 2008; January, April, July, and October, 2001
Domain	East Asia
Horizontal resolution	36 km (164×97)
Vertical resolution	23 layers from 1000 mb - 50 mb
Meteorological initial condition (IC) and boundary condition (BC)	The National Centers for Environmental Predictions Final Analysis (NCEP-FNL) reanalysis data; re-initialization every day
Shortwave radiation	Goddard shortwave radiation scheme (Chou and Max, 1994)
Longwave radiation	The rapid radiative transfer model (RRTM) (Mlawer et al., 1997)
Land surface	Community National Centers for Environmental Prediction (NCEP), Oregon State University, Air Force, and Hydrologic Research Lab-NWS Land Surface Model (NOAH) (Tewari et al., 2004)
Surface layer	Monin-Obukhov (Monin and Obukhov, 1954; Janjic, 2002)
Planetary boundary layer (PBL)	Yonsei University (YSU) PBL scheme (Hong et al., 2006)
Cumulus	Grell-Devenyi ensemble (Grell and Devenyi, 2002)
Microphysics	Purdue Lin (Lin et al., 1983; Rutledge and Hobbs, 1984; Chen and Sun, 2002)
Aerosol activation	Abdul-Razzak and Ghan (Abdul-Razzak and Ghan, 2002)
Gas-phase chemistry	Carbon-Bond mechanism version Z (CBMZ) (Zaveri and Peters, 1999)
Photolysis	Fast-J (Wild et al., 2000)
Aerosol module	Model for simulating aerosol interactions and chemistry (MOSAIC) (Zaveri et al., 2008)
Aqueous-phase chemistry	Carnegie Mellon University (CMU) mechanism (Fahey and Pandis, 2001)
Chemical IC	Community Multiscale Air Quality (CMAQ) modeling system (Binkowski and Roselle, 2003)
Chemical BC	The Goddard Earth Observing System Atmospheric Chemistry Transport Model (GEOS-Chem)
Anthropogenic emissions	Adjusted version for Wang et al. (2010) following the approach of X. Zhang (2013)
Biogenic emissions	Model of Emissions of Gases and Aerosols from Nature (MEGAN) version 2 (Guenther et al., 2006)
Dust emissions	Zender et al. (2003) implemented by K. Wang et al. (2012)
Sea-salt emissions	Gong (2003)

2.1.2 WRF-CAM5

The original Community Atmosphere Model version 5 (CAM5) is developed by the National Center for Atmospheric Research (NCAR). The major physics and chemistry options are summarized in Table 2.2. A modal aerosol module (MAM) has been developed for the CAM5 by Liu et al. (2012). MAM is capable of simulating the aerosol size distribution and both internal and external mixing between aerosol components, treating numerous complicated aerosol processes and aerosol physical, chemical, and optical properties in a physically-based manner (Liu et al., 2012). MAM3 (a version with three lognormal modes: Aitken mode (with a geometric number mean diameter (d_p) of 0.028 μm), accumulation mode (with d_p of 0.125 μm) and coarse mode (with d_p of 1.709 μm)) has been used in this study. The size distributions of each mode are assumed to be lognormal, and the geometric standard deviation (σ_g) of each mode is 1.6, 1.8, and 1.8, respectively. Thus, the main size structure difference between the two models for aerosol module is that MOSAIC in WRF/Chem uses 8 bins whereas MAM3 in CAM5 uses three log-normal modes (Aitken, accumulation, and coarse modes) to represent aerosol size distributions. In addition, some physics options used in WRF-CAM5 are different from WRF/Chem. For instance, both of short- and long- wave radiation schemes used in WRF-CAM5 are the rapid radiative transfer method for Global Climate Models (GCMs) (RRTMG) (Mlawer et al. 1997; Iacono et al. 2008), the PBL scheme used in WRF-CAM5 is from Bretherton and Park (2009), the cumulus scheme used in WRF-CAM5 is Zhang-Macfarlane (Zhang and MacFarlane, 1995) with modifications from Song and Zhang (2011), the microphysics scheme used in WRF-

CAM5 is the Morrison 2-moment scheme (Morrison and Gettelman, 2008), and the photolysis scheme used in WRF-CAM5 is the Fast Tropospheric Ultraviolet-Visible (FTUV) (Madronich,1987; Tie et al., 2003). In addition, the Cliff Mass's correction has been used for calculating the wind (Mass et al., 2010).

Table 2.2 WRF-CAM5 model configurations

Attribute	Model Configuration
Simulation period	July, August, and September 2008
Domain	East Asia
Horizontal resolution	36 km (164×97)
Vertical resolution	23 layers from 1000 mb - 50 mb
Meteorological IC and BC	The National Centers for Environmental Predictions Final Analysis (NCEP-FNL) reanalysis data; re-initialization every day
Shortwave radiation	The Rapid Radiative Transfer Method for GCMs (RRTMG) (Iacono et al., 2008; Mlawer et al., 1997)
Longwave radiation	The Rapid Radiative Transfer Method for GCMs (RRTMG) (Iacono et al., 2008; Mlawer et al., 1997)
Land surface	Community National Centers for Environmental Prediction (NCEP), Oregon State University, Air Force, and Hydrologic Research Lab-NWS Land Surface Model (NOAH) (Tewari et al., 2004)
Surface layer	Monin-Obukhov (Monin and Obukhov, 1954; Janjic, 2002)
PBL	Bretherton-Park (Bretherton and Park, 2009)
Cumulus	Zhang-Macfarlane (Zhang and MacFarlane, 1995) with modification from Song and Zhang (2011)
Microphysics	Morrison 2-moment (Morrison and Gettelman, 2008)
Aerosol activation	Abdul-Razzak and Ghan (Abdul-Razzak and Ghan, 2002)
Gas-phase chemistry	Carbon-Bond mechanism version Z (CBMZ) (Zaveri and Peters, 1999)
Photolysis	Fast Tropospheric Ultraviolet-Visible (FTUV) (Madronich, 1987)
Aerosol module	A modal aerosol module with three lognormal modes (MAM3) (Liu et al., 2012)
Aqueous-phase chemistry	Carnegie Mellon University (CMU) mechanism (Fahey and Pandis, 2001)
Chemical IC	Community Multiscale Air Quality (CMAQ) modeling system (Binkowski and Roselle, 2003)
Chemical BC	The Goddard Earth Observing System Atmospheric Chemistry Transport Model (GEOS-Chem)
Anthropogenic emissions	Adjusted version for Wang et al. (2010)
Biogenic emissions	Model of Emissions of Gases and Aerosols from Nature (MEGAN) version 2 (Guenther et al., 2006)
Dust emissions	Zender et al. (2003) implemented by K. Wang et al. (2012)
Sea-salt emissions	Gong (2003)

2.1.3 Model Improvement

2.1.3.1 Nucleation and Early Growth Parameterizations

Tables 2.3 (a) and (b) summarize the parameterizations of the default nucleation in WRF/Chem, and various nucleation schemes, as well as particle early growth, respectively, to be examined in this study. Unlike other schemes which explicitly calculate the nucleation rate, WE94 (i.e., the default module used in WRF/Chem) calculates the critical concentration in μg m^{-3}, rather than the new particle formation rate. The number of particles produced by WE94 is thus somewhat arbitrary, because it depends on the smallest bin of the model (Wexler et al., 1994). Merikanto et al. (2009) (ME09) and Wang et al. (2009) (WA09), which are default nucleation schemes in WRF-CAM5, are developed based on classical ternary (H_2SO_4-NH_3-H_2O) nucleation theory and activation/kinetic theory (based on Sihto et al. (2006)), respectively. Wang et al. (2011) (WA11) is a power law scheme (including activation, kinetic, and thermodynamic theories), which is derived based on measurement data at an urban site (Beijing) in China (Wang et al., 2011). BO08 is similar to WA09 and WA11 except that it was derived based on measurement data obtained in mountain and forest areas (Boy et al., 2008). YU10 is an ion-mediated nucleation scheme, which is suitable for the whole troposphere (Yu, 2010). As mentioned in section 1.3.1, nucleation mechanisms under different environments may be quite different which will lead to diverse formation rates of newly formed particles, especially in polluted urban areas (see Figure 1.3). Figure 2.1 shows the spatial distribution of surface land index from the U. S. Geological Survey (USGS) used in WRF/Chem. However, the land index 1 (urban and built-up land) is not included in

Figure 2.1 due to their small fractions (see Figure 2.2). Nevertheless, large differences exist in the new particle formation rates between urban and forest/mountain sites. Therefore, the fraction shown in Figure 2.2 of land index 1 (urban and built-up land) is used to determine the nucleation parameterizations to be used over urban areas. Thus, in this study, based on various land surfaces, a combination of WA11 with activation theory (WA11_ACTI) (for urban areas in PBL), BO08 with activation theory (BO08_ACTI) (for non-urban areas in PBL), and YU10 (above PBL) will be tested.

Kerminen and Kulamala (2002) (KK02) derived a simple expression (called K-K equation) relating the nucleation rate (also called the "real" nucleation rate) and the formation rate at larger size (also called the "apparent" nucleation rate) by analyzing the competition between nuclei growth and sink by background aerosols. Lehtinen et al. (2007) (LE07) updated this K-K equation using a coagulation sink instead of a condensation sink to avoid some uncertainties from the calculations. In default WRF/Chem, both schemes are not used. The updated KK equation (i.e., LE07) is incorporated into WRF/Chem with 12-bin to simulate the particle early growth. An optimal nucleation scheme is first selected based on application and evaluation of WRF/Chem with various nucleation treatments, then applied to WRF/CAM5.

Table 2.3 Nucleation parameterizations and particle early growth treatment to be examined in this work

(a) Nucleation parameterizations

Category	Reference	Theoretical Basis	Dependent variable	Equation:
Binary	Wexler et al., 1994 (WE94) (Default in WRF/Chem)	Classical binary (H_2SO_4-H_2O) nucleation theory	[a]T, [b]RH, and [c] $C_{cir,H2SO4}$	$C_{cri,H2SO4} = 0.16\exp(0.1T - 3.5RH - 27.7)$
Ternary	Merikanto et al. 2007, 2009b (ME09) (Default in WRF-CAM5)	Classical ternary (H_2SO_4-NH_3-H_2O) nucleation theory	[d]N_{sulf}, T, RH, and [e]C_{NH3}	Empirical equations suitable for temperature (235K-295K), N_{sulf} (5×10^4-10^9), C_{NH3} (0.1-1000pptv), RH (0.05-0.95) and nucleation rate over 10^{-5}cm^{-3}s^{-1}.
Power Law	Wang et al., 2011 (WA11), used for urban and polluted rural areas	Activation theory	N_{sulf}	[f] $J =$ [g] $A \times N_{sulf}$ $A = 1.95\times10^{-6}$ s^{-1}
		Kinetic theory	N_{sulf}	$J =$ [h]$K \times N_{sulf}{}^2$ $K = 3.44\times10^{-13}$ cm^3 s^{-1}
		Thermodynamic theory	N_{sulf}	$J =$ [i]$T_c \times N_{sulf}{}^3$ $T_c = 5.96\times10^{-20}$ cm^6 s^{-1}
	Boy et al., 2008b (BO08), used for mountain and forest areas	Activation theory	N_{sulf}	$J = A \times N_{sulf}$ $A = 0.28\times10^{-6}$ s^{-1}
		Kinetic theory	N_{sulf}	$J = K \times N_{sulf}{}^2$ $K = 0.18\times10^{-13}$ cm^3 s^{-1}
	Wang et al., 2009a (WA09) (Default in WRF-CAM5)	Activation theory	N_{sulf}	$J = A \times N_{sulf}$ $A = 1.0\times10^{-6}$ s^{-1}
		Kinetic theory	N_{sulf}	$J = K \times N_{sulf}{}^2$ $K = 1.0\times10^{-12}$ cm^3 s^{-1}
Ion-mediated	Yu, 2010 (YU10)	Ion-mediated nucleation (IMN) theory	N_{sulf}, T, RH, [j]Q, and [k]S	Look-up table

Table 2.3 Continued

(b) Particle early growth algorithm

Category	Reference	Theoretical Basis	Dependent variable	Equation:
Particle Early Growth	Lehtinen et al., 2007 (LE07)	Based on coagulation sink	[l]*CoagS*, [m]*GR, dx, d1* and *r*	$m = \frac{\log[CoagS(a_x)/CoagS(d_1)]}{\log[d_x/d_1]}$ $r = \frac{1}{m+1}[(\frac{d_x}{d_1})^{m+1} - 1]$ $J_x = J_1 \cdot \exp[-r \cdot d_1 \cdot \frac{CoagS(d_1)}{GR}]$

[a] T – temperature
[b] RH – relative humidity
[c] $C_{cir,H2SO4}$ – the critical concentration in μg m^{-3}
[d] N_{sulf} – number concentrations of H_2SO_4, cm^{-3}
[e] C_{NH3} – volume mixing ratio of NH_3
[f] J – formation rate
[g] A – activation coefficient
[h] K – kinetic coefficient
[i] T_c – thermodynamic coefficient
[j] Q – ionization rate, ion-pairs $cm^{-3}s^{-1}$
[k] S – surface area of pre-existing particles, $\mu m^2 cm^{-3}$
[l] *CoagS* – coagulation sink
[m] *GR* – growth rate

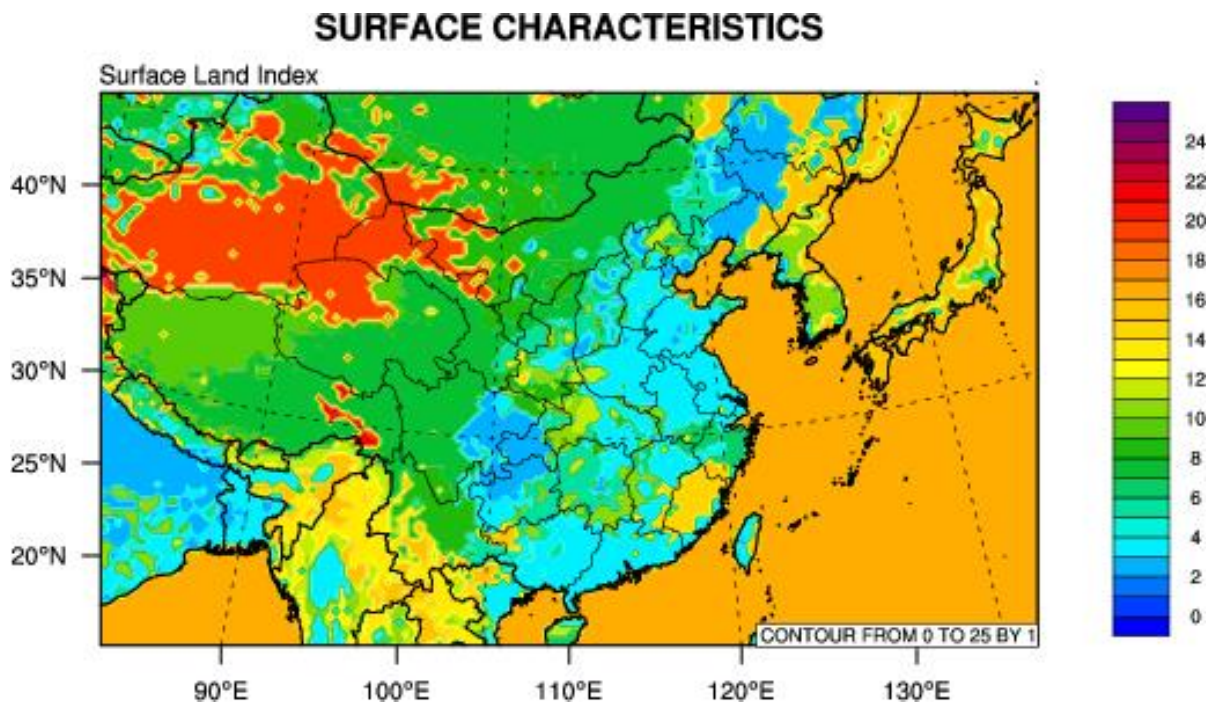

Figure 2.1 Characteristics of land covers used in the model from U. S. Geological Survey (USGS): 1 - Urban and Built-Up Land; 2 - Dryland Cropland and Pasture; 3 - Irrigated Cropland and Pasture; 4 – Mixed Dryland/Irrigated Cropland and Pasture; 5 - Cropland/Grassland Mosaic; 6 - Cropland/Woodland Mosaic; 7 - Grassland; 8 – Shrubland; 9 - Mixed Shrubland/Grassland; 10 – Savanna; 11 - Deciduous Broadleaf Forest; 12 - Deciduous Needleleaf Forest; 13 - Evergreen Broadleaf Forest; 14 - Evergreen Needleleaf Forest; 15 - Mixed Forest; 16 – Mixed Forest; 17 - Herbaceous Wetland; 18 - Wooded Wetland; 19 - Barren or Sparsely Vegetated; 20 - Herbaceous Tundra; 21- Wooded Tundra; 22 - Mixed Tundra; 23 - Bare Ground Tundra; 24 - Snow or Ice.

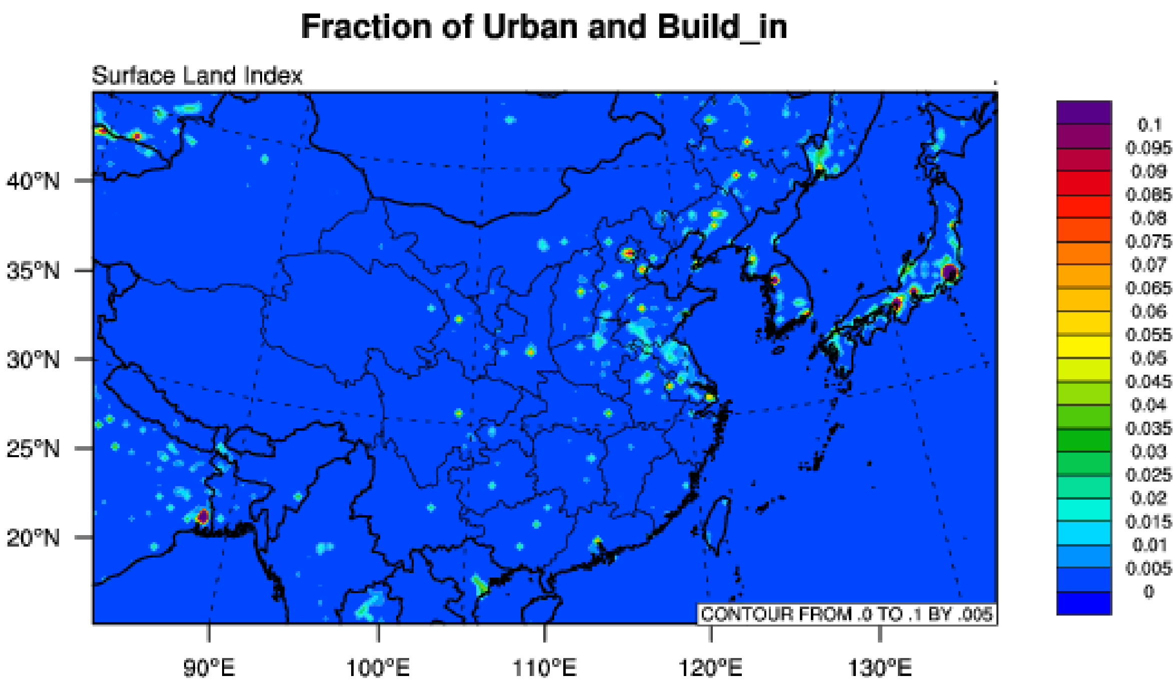

Figure 2.2 Fraction of land index 1 (urban and build_up areas).

2.1.3.2 Particle Size Distribution

The lowest size bin for the default 8-bin structure in MOSAIC has diameter ranges of 39-78 nm, which are much larger than the reported size (around 1-2 nm) of newly formed particles (Kulmala et al., 2004, 2013). This 8-bin structure used in MOSIAC is insufficient to the accurate representation of the nucleation mode (1-20 nm). In this study, the 8 size structure bin is thus first modified, then extended to 12 size structure bin with the first 4 bins for ultrafine particles with the diameters of 1-20 nm (see Table 2.4) to accurately simulate the formation and early growth of the ultrafine particles. In order to ensure consistent bin boundaries for overlapped bins between 8-bin and 12-bin structures (i.e., bins 1-8 in 8-bin structure and bins 5-12 in 12-bin structure), the default 8 bins are modified (referred to as modified 8-bin thereafter). Table 2.4 summarizes the size ranges of each bin in the 12-bin structure along with the original and updated 8-bin structures. WRF/Chem simulations with modified 8-bin and new 12-bin are referred to as WRF/Chem (8-bin) and WRF/Chme (12-bin), respectively, thereafter.

Table 2.4 The default 8-bin, modified 8-bin, and new 12-bin structure in WRF/Chem

Bin #	8-bin Default low[a]	high[b]	dcen[c]	8-bin Modified low	high	dcen	Bin #	12-bin New low	high	dcen
							01	1.0×10^{-3}	2.15×10^{-3}	1.47×10^{-3}
							02	2.15×10^{-3}	4.64×10^{-3}	3.16×10^{-3}
							03	4.64×10^{-3}	1.0×10^{-2}	6.81×10^{-3}
							04	1.0×10^{-2}	2.15×10^{-2}	1.47×10^{-2}
01	3.91×10^{-2}	7.81×10^{-2}	5.52×10^{-2}	2.15×10^{-2}	4.64×10^{-2}	3.16×10^{-2}	05	2.15×10^{-2}	4.64×10^{-2}	3.16×10^{-2}
02	7.81×10^{-2}	1.56×10^{-1}	1.10×10^{-1}	4.64×10^{-2}	1.0×10^{-1}	6.81×10^{-2}	06	4.64×10^{-2}	1.0×10^{-1}	6.81×10^{-2}
03	1.56×10^{-1}	3.13×10^{-1}	2.21×10^{-1}	1.0×10^{-1}	2.15×10^{-1}	1.47×10^{-1}	07	1.0×10^{-1}	2.15×10^{-1}	1.47×10^{-1}
04	3.13×10^{-1}	6.25×10^{-1}	4.42×10^{-1}	2.15×10^{-1}	4.64×10^{-1}	3.16×10^{-1}	08	2.15×10^{-1}	4.64×10^{-1}	3.16×10^{-1}
05	6.25×10^{-1}	1.25	8.84×10^{-1}	4.64×10^{-1}	1	6.81×10^{-1}	09	4.64×10^{-1}	1	6.81×10^{-1}
06	1.25	2.5	1.77	1	2.15	1.47	10	1	2.15	1.47
07	2.5	5	3.54	2.15	4.64	3.16	11	2.15	4.64	3.16
08	5	10	7.07	4.64	10	6.81	12	4.64	10	6.81

[a]low – Low bound diameter of the bin in μm
[b]high – High bound diameter of the bin in μm
[c]dcen – Geometric mean diameter of the bin in μm

In addition to the aforementioned new treatments, a new dust module named Dust Entrainment and Deposition (DEAD) (Zender et al., 2003) has been implemented by another group member into WRF/Chem and WRF-CAM5 following Wang et al. (2012). For this newly coupled module, the dust emissions are mainly calculated based on land erosion. The default dust scheme used in MOSAIC is based on the various land categories (Shaw et al., 2008).

2.2 Episode Selection

During the past three decades, East Asia has experienced continuous rapid economic and population growth, industrialization, and urbanization, which have caused significant degradation of air quality on regional and global scales (Jaffe et al., 1999; Akimoto, 2003; Weiss-Penzias et al., 2006). In addition, East Asia has special topography and geographical locations and distinct climatic conditions in terms of temperature, pressure, airflow, and rainfall (Saha, 2010). Thus, East Asia provides a supreme testbed for improving and testing the performance of WRF/Chem and WRF-CAM5. Two simulation periods have been selected with different purposes (1) July in 2008, and (2) four representative months in 2001 (January, April, July, and October, one for each season).

July 2008, one month before 2008 Olympics in Beijing China, is selected for nucleation scheme testing because of the availability of relevant observations for model validation during the Campaigns of Air Quality Research in Beijing and Surrounding Region 2008 (CAREBeijing2008) (Wang et al., 2011; Wang, 2012). The model predictions using WRF/Chem (8-bin) and WRF/Chem (12-bin) will be evaluated with available observations.

Based on the July 2008 evaluation results using various nucleation schemes, an optimal nucleation scheme or a combination of several schemes will be selected to represent nucleation and particle growth processes for multi-month simulations in 2001. WRF/Chem (12-bin) with the optimal new particle parameterization is then applied to the four representative months of 2001 to simulate anthropogenic aerosols and their interactions with meteorology. 2001 represents a heavy-pollution episode (K. Wang et al., 2009) during which the concentrations of aerosols are high, and the aerosol-meteorology interactions may be potentially significant. In addition, according to previous studies, several dust storms have been reported in 2001 (Zhang et al., 2003; Gong et al., 2003), and also NPF in anthropogenic plumes advecting from East Asia has been observed in 2001 during the National Atmospheric and Space Administration (NASA) Transport and Chemical Evolution over Pacific (TRACE-P) mission (Weber et al., 2003). In addition to the 2001 baseline simulations, sensitivity simulations without anthropogenic aerosols using WRF/Chem with default 12-bin are carried out to quantify the impacts of anthropogenic aerosols on simulated air quality and climate. In those sensitivity simulations, the emissions of primary aerosols and the formation pathways of secondary aerosols are turned off.

2.3 Database for Model Evaluation

One of the main objectives of this study is to evaluate the updated WRF/Chem and WRF-CAM5 model performances for simulating the ultrafine particles and also other meteorological and chemical variables. Therefore, numerous observational data are needed. The observational datasets include data from the National Oceanic and Atmospheric

Administration (NOAA) (http://www.ncdc.noaa.gov/oa/climate/climatedata.html), the Ministry of Environmental Protection of China (MEP) (http://datacenter.mep.gov.cn/), the Environmental Protection Department (EPD) of Hong Kong (http://epic.epd.gov.hk/), the Taiwan Air Quality Monitoring Network (AQMN) (http://taqm.epa.gov.tw/taqm/en/default.aspx), the National Institute of Environmental Studies in Japan (NIES) (http://www.nies.go.jp/igreen/index.html), the Tropospheric Emission Monitoring Internet Service (TEMI) (http://www.temis.nl/), and NASA (http://modis.gsfc.nasa.gov/). In addition, some nucleation and PM composition data are obtained from Wang (2012) and Tsinghua University, respectively.

2.3.1 Meteorological Data

The meteorological variables include temperature at 2 meters (T2), water vapor mixing ratios at 2 meters (Q2), atmospheric pressure (P), wind speeds and directions at 10 meters (WS10 and WD10, respectively), and precipitation. These variables are evaluated using hourly global surface observational data from the National Climatic Data Center (NCDC).

2.3.2 Chemical Data from Surface Networks

The chemical species evaluated include the surface concentrations of PM_{10}, $PM_{2.5}$, carbon monoxide (CO), nitrogen monoxide (NO), nitrogen dioxide (NO_2), ozone (O_3), volatile organic compounds (VOCs), sulfur dioxide (SO_2), sulfuric acid (H_2SO_4), PM number and particle size distribution (PSD), and the column mass concentrations of CO, NO_2, SO_2 and O_3. The chemical surface concentrations are evaluated using surface measurements over mainland China (derived from the Air Pollution Index (API) in 42 major cities), Hong Kong (about 9 sampling sites), Taiwan (about 65 sampling sites), Japan (over 2000 sampling sites), and Tsinghua University (two sites in Beijing). In addition, important parameters are analyzed to study the NPF events and particle early growth processes. These include the formation rate (*J*), the condensation sink (*CS*), the particle growth rate (*GR*), H_2SO_4 concentration, PM number concentration, and PSD (Wang, 2012).

2.3.3 Satellite Data

The column abundances of chemical species are evaluated using various satellite data. These include the Measurements of Pollution in the Troposphere (MOPITT) for CO column mass, the Global Ozone Monitoring (GOME) and Scanning Imaging Absorption spectrometer (SCIAMACHY) for NO_2 column mass, and the Total Ozone Mapping Spectrometer (TOMS) and Ozone Monitoring Instrument (OMI) for tropospheric ozone residual (TOR), and SCIAMACHY for SO_2 column mass. Additional aerosol and cloud properties are also evaluated. These include aerosol optical depth (AOD), CCN, cloud fraction (CF), cloud optical thickness (COT), cloud water path (CWP), and precipitable water vapor (PWV) from Terra Moderate-resolution Imaging Spectroradiometer (MODIS). Table 2.5 summarize all observational data mentioned above.

Table 2.5 Summary of observational databases used in model evaluation

Database	Variables/Species	Data Frequency
For meteorology		
NCDC	Precip (mm day^{-1})	Hourly
NCDC	T2 (^{o}C)	Hourly
NCDC	RH2 (%)	Hourly
NCDC	Q2 (kg kg^{-1})	Hourly
NCDC	WS10 (m s^{-1})	Hourly
NCDC	WD10 (^{o})	Hourly
For gaseous species		
Wang (2012) (for Beijing)	H_2SO_4	
SCIAMACHY (column mass for the whole domain)	SO_2	Monthly
API (for Beijing)		Daily
NIES (for Japan)		Monthly
AQMN (for Taiwan)		Daily
EPD (for Hong Kong)		Daily
TOMS and OMI (column mass for the whole domain)	O_3	Monthly
TOMS (column mass for the whole domain)		Monthly
API (for Beijing)		Daily
NIES (for Japan)		Monthly
AQMN (for Taiwan)		Daily
EPD (for Hong Kong)		Daily
MOPITT (column mass for the whole domain)	NO_2	Monthly
API (for Beijing)		Daily
NIES (for Japan)		Monthly
AQMN (for Taiwan)		Daily
EPD (for Hong Kong)		Daily
NIES (for Japan)	NO	Monthly
AQMN (for Taiwan)		Daily
EPD (for Hong Kong)		Daily
MOPITT (column mass for the whole domain)	CO	Monthly
API (for Beijing)		Daily
NIES (for Japan)		Monthly
AQMN (for Taiwan)		Daily
EPD (for Hong Kong)		Daily

Table 2.5 Continued

	VOCs	
Wang et al. (2010a) (For Beijing)		Monthly
Cai et al. (2010) (For Shanghai)		Monthly
For PM		
API (for China mainland)	PM_{10}	Daily
NIES (for Japan)		Monthly
AQMN (for Taiwan)		Daily
EPD (for Hong Kong)		Daily
For Miyun and Tsinghua	$PM_{2.5}$	Daily
AQMN (for Taiwan)		Daily
EPD (for Hong Kong)		Daily
For PM composition		
For Miyun and Tsinghua	Na^+	Daily
For Miyun and Tsinghua	NH_4^+	Daily
For Miyun and Tsinghua	Cl^-	Daily
For Miyun and Tsinghua	NO_3^-	Daily
For Miyun and Tsinghua	SO_4^{2-}	Daily
For Nucleation		
Wang (2012) (for Beijing)	Formation rate	Daily
Yue et al. (2010) (for Beijing)	Particle size distribution	Monthly
Wang (2012) (for Beijing)	Condensation sink	Daily
For satellite		
MODIS	COT	Monthly
MODIS	CWP (g m^{-2})	Monthly
MODIS	PWV (cm)	Monthly
MODIS	AOD	Monthly

2.4 Evaluation Methodology

The performance evaluation of WRF/Chem and WRF-CAM5 predictions are conducted in terms of statistical, spatial, and temporal comparisons. Observed and simulated values of nearly all meteorological and chemical variables are compared through the calculation of statistical measures including the normalized mean bias (NMB), the normalized mean error (NME), the mean bias (MB), and the root mean square error (RMSE). The formulas are as follows (Yu et al., 2006):

$$NMB = \frac{\sum_{i=1}^{N}(S_i - O_i)}{\sum_{i=1}^{N} O_i} \times 100\% \quad (1)$$

$$NMB = \frac{\sum_{i=1}^{N}| S_i - O_i |}{\sum_{i=1}^{N} O_i} \times 100\% \quad (2)$$

$$MB = \frac{1}{N}\sum_{i=1}^{N}(S_i - O_i) = \bar{S} - \bar{O} \quad (3)$$

$$RMSE = [\frac{1}{N}\sum_{i=1}^{N}(S_i - O_i)^2]^{\frac{1}{2}} \quad (4)$$

Where O_i and S_i are the observed and simulated values at a specific time or location *i* (up to *N* time periods or locations) in a given time period or location. NMB is about the tendency of the model to overpredict or underpredict variables. Nevertheless, it is worth to note that the summation of positive and negative biases can lead to cancellation of the absolute magnitude of discrepancies. Therefore, NME has also been calculated, which is based on the summation of the absolute values of NMB at each *i*. In addition, spatial trends over the whole domain are preferred. Monthly-averaged predictions overlaid with observed values are plotted by applying the National Center for Atmospheric Research (NCAR) Command Language (NCL). A comparison of the color shading at each point allows for estimating the capability of model to reproduce observed variables. The temporal evaluation is completed for the July 2008 case study in Beijing.

3. APPLICATION AND EVALUATION OF WRF/Chem

3.1 Model Setup and Input

The default and improved WRF/Chem are applied to East Asia at a horizontal resolution of 36-km. The vertical resolution is 23 layers from the surface to ~50 mbar. For July 2008, WRF/Chem simulations with the BO08, WA11, YU10, and a combination of them are performed. A simulation without nucleation is also performed. The simulation results is evaluated using observations in July 2008. Based on the July 2008 evaluation results, an optimal nucleation scheme or a combination of several schemes is selected to represent nucleation and particle growth processes for multi-month simulations in 2001. WRF/Chem with the optimal new particle parameterization is then applied to the four representative months of 2001. In addition to the 2001 baseline simulations, sensitivity simulations without anthropogenic aerosols are carried out to quantify the impacts of anthropogenic aerosols on simulated air quality and climate. In those sensitivity simulations, the emissions of primary aerosols and the formation pathways of secondary aerosols are turned off.

The meteorological initial and boundary conditions are based on the National Centers for Environmental Prediction (NCEP) Final (FNL) Operational Global Analysis data. The chemical initial and boundary conditions are based on Liu et al. (2010) over East Asia. The anthropogenic emissions are based on an updated version of the Transport and Chemical Evolution over the Pacific (TRACE-P) over China for 2001 simulations (Jacob et al., 2003; Carmichael et al., 2003), and the Intercontinental Chemical Transport Experiment-Phase B

(INTEX-B) emission for 2008 simulations (Zhang et al., 2009). The natural emissions of biogenic VOCs are simulated online based on the Model of Emissions of Gases and Aerosols from Nature (MEGAN) version 2 (Guenther et al., 2006). The dust emissions are simulated online based on the DEAD scheme using the erosion data (Zender et al., 2003). The sea-salt emissions are simulated as a function of surface wind speed based on Gong (2003) (assuming that sea salt is pure NaCl).

3.2 Testing of Nucleation and Early Growth Parameterizations for July 2008

Table 3.1 summarizes all testing runs in July 2008. Figure 3.1 shows the zonal mean values of calculated nucleation rates using WRF/Chem with modified 8-bin and different nucleation schemes. BO08_ACTI and BO08_KINE give similar results due to much lower prefactor compared with WA11_ACTI and WA11_KINE. The nucleation rates predicted by WA11_ACTI for the zonal mean values range from 0.04 to 11.7 cm^{-3} s^{-1}. However, the nucleation rates predicted by WA11_KINE (range from 0 to 169.2 cm^{-3} s^{-1}) and WA11_THER (range from 0 to 4726 cm^{-3} s^{-1}) for the zonal mean values are far beyond the observational J values in polluted urban areas (i.e., 3.3 to 81.4 cm^{-3} s^{-1} reported by Wu et al. (2007) from March 2004 to February 2005). ME09 gives much higher J values in the top of the modeling domain between 300-100 mb, but negligible J values below. This indicates that no significant nucleation occurs when temperatures are above 295K, consistent with the finding of Merikanto et al. (2009). ME09 may not be appropriate for simulating J values in PBL during summer due to high temperatures.

Table 3.1 Summary of testing simulations in July 2008

Nucleation schemes	Modified 8-bin (without LE07)	12-bin (with LE07)
BO08_ACTI	YES	YES
BO08_KINE	YES	NO
WA11_ACTI	YES	YES
WA11_KINE	YES	NO
WA11_THER	YES	NO
ME09	YES	NO
YU10	NO	YES
COMB	NO	YES
NO_NUCLEATION	YES	YES

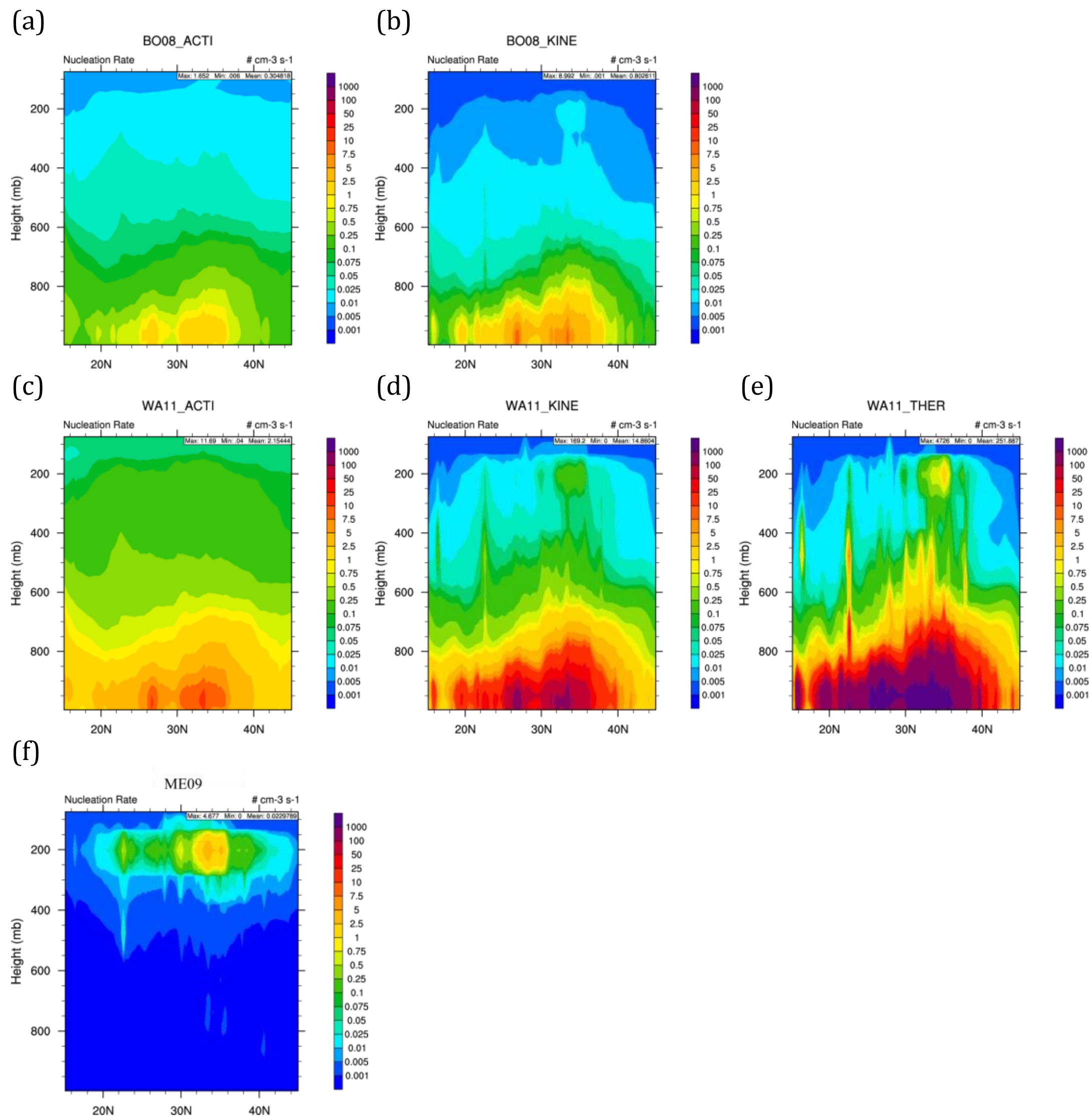

Figure 3.1 Zonal mean values of nucleation rate (J) predicted with WRF/Chem with updated 8-bin and various nucleation parameterizations: (a) BO08_ACTI, (b) BO08_KINE, (c) WA11_ACTI, (d) WA11_KINE, (e) WA11_THER, and (f) ME09.

According to the work of Yue et al. (2009) in Beijing, the observed particle number size distributions (N-PSD) are quite different during polluted (PM_{10} > 150 μg m^{-3}) and nonpolluted days (PM_{10} ≤ 150 μg m^{-3}) at the Beijing urban site, e.g., the average N-PSD showed significant shifts to larger sizes on polluted days than nonpolluted days (see Figure 3.2 a). Figures 3.2 b and 3.2 c compare predicted monthly-averaged N-PSD using WRF/Chem (8-bin) without nucleation, and WRF/Chem (12-bin) simulations with and without nucleation parameterizations. For WRF/Chem (12-bin), the simulations are performed with YU10 and a combination of WA11_ACTI (for urban areas in PBL), BO08_ACTI (for non-urban areas in PBL), and YU10 (above PBL) (referred to as COMB). As shown in Figure 3.2 b, WRF/Chem (8-bin) can only simulates the accumulation mode of the N-PSD due to the higher low bound (~22 nm) of the first bin compared with WRF/Chem (12-bin) (~1 nm), which is insufficient to study the NPF events. As shown in Figure 3.2 c, comparing to the N-PSD predicted by WRF/Chem without simulating nucleation, WRF/Chem (12-bin) with various nucleation schemes can explicitly track the new particle formation and early growth. According to previous studies (Wu et al., 2007; Yu et al., 2010), at a lower background PM level (non-polluted) in Beijing, NPF events can occur more easily, which would lead to higher number concentrations of ultrafine particles (< 0.1 μm) compared with polluted days. The simulation results show higher PM number concentration in the nucleation mode on polluted days than those on non-polluted days, consistent with observations.

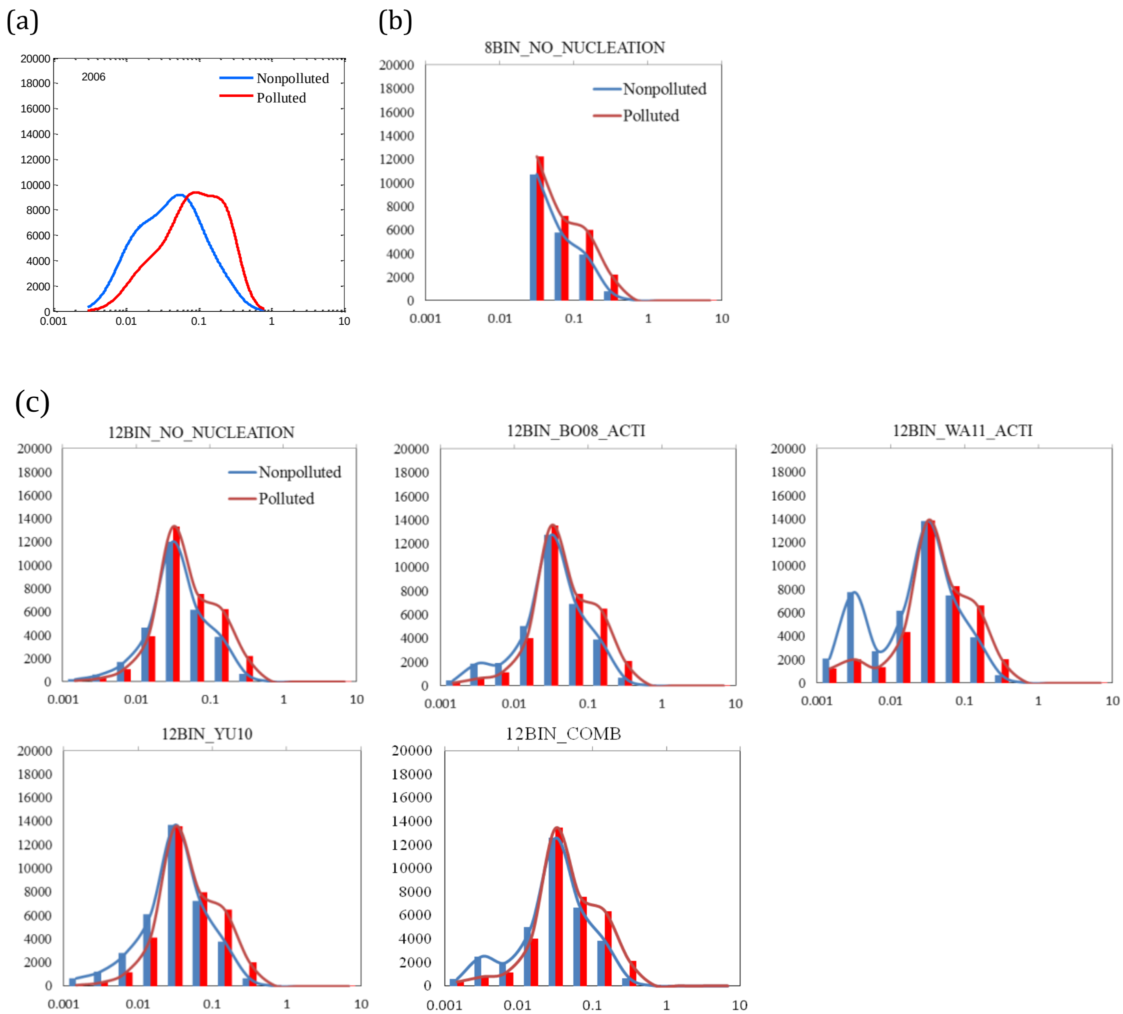

Figure 3.2 Monthly-averaged particle number size distributions on non-polluted and polluted days at Beijing urban site in Beijing in the summer of 2006, (a) measurement data, (b) predictions with WRF/Chem with the modified 8-bin, (c) predictions with WRF/Chem with 12-bin (Note: Polluted is related to PM_{10} > 150 μg m^{-3}; nonpolluted is related to $PM_{10} \leq$ 150 μg m^{-3}).

The criterion for discerning NPF events is the burst of the nucleation mode particles with usually maximum number concentrations > 10^4 cm^{-3} for 3 nm – 10 nm particles (Birmili and Wiedensohler, 2000; Wu et al., 2007). Figure 3.3 shows the comparison of the time series of N-PSD between observational data (Wang, 2012) measured during the CAREBeijing2008 campaign and the modeling results with and without various nucleation schemes (NO_NUCL, BO08_ACTI, WA11_ACTI, YU10, and COMB coupled with the LE07 particle early growth parameterization. Comparing to the N-PSD without accounting for nucleation, the N-PSDs predicted with various nucleation parameterizations show great improvement for nucleation and Aitken modes. WRF/Chem (12-bin) with these nucleation parameterizations capture the three reported NPF events in July 2008 (i.e., July 12, 17, and 30, corresponding to Junior days 194, 199, and 212, respectively) (Wang, 2012). However, there remain some uncertainties, which will be discussed later.

Gaseous sulfuric acid, H_2SO_4, is a key component for nucleation (Seinfeld and Pandis, 2006; Yue et al., 2010; Wang et al., 2011), and it is predominantly produced through the oxidation of SO_2 by hydroxyl radical (OH) in the presence of oxygen (O_2) and water (H_2O) as follows (Seinfeld and Pandis, 2006):

$$O_3 + hv \rightarrow O(^1D) + O_2 \quad \text{(R1)}$$

$$O(^1D) + H_2O \rightarrow 2OH \quad \text{(R2)}$$

$$SO_2 + OH + M \rightarrow HSO_3 + M \quad \text{(R3)}$$

$$HSO_3 + O_2 \rightarrow SO_3 + HO_2 \quad \text{(R4)}$$

$$SO_3 + H_2O \rightarrow H_2SO_4 \quad \text{(R5)}$$

The reaction between SO_2 and OH represents the primary pathway to form H_2SO_4 ((R3)-(R5)). (R1)-(R2) represent the major known initiation reactions, which produce OH radical through the photolysis. Since (R2) is the major source of OH in the atmosphere, ozone (O_3), solar radiation, and water vapor are three key factors that dominate the production of OH radicals. Other important parameters describing NPF including the formation rate (FR) and growth rate (GR) of new particles, as well as the condensation sink (CS) should also be analyzed. In addition, the background PM concentration is another key parameter for the occurrences of NPF events. The WRF/Chem simulation with COMB shows the occurrence of the NPF event on July 3 (Julian day 185), 7 (189), 13 (195), 16 (198), 19 (201), 20 (202), 21 (203), and 22 (204), which are inconsistent with the observational data (see Figure 3.3). The detailed reasons are discussed next.

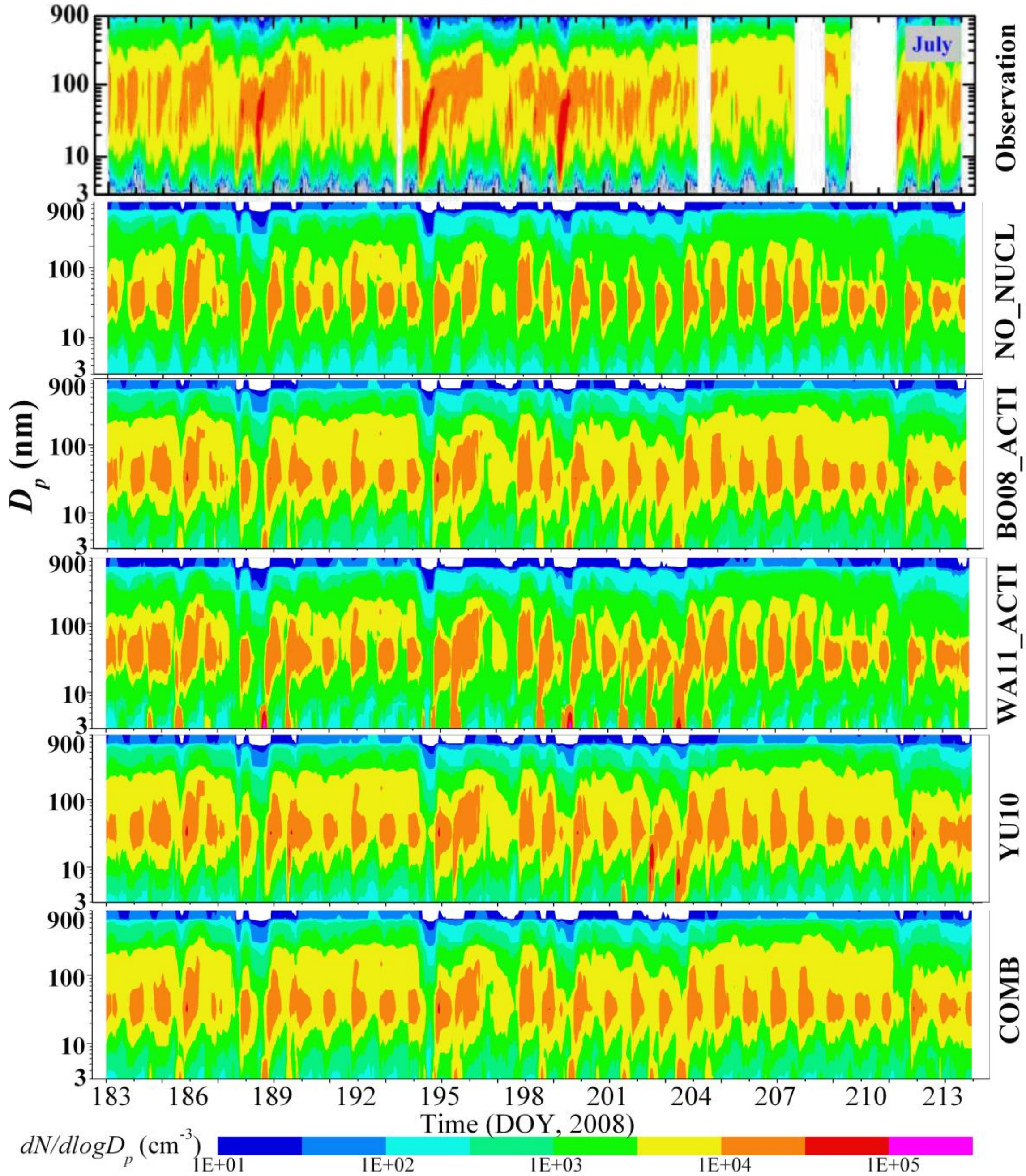

Figure 3.3 Comparison of the time series of particle number size distributions (3-900 nm) between observational data (Wang, 2010) and modeling results using 12-bin WRF/Chem with and without various nucleation schemes (NO_NUCL, BO08_ACTI, WA11_ACTI, YU10, and COMB) at an urban site in Beijing in July 2008. The color bar represents $dN/dlogD_p$ (cm^{-3}).

Two methods have been used to calculate the growth rates: (1) the maximum concentration method (MCM) (Lehtinen et al., 2003; Hirsikko et al., 2005), and (2) the mode fitting method (MFM) (Dal Maso et al., 2005):

$$GR = \frac{\Delta D_m}{\Delta t} \tag{3}$$

where, t is the change of time; for method 1 (MCM), D_m is calculated based on the maximum number concentration of each mode or section; and for method 2 (MFM), D_m is the geometric mean diameter of each mode or section. Figure 3.4 shows that the MFM (black dots and line) does not clearly show the particle growth under 5-nm because of the calculated large geometric mean diameter, which would lead to zero GR in the small size range. By contrast, MCM overcomes this problem by selecting the size bin, which has the maximum concentration for the specific time step. However, the shortcoming of MCM is that the GR results are greatly influenced by primary emissions, especially in polluted areas. As shown in Figure 3.4, the GR results calculated with the two methods are quite different, with higher GR values by MCM than by MFM. Our modeling results show the same trend (GR_{MCM} > GR_{MFM}) of the two methods with the observational results (Wang, 2012), suggesting that, for the calculation of GR for newly-formed particles with diameter within several nms, MCM might be a better choice for the calculation of GR in this study.

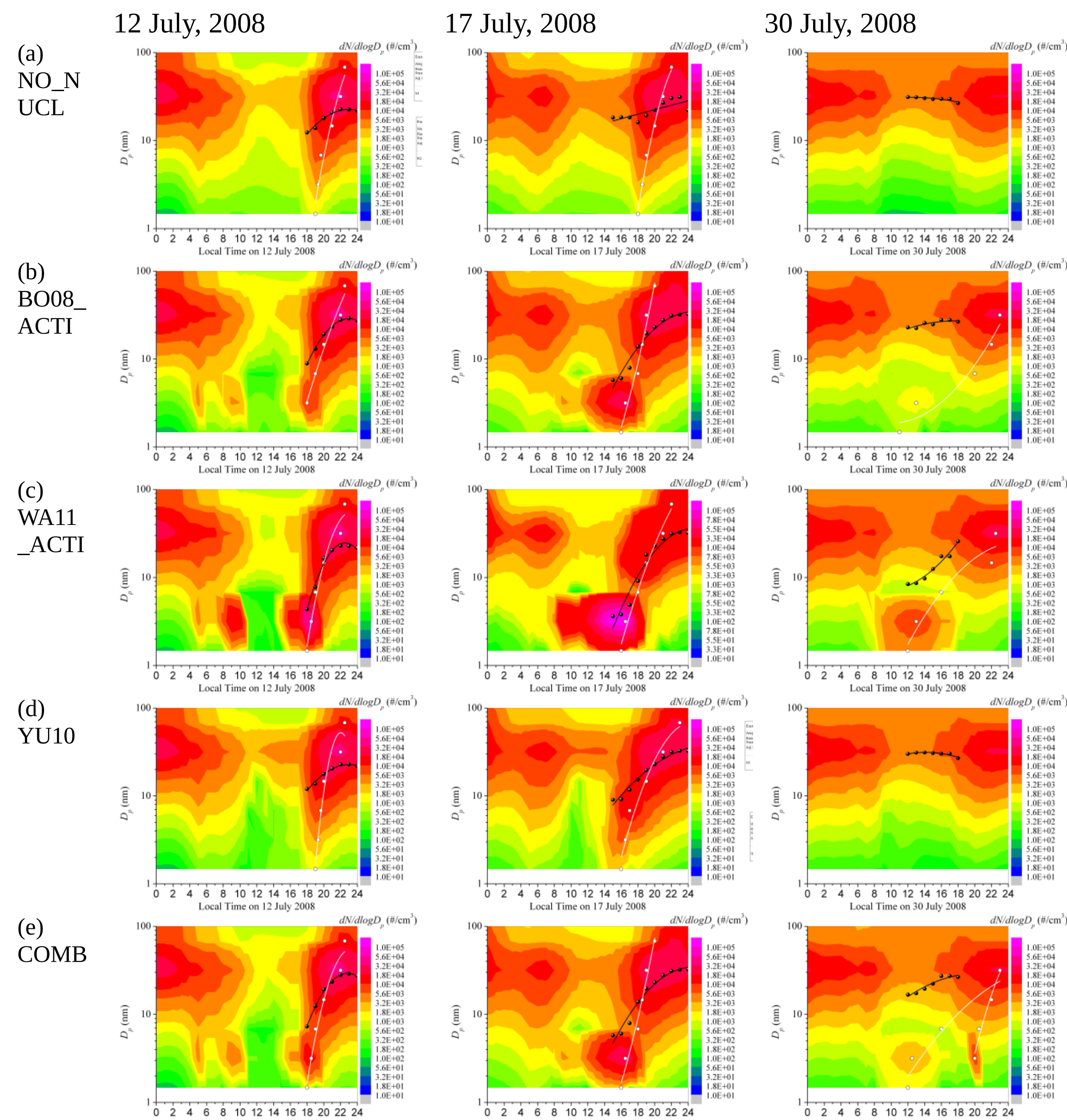

Figure 3.4 Predicted particle number size distribution on three new particle formation days (i.e., 12, 17, 30) in July 2008 at an urban site in Beijing by WRF/Chem (12-bin) simulations with (a) NO_NUCL, (b) BO08_ACTI, (c) WA11_ACTI, (d) YU10, and (e) COMB (black dots and line represent the MCM method, and white dots and line represent MFM method).

Figure 3.5 shows the time series for H_2SO_4, CS, FR, PM_{10}, SO_2, O_3, and NO_2, and Tables 3.2 and 3.3 summarize the correpsonding performance statistics. As shown in Figure 3.5, the PM_{10} concentrations are underpredicted on July 3 (185), 13 (195), 19 (201), 20 (202), 21 (203), and 22 (204), which may lead to the underpredictions of the coagulation scavenging rates due to fewer particles in the atmosphere. Since the newly-formed nuclei undergo two competitive processes: coagulation scavenging and condensational growth (Kerminen et al., 2001), the prediction of atmospheric PM concentrations may be a source of uncertainties in predicting NPF events. In order to better analyze the model performance, the statistics for meteorological predictions and some chemical species (PM_{10}, SO_2, O_3 and NO_2) using WRF/Chem (12-bin) are summarized in Table 3.1 (since the results for all tested nucleation schemes (WA11_ACTI, BO08_ACTI, YU10_ACTI and COMB) are similar, only results from WRF/Chem with COMB are shown here). As mentioned before, atmospheric PM concentrations might be important for predicting NPF events, however, the PM_{10} concentrations are well predicted on July 7 (189) and 16 (198). The NPF events are still overpredicted during the two days, which might be due to other factors such as precipitation. Wang (2012) reported precipitation during the two days, which is not captured by the simulation. Precipitation could lead to a strong wet deposition, removing newly-formed particles before they can grow into larger particles. While these newly-formed particles contribute to PM number concentrations, their contributions to PM_{10} mass concentrations are negligible. Precipitation in Beijing is mainly concentrated in summer months, accounting for 75% of the total annual precipitation (Yue et al., 2009). As shown in Table 3.1, 24-hour precipitation is poorly estimated (with values of R of 0.01 – 0.02). Therefore, poor model performance in predicting observed daily precipitation may be another source of uncertainties in accurately predicting NPF events**.**

As shown in Figure 3.5, the mixing ratios of key precursor SO_2 are underpredicted, and the number concentrations of H_2SO_4 are overpredicted, which may be due to several reasons. First, the overprediction of O_3 may have produced too much OH radicals, which may lead to overpredictions of H_2SO_4. The atmospheric oxidation capability in the ambient environbment in Beijing during July 2008 may not be as strong as what WRF/Chem predicts. According to previous studies (Wang et al., 2006; Duan et al., 2008; Ran et al., 2009; Cai et al., 2010a), the mixing ratios of both VOCs and NO_x are significant in controlling O_3 formation in megacities (such as Beijing and Shanghai) in China. Table 3.2 compares observed and simulated mixing ratios of VOCs. Those results indicate that, in both Beijing and Shanghai, the mixing ratios of anthropogenic VOCs (e.g., TOL and XYL) are significantly underpredicted by -80.9 to -54.2% and -70.0% to -48.9%, respectively, but those of the typical biogenic VOCs (e.g., isoprene) are overpredicted by MEGAN2, possible reasons for the underprediction are the mixing ratios of anthropogenic VOCs include the use of the coarse resolution or the underestimations of emissions. The mixing ratios of NO_2 are generally underpredicted with an NMB of ~ -36%. Thus, the overpredictions of O_3 in both cities may be due to insufficient titration as a result of the underprediction of NO mixing ratios. Large uncertainties exist in emissions of NO, which may help explain in part the underpredictions of NO. Second, the underpredition of CS (see Figure 3.5) might be another reason for the overprediction of H_2SO_4. The overall GR is largely underpredicted for the three NPF events occurred during July (see Table 3.3) in Beijing. The FR values predicted by BO08_ACTI and COMB show a closer agreement with observations than other two nucleation schemes, with NMBs of -12.4% and 56.5%.

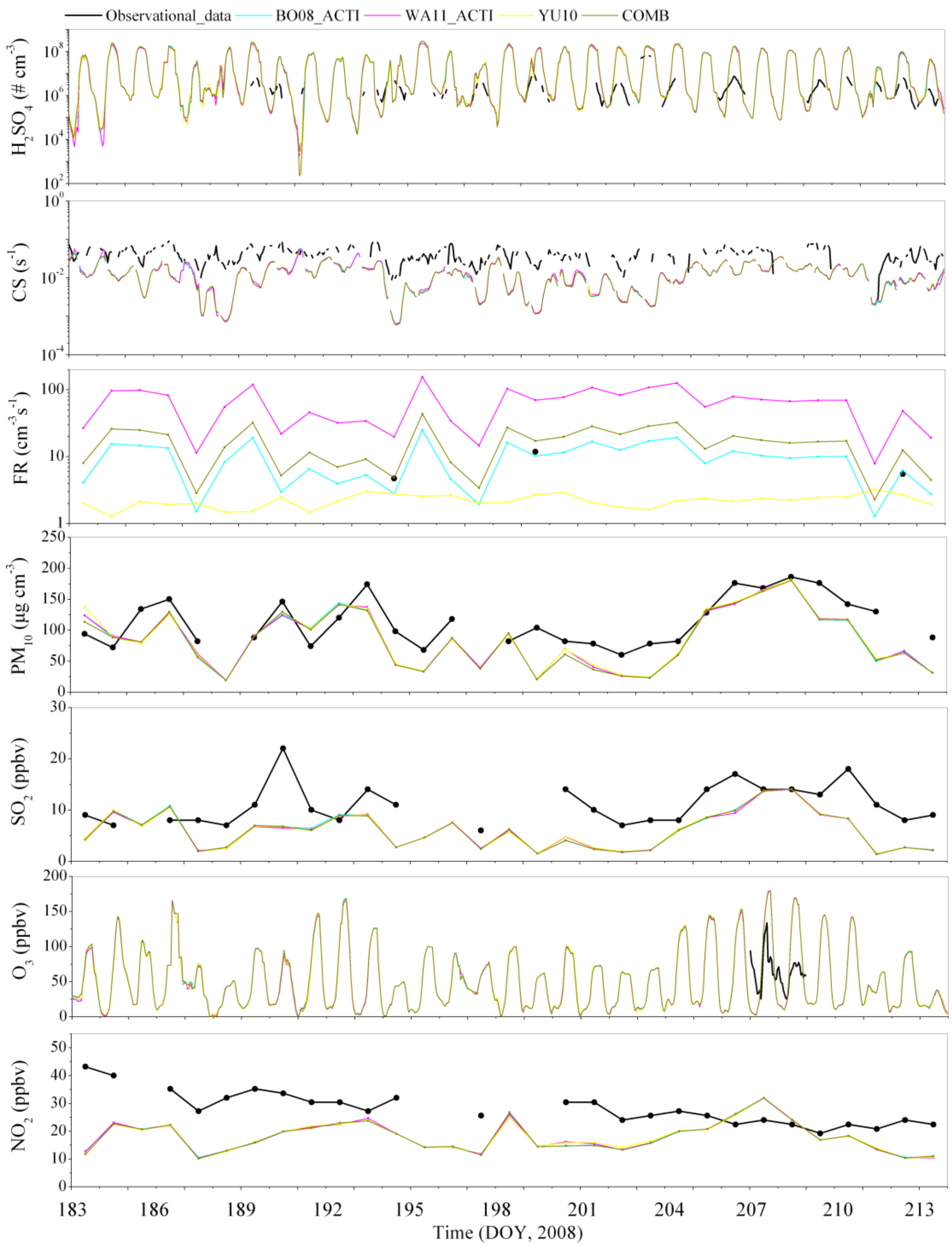

Figure 3.5 Comparison of the time series for H_2SO_4, CS, FR, PM_{10}, SO_2, O_3 and NO_2 from WRF/Chem (12-bin).

Table 3.2 Performance statistics for meteorological and chemical predictions using updated 12-bin WRF/Chem model with COMB[a] for July 2008.

Variable	Dataset	July 2008							
		Mean Obs	Mean Mod	Data #	MB	RMSE	NMB, %	NME, %	R
T2[b], °C	NCDC[g]	24.9	23.7	317429	-1.2	25.6	-4.8	15.506	0.56
P[c], mb	NCDC	956.6	942.5	188681	-14.1	1331.8	-1.5	2.3	0.94
Q2[d], g kg^{-1}	NCDC	14.5	15.2	188542	0.7	5.6	4.6	12.8	0.87
WS10[e], m s^{-1}	NCDC	2.5	3.7	316728	1.2	8.2	49.1	88.9	0.26
WD10[f], degree	NCDC	183.2	179.1	283878	-4.1	13389.1	-2.2	48.2	0.16
24-h rain, mm	NCDC	4.9	3.8	22321	-1.0	350.8	-21.3	1.5	0.01
PM_{10}, µg cm^{-3}	API[h]	113.5	88.7	28	-24.8	38.5	-21.9	28.4	0.76
SO_2, ppbv	API	11.0	6.1	26	-4.9	6.3	-44.7	49.1	0.45
TOL[i], ppbv (Beijing)	Wang et al., 2010a	3.67	0.70		-2.97		-80.9		
TOL, ppbv (Shanghai)	Cai et al., 2010b	7.74	2.32		-5.42		-70.0		
XYL[j], ppbv (Beijing)	Wang et al., 2010a	1.20	0.55		-0.65		-54.2		
XYL, ppbv (Shanghai)	Cai et al., 2010	2.23	1.14		-1.09		-48.9		
Isoprene, ppbv (Beijing)	Wang et al., 2010a	0.68	0.83		0.15		22.1		
Isoprene, ppbv (Shanghai)	Cai et al., 2010	0.13	0.28		0.15		115.4		
O_3, ppbv	He et al., 2010	63.8	75.6	48	11.9	53.7	18.6	70.5	0.62
NO_2, ppbv	API	28.2	17.9	26	-10.3	13.1	-36.4	40.0	-0.02

Table 3.2 Continued.

[a]COMB – Combination of BO08_ACTI, WA11_ACTI and YU10
[b]T2 – Temperature at 2 meters
[c]P – Atmospheric pressure
[d]Q2 – Water vapor mixing ratios at 2 meters
[e]WS10 – Wind speeds at 10 meters
[f]WD10 – Wind directions at 10 meters
[g]NCDC – National Climatic Data Center
[h]API – Air Pollution Index
[i]TOL – Benzene, Toluene, Ethylbenzene, i-Propylbenzene, n-Propylbenzene
[j]XYL – m,p,o-Xylene, Styrene, 1,3,5-Trimethylbenzene, 1,2,4-Trimethylbenzene, 1,2,3-Trimethylbenzene, p-Ethyltoluene

Table 3.3 Evaluation of nucleation related variables (predicted with WRF/Chem 12-bin) with various nucleation schemes.

Variable	Scheme	July 2008							
		Mean Obs	Mean Mod	Data #	MB	RMSE	NMB, %	NME, %	R
H_2SO_4, cm^{-3}	BO08_ACTI[a]	4.3×10^6	3.9×10^7	228	3.5×10^7	6.7×10^7	808.2	858.7	0.25
	WA11_ACTI[b]	4.3×10^6	3.6×10^7	228	3.2×10^7	5.9×10^7	739.3	789.9	0.25
	YU10[c]	4.3×10^6	3.8×10^7	228	3.4×10^7	6.5×10^7	787.6	839.4	0.25
	COMB[d]	4.3×10^6	3.9×10^7	228	3.5×10^7	6.7×10^7	816.0	866.3	0.25
CS[e], s^{-1}	BO08_ACTI	4.1×10^{-2}	1.2×10^{-2}	420	-2.9×10^{-2}	3.2×10^{-2}	-69.9	70.8	0.51
	WA11_ACTI	4.1×10^{-2}	1.3×10^{-2}	420	-2.8×10^{-2}	3.2×10^{-2}	-69.1	70.4	0.49
	YU10	4.1×10^{-2}	1.2×10^{-2}	420	-2.9×10^{-2}	3.2×10^{-2}	-70.4	71.2	0.52
	COMB	4.1×10^{-2}	1.2×10^{-2}	420	-2.9×10^{-2}	3.2×10^{-2}	-71.1	71.7	0.55
GR[f], nm h^{-1} (3-7nm)	BO08_ACTI	12.5	2.9		-9.6		-77.1		-
	WA11_ACTI	12.5	3.4		-9.1		-73.1		-
	YU10	12.5	4.1		-8.4		-66.8		-
	COMB	12.5	4.9		-7.6		-60.6		-
FR[g], cm^{-3} s^{-1} (three cases)	BO08_ACTI	7.3	6.4		-0.9		-12.4		-
	WA11_ACTI	7.3	45.9		38.6		526.4		-
	YU10	7.3	2.7		-4.6		-63.0		-
	COMB	7.3	11.5		4.2		56.5		-

[a]BO08_ACTI – Activation theory of Boy et al. 2008
[b]WA11_ACTI – Activation theory of Wang et al. 2011
[c]YU10 – Ion-mediated nucleation of Yu, 2010
[d]COMB – Combination of BO08_ACTI, WA11_ACTI, and YU10
[e]CS – Condensation sink
[f]GR – Growth rate
[g]FR – Formation rate

According to the studies of Wu et al. (2007), the formation rate of 3-nm particles in Beijing ranges from 3.3 to 81.4 cm^{-3} s^{-1} from March 2004 to February 2005. Figure 3.6 shows the spatial distributions of the formation rate of bin-1 from WRF/Chem (12-bin) simulations using various nucleation schemes. The maximum formation rate predicted by YU10 near the surface over the whole domain is ~8.2 cm^{-3} s^{-1}, which may underestimate FR values. On the other hand, WA11_ACTI gives the maximum value of around 251.6 cm^{-3} s^{-1}, which may overpredict FR values. BO08_ACTI (range from 0 - 42.7 cm^{-3} s^{-1}) and COMB (range from 0 - 42.9 cm^{-3} s^{-1}) give similar formation rates on the surface. Although BO08_ACTI gives the smallest NMB at Beijing (see Table 3.3), the BO08_ACTI gives much lower FR in upper layers than YU20. Based on the above analyses, both of BO08_ACTI and COMB may generate reasonable FR values near surface. The spatial distribution pattern of formation rate is similar with that of H_2SO_4 (see Figure 3.7).

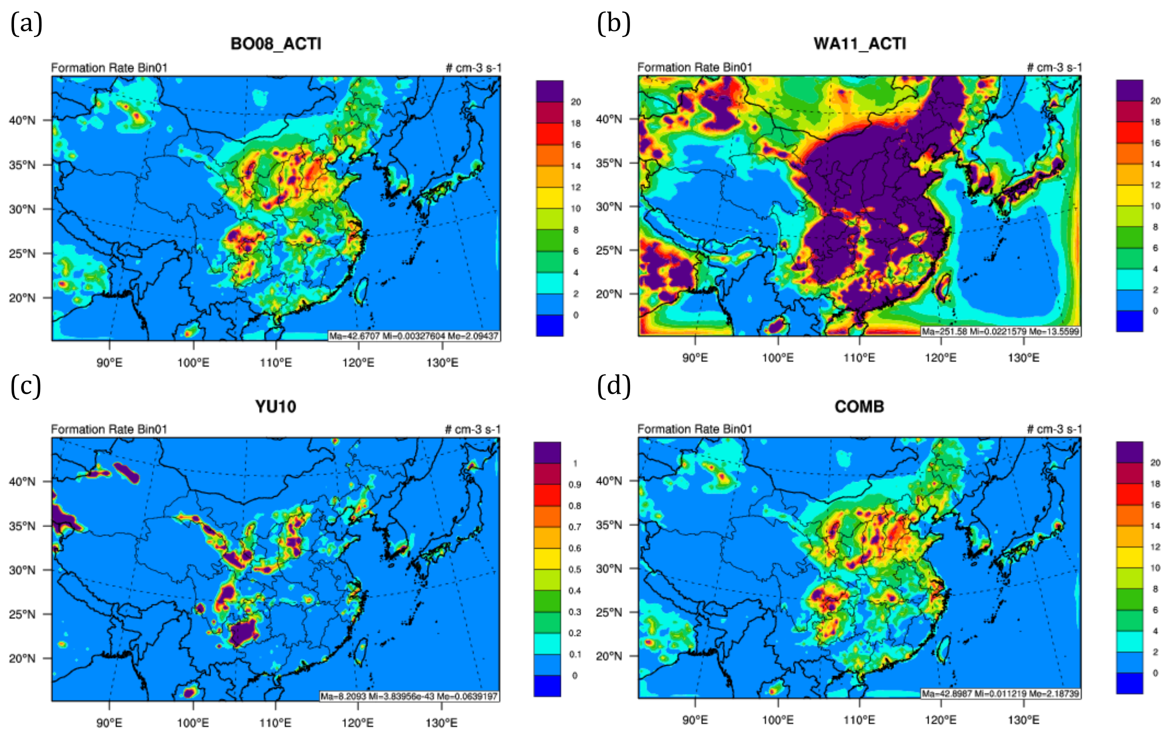

Figure 3.6 Spatial distributions of the formation rate of bin-1 from WRF/Chem with 12-bin using various nucleation schemes, (a) BO08_ACTI, (b) WA11_ACTI, (c) YU10, and (d) COMB.

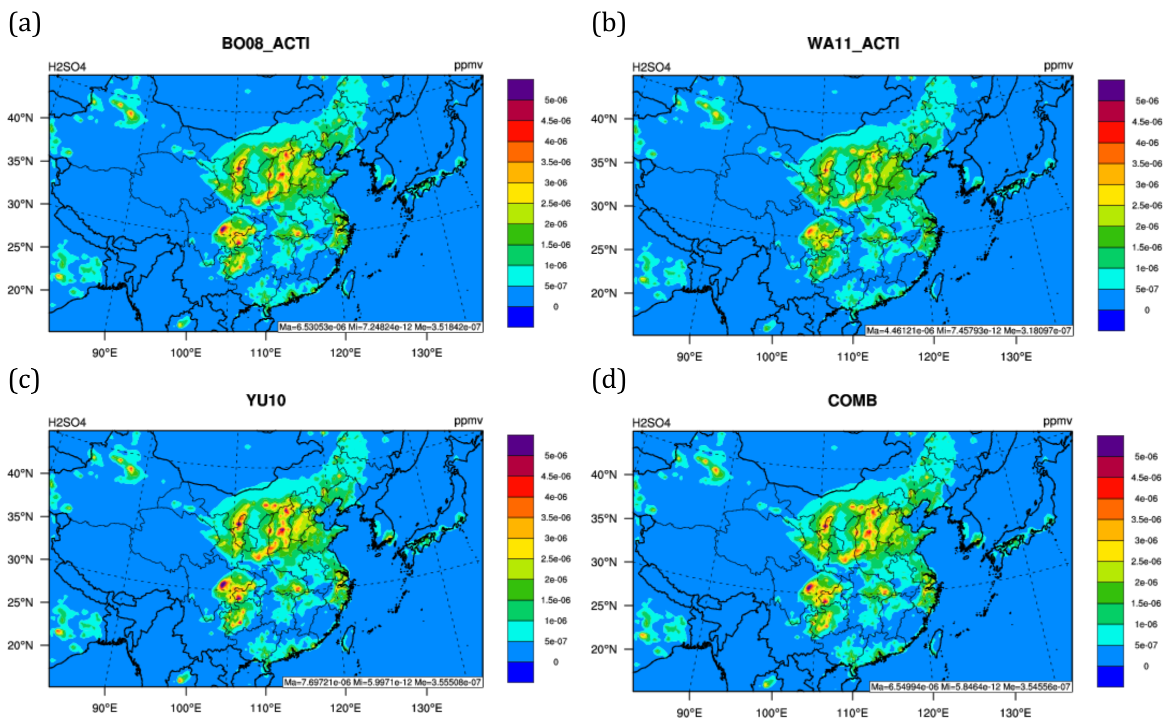

Figure 3.7 Spatial distributions of the H_2SO_4 from WRF/Chem with 12-bin using various nucleation schemes, (a) BO08_ACTI, (b) WA11_ACTI, (c) YU10, and (d) COMB.

Figure 3.8 compares the zonal mean values of FR of bin-1 using various schemes. Since WA11_ACTI is developed at a heavily-polluted urban site in Beijing, it gives very high values (~10.6 cm^{-3} s^{-1}) over the whole zonal areas (see Figure 3.8a). As shown in Figure 3.8b, BO08_ACTI predicts large FR values (from 1.0 to 4.8 cm^{-3} s^{-1}) in the lower portion of the atmosphere (1000-500 mb), but much smaller values (< 1 cm^{-3} s^{-1}) in upper atmosphere (< 500 mb), which is inconsistent with the FR values in upper atmosphere reported by previous studies. For example, recent modeling studies (Yu and Turco, 2000b, 2011) and laboratory measurements (Enghoff et al., 2011; Kirkby et al., 2011) clearly showed an important role of ionization in promoting nucleation. The ionization rate is high in upper atmosphere (see Figure 3.8e) due to strong galactic cosmic rays. Figure 3.8f shows the measured ultrafine particle number concentrations (cm^{-3}) completed by Yu et al. (2008), which can provide a qualitative evaluation of the model performance. The ion-mediated nucleation scheme YU10 gives low values in lower atmosphere (see Figure 3.7c) due to the low ionization rate (see Figure 3.8e). A comparison of Figures 3.8 (d) and (f) indicates that the simulation COMB appears to capture the vertical spatial patterns of the observed ultrafine particle number concentrations.

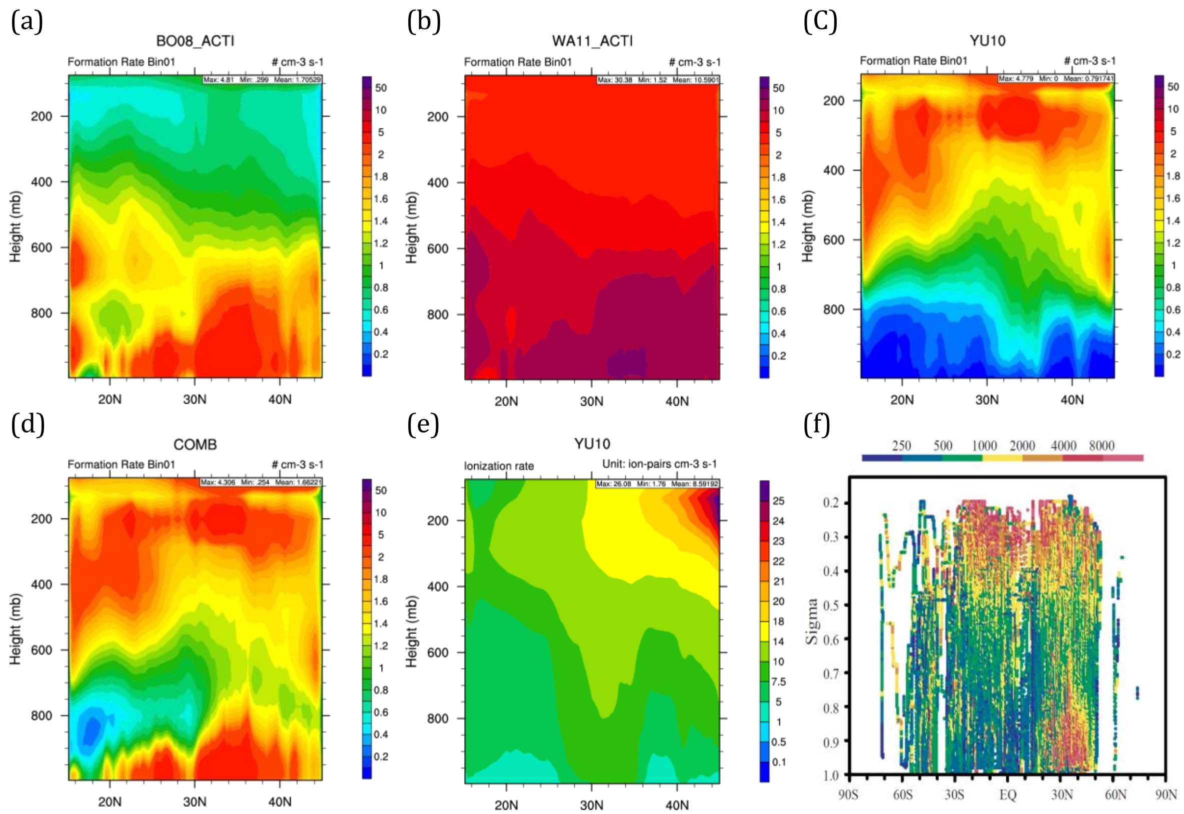

Figure 3.8 Zonal mean values of formation rate (J) using various nucleation schemes, (a) BO08_ACTI, (b) WA11_ACTI, (c) YU10, and (d) COMB, and the ionization rate (e) simulated by WRF/Chem with 12-bin and COMB scheme. (f) ultrafine particle number concentrations (cm^{-3}) based on the measurement data (Yu et al., 2008) (sigma is the height index used in Global Chemical Transport Model (GEOS-Chem), 48 vertical sigma levels extending from the surface to approximately 0.01 hPa).

Table 3.4 summarizes the model evaluation for PM composition at an urban site (Tsinghua, which is 20 km away from downtown and 2 km from 4th Ring Road) in Bejing and a rural site (Miyun, which is 60 km away from downtown), respectively. There are no obvious differences in predictions of PM composition among simulations with various nucleation schemes. The underpredictions of SO_4^{2-} might be due to the underestimation of SO_x emissions (Wang and Zhang, 2012) and the CS. The WRF/Chem tends to overpredict NO_3^- concentrations, and the overprediction of NO_3^- might be due the underpredictions of NH_3 and NO_x emissions, or the underestimation of the NO_3^- wet deposition (Wang and Zhang, 2012). In addition, the underpredictions of both of Na^+ and Cl^- might be due to the underestimations of sea-salt aerosols, which may be due to limitations in the sea-salt emission scheme used in the WRF/Chem simulations.

Table 3.4 Evaluation of PM composition predicted with WRF/Chem (12-bin) with COMB nucleation scheme in July 2008.

Tsinghua site	July 2008							
	Mean Obs.	Mean Mod.	Data #	MB,	RMSE,	NMB, %	NME, %	R
$PM_{2.5}$, µg cm^{-3}	77.8	69.6	31	-8.3	22.9	-10.6	24.9	0.91
Na^{+}, µg cm^{-3}	0.26	0.14	31	-0.12	0.25	-46.9	84.2	0.04
NH_4^{+}, µg cm^{-3}	7.9	11.1	31	3.2	6.8	39.9	68.6	0.85
Cl^{-}, µg cm^{-3}	1.3	0.3	31	-1.1	1.3	-86.6	89.6	-0.03
NO_3^{-}, µg cm^{-3}	15.4	22.0	31	6.6	15.6	42.9	80.6	0.76
SO_4^{2-}, µg cm^{-3}	27.7	13.2	31	-14.6	18.7	-52.5	55.4	0.84
Miyun site	July 2008							
	Mean Obs.	Mean Mod.	Data #	MB,	RMSE,	NMB, %	NME, %	R
$PM_{2.5}$, µg cm^{-3}	65.6	63.8	31	-1.8	29.6	-2.7	34.8	0.81
Na^{+}, µg cm^{-3}	0.26	0.14	31	-1.2	0.27	-46.9	84.2	0.04
NH_4^{+}, µg cm^{-3}	7.9	11.1	31	3.2	6.4	39.9	68.6	0.85
NO_3^{-}, µg cm^{-3}	15.4	22.0	31	6.6	15.5	42.9	80.6	0.76
SO_4^{2-}, µg cm^{-3}	27.7	13.2	31	-14.5	15.2	-52.5	55.4	0.84

The aforementioned analyses show that COMB is able to give reasonable results for capturing the vertical distribution of newly formed particles. The combination of WA11_ACTI, BO08_ACTI, and YU10 parameterizations used in the simulation COMB will be therefore selected for the 2001 4-month applications. In order to understand the favorable conditions for NPF events in Beijing, the time series of temperature (T), relative humidity (RH), N-PSD, H_2SO_4, PM_{10}, and CS predicted from COMB are shown in Figure 3.9. These plots suggest that NPF events occur under the certain conditions with low RH, high H_2SO_4 concentrations, low PM_{10} concentrations, and low CS. These results from COMB are consistent with the observational discrepancies of RH, H_2SO_4, PM_{10}, and CS during NPF and Non_NPF events analyzed by Wu et al. (2007) and Wang (2012) in Beijing. Figure 3.10 compares the diurnal variations of the four variables from WRF/Chem (12-bin) with COMB: RH, H_2SO_4, PM_{10}, and CS during NPF and Non_NPF events in July, 2008. This comparison indicates that RH, PM_{10}, and CS are 23%, 54%, and 54% lower during NPF days than those on Non_NPF days; however H_2SO_4 concentration is about 139% higher on NPF days than on Non_NPF days.

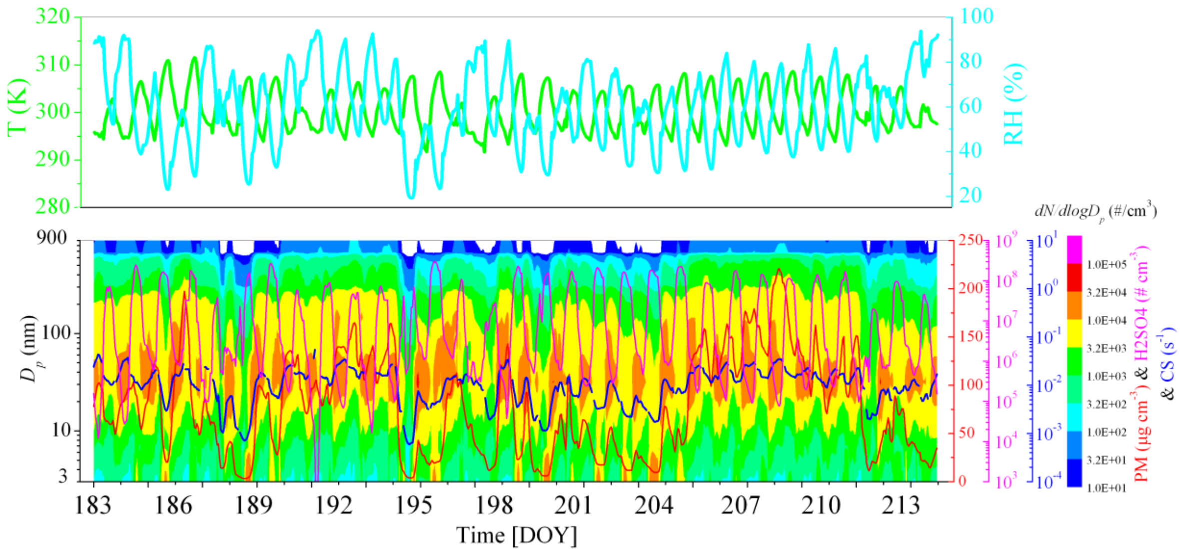

Figure 3.9 Times series of T2, RH2, Particle number size distribution, number concentrations of H_2SO_4, mass concentrations of PM_{10}, and CS simulated by WRF/Chem with 12-bin and COMB.

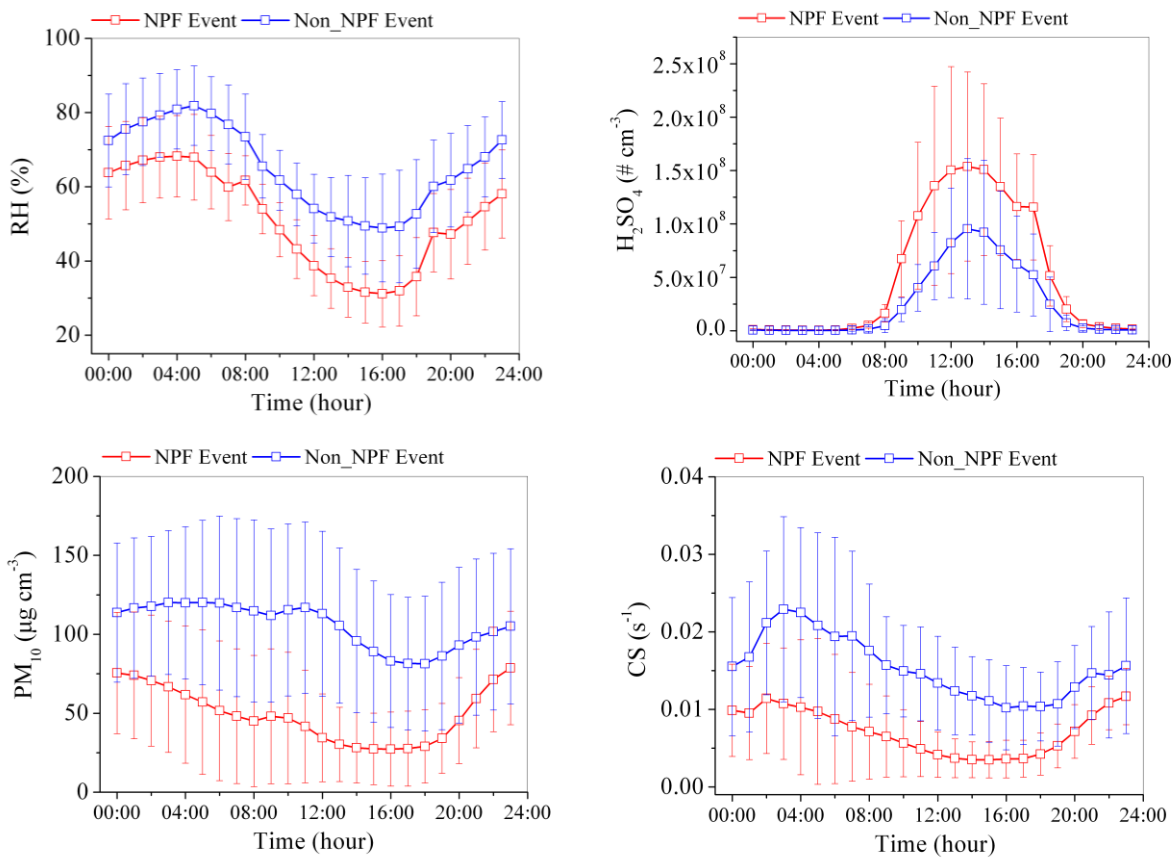

Figure 3.10 Average diurnal variations during the NPF days and no NPF event (Non_NPF Event) days at an urban site in Beijing in July 2008 for RH2, number concentrations of H_2SO_4, mass concentrations of PM_{10}, and CS.

Figure 3.11 compares simulated column SO_2, O_3, NO_2, and CO mass concentrations from the WRF simulation with 12-bin and COMB scheme with the satellite data. Figure 3.12 compares model predictions with the aerosol and cloud level 3 products from both MODIS Aqua and Terra satellite. Table 3.5 summarizes the corresponding statistics of these variables. The evaluation suggests that column concentrations of SO_2, O_3, NO_2, and CO, AOD, CF, and CCN at 0.5% super-saturation (i.e., CCN5) are simulated reasonably well, with NMBs of -34% to 10% and R of 0.53 – 0.81. According to previous studies (Liu et al., 2010; Wang et al., 2010b), the high AOD over the northwest of China cannot be captured, but in this study, the newly coupled dust module (DEAD) is able to capture this characteristic (see Figure 3.12). However, the model severely underestimates COT and CWP, especially in the northern part of East Asia (see Figure 3.12), which may be due in part to the poor performance on simulating ice clouds by current model (Zhang et al., 2013) and the underestimations of the subgrid convective clouds and the related aerosol effects (Yu et al., 2013). Our knowledge about ice particle formation and transformation is still very limited compared to the understanding of processes in warm clouds (Zhang et al., 2013). For example, details of homogeneous and heterogeneous nucleation processes, and their contributions to the formation of ice crystals in cold clouds remain unclear (Prenni et al., 2007; Spichtinger and Gierens, 2009; Zhang et al., 2013). Nevertheless, overall, the improved 12-bin WRF/Chem model with COMB nucleation scheme could reasonably well reproduce the real conditions in the atmosphere.

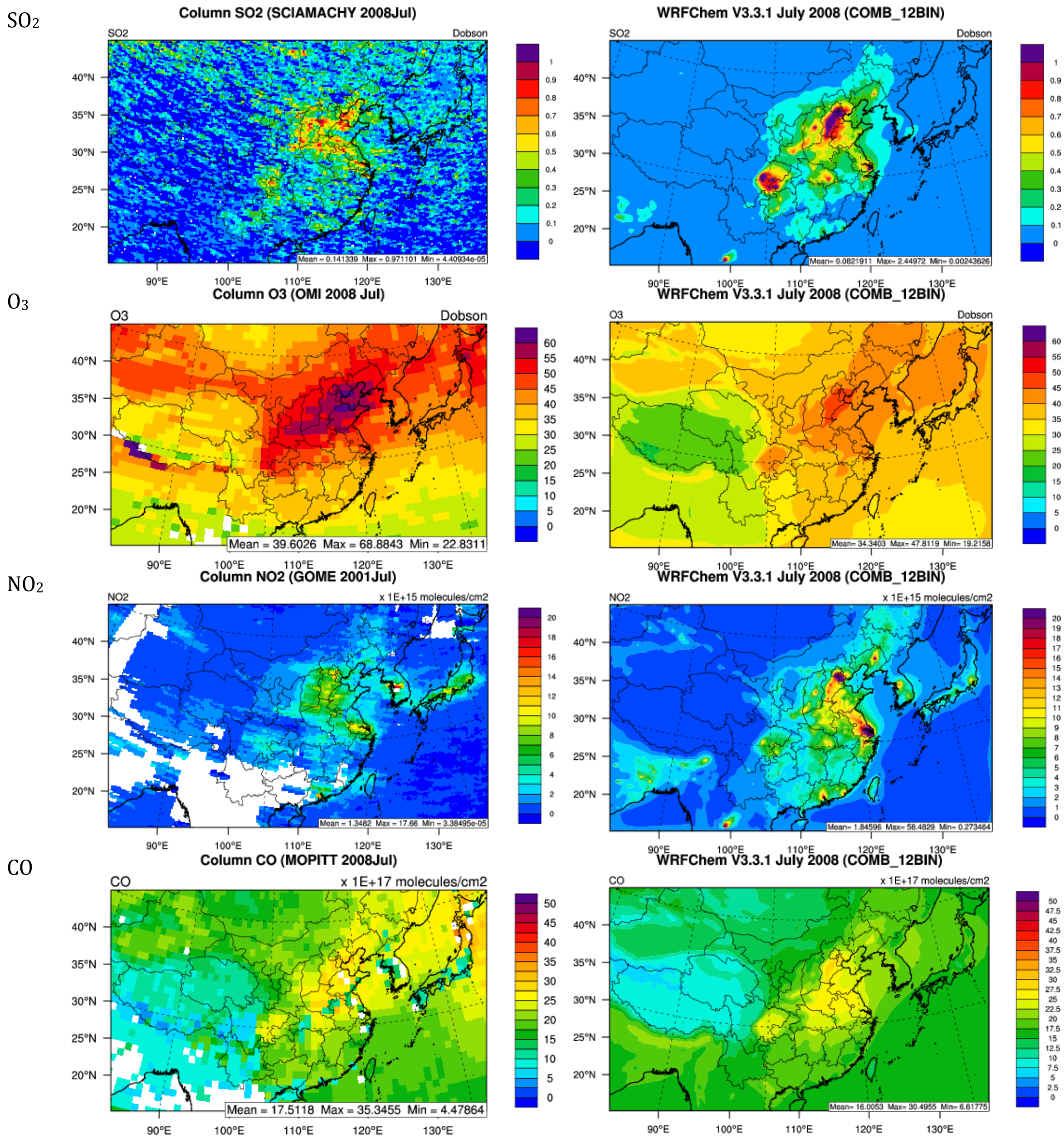

Figure 3.11 Observed and simulated spatial distributions of column concentrations of SO_2, O_3, NO_2, and CO in July 2008. The simulation is based on WRF/Chem with 12-bin and COMB. The observations for column SO_2, O_3, NO_2, and CO are taken from satellite data.

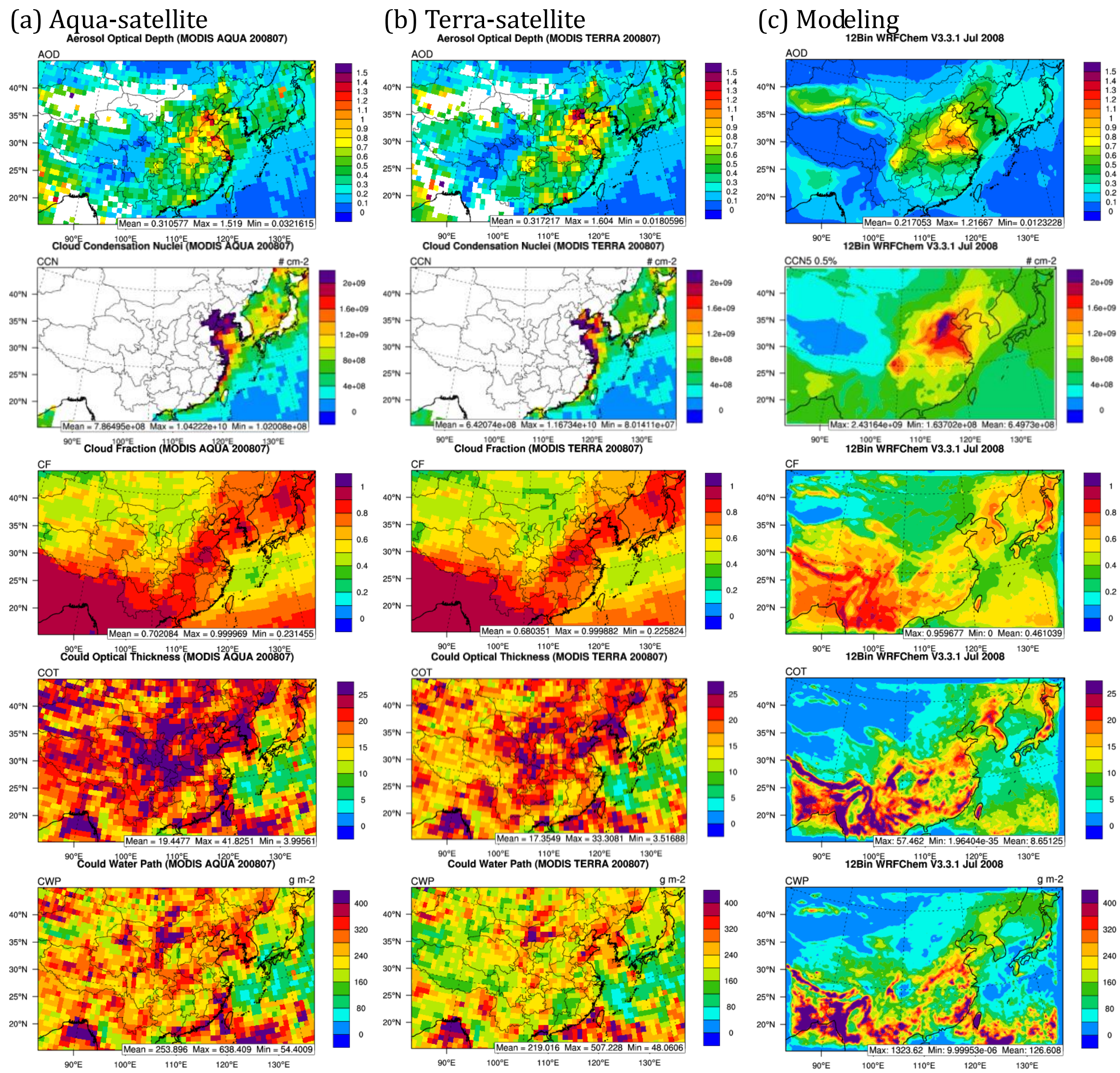

Figure 3.12 Observed and simulated spatial distributions of simulated and observed AOD CCN5, CF, COT, and CWP in July 2008. The simulation is based on WRF/Chem with 12-bin and COMB. The observations are taken from two satellites (MODIS Aqua and Terra).

Table 3.5 Evaluation of column variables predicted with WRF/Chem model (12-bin) with COMB in July 2008.

Variable	Scheme	July 2008							
		Mean Obs	Mean Mod	Data #	MB	RMSE	NMB, %	NME, %	R
SO_2, DU	SCIAMACHY[a]	0.14	0.11	10392	-0.03	0.14	-24.4	67.8	0.57
O_3, DU	OMI[b]	39.6	34.3	15898	-5.3	8.4	-13.3	17.6	0.61
NO_2, $\times 10^{15}$ molecules cm^{-2}	SCIAMACHY	1.8	2.0	12649	0.2	2.5	10.1	60.4	0.72
CO, $\times 10^{17}$ molecules cm^{-2}	MOPITT[c]	17.5	16.0	15606	-1.5	5.2	-8.7	25.0	0.53
Aqua satellite:		July 2008							
		Mean Obs	Mean Mod	Data #	MB	RMSE	NMB, %	NME, %	R
AOD	MODIS[d]	0.31	0.21	14952	-0.10	0.20	-31.1	43.8	0.65
CCN5[e],$\times 10^8$ # cm^{-2}	MODIS	8.0	7.0	5496	-1.0	8.9	-12.2	55.3	0.81
CF[f]	MODIS	0.70	0.46	15908	-0.24	0.28	-34.4	34.8	0.69
COT[g]	MODIS	19.4	9.0	15908	-10.5	13.5	-53.9	60.6	0.23
CWP[h], g m^{-2}	MODIS	253.9	126.6	15908	-127.3	178.0	-50.1	61.4	0.33
Terra satellite:		July 2008							
		Mean Obs	Mean Mod	Data #	MB	RMSE	NMB, %	NME, %	R
AOD	MODIS	0.32	0.22	15047	-0.10	0.21	-32.0	44.7	0.65
CCN5,$\times 10^8$ # cm^{-2}	MODIS	6.5	7.0	5519	0.5	8.5	7.5	59.2	0.72
CF	MODIS	0.68	0.46	15908	-0.22	0.27	-32.3	32.8	0.70
COT	MODIS	17.4	9.0	15908	-8.4	11.7	-48.4	58.6	0.24
CWP, g m^{-2}	MODIS	219.0	126.6	15908	-92.4	156.4	-42.2	60.1	0.28

Table 3.5 Continued

[a]SCIAMACHY – Scanning Imaging Absorption spectrometer
[b]OMI – Ozone Monitoring Instrument
[c]MOPITT – Measurements Of Pollution In The Troposphere
[d]MODIS – Terra moderate-resolution imaging
[e]CCN5 – Cloud condensation nuclei at 0.5% super-saturation
[f]CF – Cloud fraction
[g]COT – Cloud optical thickness
[h]CWP – Cloud water path; AOD – Aerosol optical depth

3.3 2001 Application and Evaluation

In this section, a comprehensive model evaluation are performed for simulations with WRF/Chem (12-bin) with the COMB nucleation scheme for the four months (January, April, July and October) in 2001.

3.3.1 Meteorological Predictions

Meteorological variables are significant in predicting chemical species. Table 3.6 summarizes the performance statistics for meteorological variables using NCDC data. The evaluation indicates that T2, Q2, and P are simulated reasonably well by WRF/Chem (12-bin), with NMBs of -10% to 40% and R of 0.55~0.94. However, WS10 is overpredicted for all four months with NMBs of 48% to 82%, the overprediction tendency of WRF in this study is similar with previous studies (Cheng and Steenburgh, 2005), which might be due to either too much mixing vertically or not enough drag in low-level. Thus, in WRF-CAM5 simulation, the friction velocity in PBL module is multiplied by a factor of 1.5 to increase the low-level drag (Mass et al., 2010). In addition, daily total precipitation is poorly estimated with R values of 0.04~0.17 and NMBs of -46% to -37%, which might be due to the large uncertainties in cloud formation and aerosol-cloud-precipitation interactions.

Table 3.6 Evaluation of meteorological variables predicted with WRF/Chem (12-bin) with COMB in 2001.

Variable	Month	Mean Obs.	Mean Mod.	Data #	MB,	RMSE,	NMB, %	NME, %	R
T2[a], °C	Jan.[f]	1.1	1.5	299396	0.4	26.9	40.0	36.4	0.89
	Apr.[g]	13.6	12.3	297625	-1.3	40.2	-9.7	35.3	0.69
	Jul.[h]	25.2	23.8	302284	-1.4	30.0	-5.6	16.3	0.55
	Oct.[i]	15.9	15.5	303799	-0.4	28.0	-2.5	25.3	0.74
P[b], mb	Jan.	965.0	949.9	175620	-15.2	1641.2	-1.6	2.6	0.93
	Apr.	962.1	948.0	171534	-14.1	1508.4	-1.5	2.4	0.93
	Jul.	957.4	943.5	178249	-13.8	1367.1	-1.4	2.3	0.94
	Oct.	964.2	949.8	175746	-14.4	1478.3	-1.5	2.4	0.94
Q2[c], g kg^{-1}	Jan.	3.4	3.9	175430	0.5	1.6	14.6	25.5	0.92
	Apr.	6.2	6.4	171193	0.3	2.8	4.2	20.0	0.90
	Jul.	14.8	15.1	177205	0.3	5.9	2.4	12.8	0.87
	Oct.	8.3	8.8	174734	0.5	3.2	5.9	16.1	0.91
WS10[d], m s^{-1}	Jan.	3.2	5.8	295637	2.6	18.6	82.3	105.9	0.43
	Apr.	3.2	5.1	293157	1.8	13.3	55.8	88.8	0.31
	Jul.	2.6	3.9	306316	1.3	8.2	48.7	86.0	0.29
	Oct.	2.7	4.8	301608	2.1	12.1	79.0	102.6	0.44
WD10[e], degree	Jan.	210.1	207.4	248091	-2.7	17978.0	-1.3	45.1	0.25
	Apr.	190.8	183.9	264684	-6.9	16761.1	-3.6	48.9	0.21
	Jul.	183.2	175.1	267535	-8.1	14291.2	-4.4	49.2	0.14
	Oct.	181.7	173.1	254266	-8.6	20521.8	-4.7	57.6	0.23
24-h rain, mm	Jan.	1.9	1.2	21215	-0.7	45.4	-37.4	118.9	0.17
	Apr.	1.9	1.1	22142	-0.8	61.1	-40.4	128.5	0.16
	Jul.	5.0	3.0	21882	-2.0	290.3	-40.7	125.5	0.10
	Oct.	2.7	1.5	22865	-1.2	139.1	-44.5	135.6	0.04

Table 3.6 Continued

[a]T2 – Temperature at 2 meters
[b]P – Atmospheric pressure
[c]Q2 – Water vapor mixing ratios at 2 meters
[d]WS10 – Wind speeds at 10 meters
[e]WD10 – Wind directions at 10 meters
[f]Jan. – January
[g]Apr. – April
[h]Jul. – July
[i]Oct. – October

3.3.2 Chemical Predictions

3.3.2.1 Model Evaluation Using Surface Measurement Data

In this section, the surface measurement data are used to evaluate the model performance. The simulated spatial distributions of PM_{10} (see Figure 3.13) show that the northwestern China, northern China, and southern Mongolian are the three regions with the largest dust aerosol sources in East Asia, which are consistent with previous studies on dust storms over East Asia (Gong et al., 2003; Zhang et al., 2003). The API-derived PM_{10} concentrations are overall well reproduced with NMBs of -25% to -11%, and R values of 0.53 - 0.81 (see Table 3.7). The model reproduces well the seasonality of PM_{10} concentrations over mainland China, with the highest concentrations in winter, followed by spring, fall, and summer. However, over Taiwan in all months and Japan in January and July 2001, PM_{10} concentrations are moderately-to-significantly underpredicted with NMBs from -56% to -35%, probably caused by the underestimation of the dust transport from desert or the emissions of local natural and anthropogenic sources or the underestimations of $PM_{2.5}$. Over Hong Kong, PM_{10} concentrations are well estimated with NMBs of -5.5% to 15.0%. The surface concentrations of CO, NO_2 and SO_2 are underpredicted in nearly all months (except for SO_2 in July over Taiwan) (with NMBs of -84% to -27% for CO, -89% to -26% for NO_2 and -84% to -17% for SO_2) over Taiwan, Hong Kong, and Japan, likely due to the underestimation of anthropogenic emissions or limited capabilities of the model on simulating some meteorological variables which significantly affect air quality (e.g., the planetary boundary layer height (PBLH) and wind speed/direction (WS/WD)). For instance, high wind speeds favor the air pollutant dispersion. Thus, the overprediction of wind speeds may lead to the underprediction of some chemical species. O_3 surface mixing ratios are overpredicted in nearly all months over Japan and Taiwan (except for April over Japan) (with NMBs of -16% to 36%), likely due to inaccurate predictions of its precursors (such as NO_x and VOCs) which have been discussed in section 3.2. Figure 3.14 compares simulated and observed monthly average PM composition at an urban site (Tsinghua) in Beijing indicating that nearly all PM species have been largely underestimated in January, which might be due to the most overestimation of wind speed in January compared with other months (see Table 3.6). T2 has also been overpredicted, indicating a higer PBLH and thus enhancing the air pollutant dispersion. In addition, during winter, SOA precursors are accumulated due to the low mixing heights, thus accelerating the SOA formation (Strader et al., 1999); however, the MOSAIC used here does not treat SOA. The underpredictions of SO_4^{2-} may be due to the underestimation of SO_x emissions (Wang and Zhang, 2012) and the CS. The WRF/Chem tends to overpredict NO_3^- concentrations, and the overprediction of NO_3^- might be due the underestimates of NH_3 and NO_x emissions, or the underestimation of the NO_3^- wet deposition (Kai et al., 2012). In addition, the underpredictions of both of Na^+ and Cl^- might be due to the underestimations of sea-salt aerosol emissions and transport.

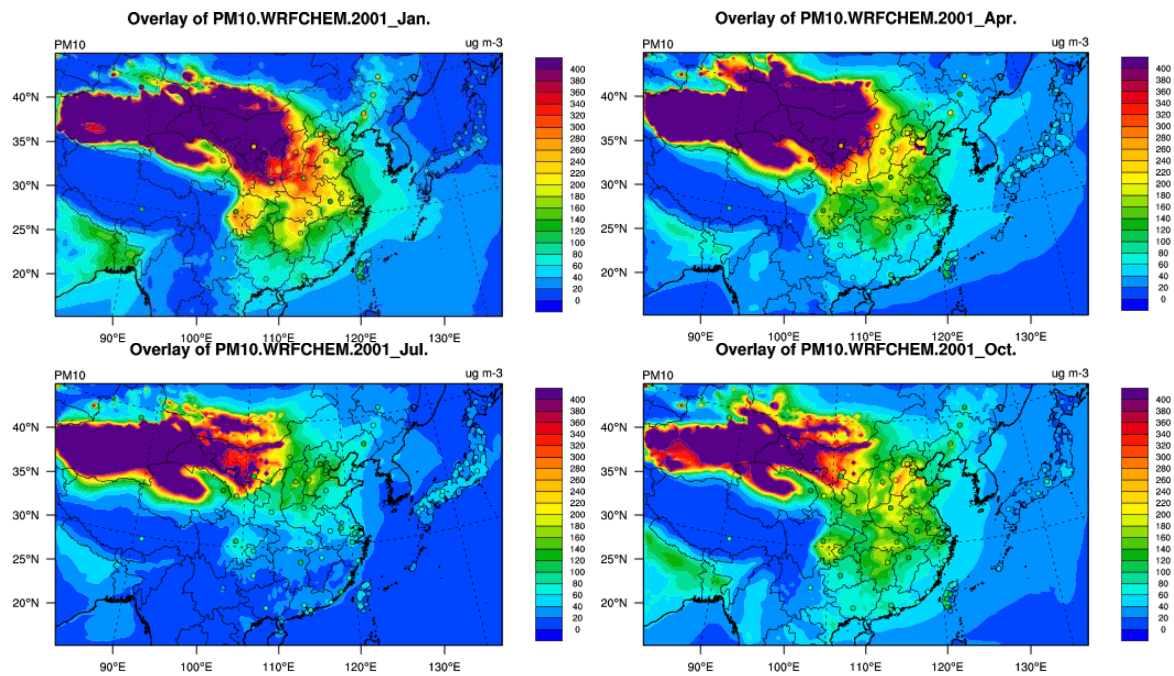

Figure 3.13 Overlay of observed and simulated monthly-mean PM_{10} during the four months (Jan. Apr. Jul. and October) in 2001. The simulation is based on WRF/Chem with 12-bin and COMB. The observations are derived from China API, Hong Kong EPD, Taiwan AQMN, and Japan NIES.

Table 3.7 Evaluation of the concentrations of gases and particles predicted with WRF/Chem (12-bin) using surface measurement data 2001.

Variable	Month	Mean Obs	Mean Mod	Data #	MB	RMSE	NMB, %	NME, %	R
Mainland China									
PM_{10}, $\mu g\ cm^{-3}$	Jan.[a]	161.5	143.3	40	-18.2	126.5	-11.3	52.2	0.53
	Apr.[b]	148.05	115.8	42	-32.2	72.5	-21.8	37.0	0.81
	Jul.[c]	91.5	68.6	42	-22.9	45.3	-25.0	40.2	0.69
	Oct.[d]	113.2	92.1	42	-21.0	51.1	-18.6	34.0	0.58
Taiwan									
PM_{10}, $\mu g\ cm^{-3}$	Jan.	65.7	28.6	134	-17.9	28.4	-56.4	67.2	0.22
	Apr.	67.4	32.6	144	-18.8	25.5	-51.7	57.0	0.50
	Jul.	38.0	19.6	123	-10.8	16.0	-48.3	52.9	-0.12
	Oct.	64.7	32.7	145	-17.8	25.8	-49.5	57.0	0.07
$PM_{2.5}$, $\mu g\ cm^{-3}$	Jan.	36.0	18.1	134	-17.9	28.4	-49.8	64.5	-0.08
	Apr.	39.6	20.8	144	-18.8	25.5	-47.4	53.6	0.18
	Jul.	27.4	16.6	123	-10.8	16.0	-39.3	46.1	0.17
	Oct.	39.0	21.2	145	-17.8	25.8	-45.7	51.2	0.27
SO_2, ppbv	Jan.	4.6	3.5	1896	-1.0	5.0	-22.6	69.0	0.22
	Apr.	4.6	3.6	1912	-0.9	4.5	-19.8	65.5	0.24
	Jul.	3.0	3.5	1917	0.5	3.8	17.8	87.9	0.17
	Oct.	3.8	3.2	1953	-0.7	3.3	-16.9	60.4	0.30
NO_2, ppbv	Jan.	24.1	7.3	1933	-16.8	19.6	-69.8	70.4	0.41
	Apr.	24.1	6.8	1881	-17.3	19.5	-71.8	72.1	0.49
	Jul.	14.4	6.2	1927	-8.2	10.5	-57.1	59.6	0.44
	Oct.	19.7	6.1	1944	-13.6	15.5	-68.9	69.2	0.43

Table 3.7 Continued

NO, ppbv	Jan.	11.1	0.7	1905	-10.4	15.8	-93.9	94.1	0.29
	Apr.	8.0	0.6	1857	-7.5	11.7	-93.0	93.2	0.38
	Jul.	6.3	0.6	1906	-5.6	8.6	-89.7	90.2	0.32
	Oct.	4.7	0.5	1890	-4.3	6.9	-90.3	90.7	0.18
CO, ppmv	Jan.	0.7	0.3	1985	-0.4	0.5	-53.2	54.2	0.12
	Apr.	0.7	0.3	1914	-0.5	0.6	-61.5	61.7	0.21
	Jul.	0.5	0.2	1933	-0.3	0.4	-63.2	63.8	0.16
	Oct.	0.6	0.3	1980	-0.3	0.4	-53.0	53.3	0.36
O_3, ppbv	Jan.	23.0	31.2	1953	8.2	12.1	35.8	43.6	0.36
	Apr.	27.6	33.9	1901	6.3	12.3	22.9	37.1	0.39
	Jul.	20.4	27.2	1952	6.8	11.5	33.4	47.5	0.21
	Oct.	34.3	38.1	1977	3.8	12.6	11.0	28.9	0.28
Hong Kong									
PM_{10}, μg cm^{-3}	Jan.	57.6	66.3	31	8.6	27.4	15.0	38.4	0.48
	Apr.	51.9	49.5	30	-2.5	23.0	-4.7	34.8	0.67
	Jul.	31.9	30.1	31	-1.8	11.0	-5.5	22.4	0.61
	Oct.	62.1	64.1	31	2.1	22.1	3.3	25.1	0.22
SO_2, μg m^{-3}	Jan.	14.2	6.6	31	-7.6	10.4	-53.5	53.4	0.56
	Apr.	14.4	4.8	30	-9.6	12.2	-66.9	67.0	0.12
	Jul.	19.8	3.3	31	-16.6	20.9	-83.5	83.5	0.60
	Oct.	11.0	6.1	31	-4.9	8.4	-44.2	46.6	0.34
NO_2 μg m^{-3}	Jan.	33.4	10.2	31	-23.2	24.7	-69.5	69.5	0.40
	Apr.	61.7	9.2	30	-52.5	53.6	-85.1	85.1	0.56

Table 3.7 Continued

	Jul.	48.0	3.9	31	-44.1	47.0	-91.8	91.8	0.36
	Oct.	63.2	7.0	31	-56.3	57.5	-89.0	89.0	0.13
NO	Jan.	73.4	0.3	31	-73.1	83.1	-99.6	99.6	0.00
μg m^{-3}	Apr.	66.1	0.4	30	-65.7	70.9	-99.4	99.4	0.00
	Jul.	77.6	0.2	31	-77.4	84.4	-99.8	99.8	-0.18
	Oct.	40.8	0.2	31	-40.6	43.7	-99.5	99.5	-0.07
CO	Jan.	1045.6	640.7	31	-404.9	446.0	-38.7	38.7	0.62
μg m^{-3}	Apr.	843.0	377.3	30	-465.6	503.0	-55.2	55.2	0.36
	Jul.	1277.9	207.0	31	-1070.9	1158.0	-83.8	83.8	-0.07
	Oct.	932.1	499.8	31	-432.3	481.3	-46.4	46.4	0.24
O_3	Jan.	27.6	67.2	31	39.6	41.4	143.4	143.4	0.26
μg m^{-3}	Apr.	34.4	58.5	30	24.1	28.5	69.9	69.9	0.50
	Jul.	18.5	49.0	31	30.5	32.1	164.5	164.5	0.05
	Oct.	53.9	81.3	31	27.4	31.6	50.9	50.9	0.32
Japan									
PM_{10}	Jan.	22.2	12.4	1470	-9.8	13.3	-44.1	52.3	0.29
μg cm^{-3}	Apr.	33.9	31.0	1537	-2.9	7.7	-8.6	18.2	0.30
	Jul.	35.1	22.6	1537	-12.5	15.6	-35.5	38.2	0.29
	Oct.	27.6	26.4	1541	-1.2	7.3	-4.3	20.6	0.44
SO_2, ppbv	Jan.	3.9	2.1	1478	-1.8	3.3	-46.4	69.1	0.18
	Apr.	6.0	2.5	1490	-3.5	4.6	-57.6	65.2	0.29
	Jul.	5.3	2.8	1453	-2.6	4.6	-48.3	70.2	0.23
	Oct.	4.2	2.6	1444	-1.6	3.3	-38.8	64.2	0.36

Table 3.7 Continued

NO_2, ppbv	Jan.	17.8	6.7	1467	-11.1	12.7	-62.1	62.7	0.65
	Apr.	16.9	7.7	1465	-9.1	11.4	-54.1	57.4	0.54
	Jul.	12.6	9.3	1465	-3.3	7.7	-26.4	48.8	0.50
	Oct.	16.9	8.5	1468	-8.4	10.3	-49.6	52.2	0.69
NO, ppbv	Jan.	15.4	0.03	1456	-15.4	19.4	-99.8	99.8	0.19
	Apr.	6.6	0.04	1448	-6.6	8.2	-99.4	99.4	0.03
	Jul.	5.5	0.05	1446	-5.5	6.7	-99.2	99.2	-0.03
	Oct.	9.9	0.05	1452	-9.9	12.2	-99.5	99.5	0.21
CO, ppmv	Jan.	0.6	0.2	132	-0.3	0.4	-56.2	56.8	0.34
	Apr.	0.4	0.3	131	-0.2	0.2	-42.2	42.9	0.30
	Jul.	0.3	0.2	131	-0.1	0.1	-27.0	31.1	0.43
	Oct.	0.5	0.3	130	-0.2	0.2	-41.9	42.9	0.49
O_3, ppbv	Jan.	26.7	29.1	202	2.4	5.9	9.1	17.7	0.38
	Apr.	43.2	36.5	200	-6.7	9.9	-15.5	19.4	0.17
	Jul.	28.7	34.6	202	5.9	9.6	20.5	27.6	0.41
	Oct.	26.0	30.4	202	4.4	7.7	17.1	23.4	0.38

[a]Jan. – January
[b]Apr. – April
[c]Jul. – July
[d]Oct. – October

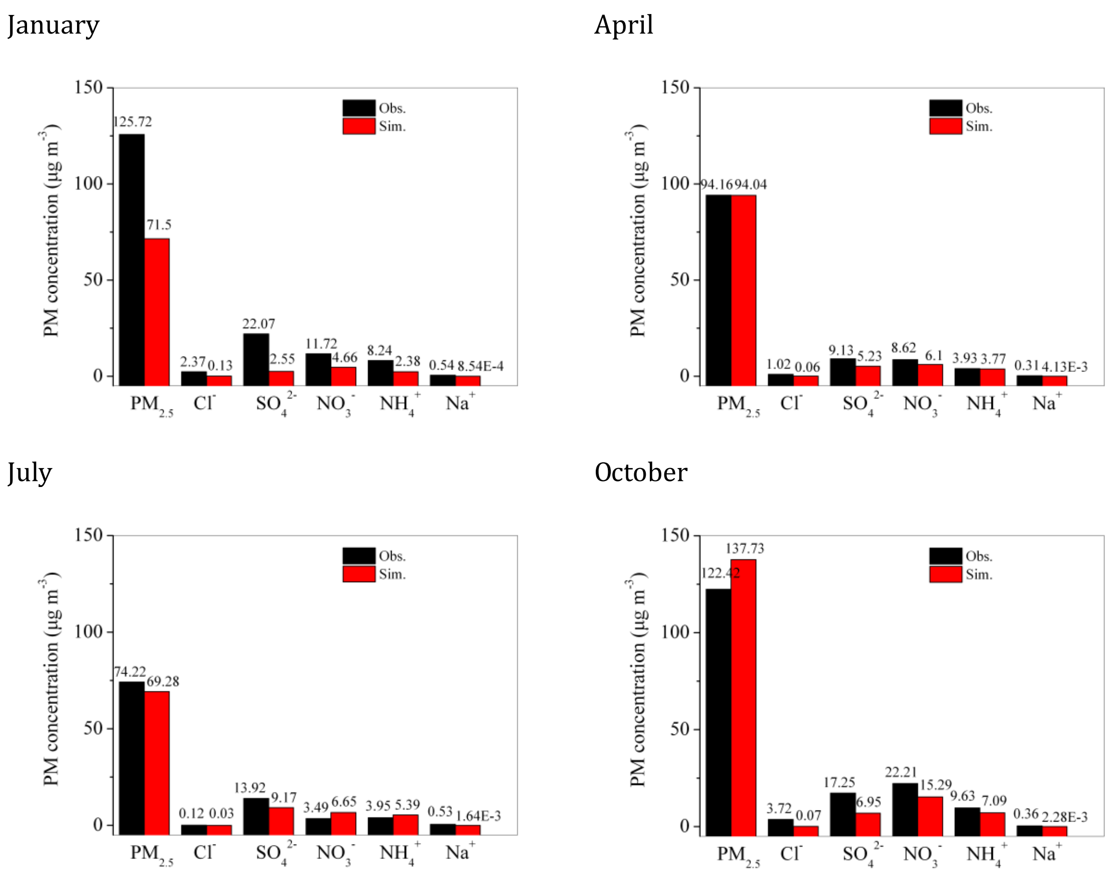

Figure 3.14 Observed and simulated monthly mean concentrations of $PM_{2.5}$ and its composition (NH_4^+, SO_4^{2-}, NO_3^-, Na^+, and Cl^- at an urban site (Tsinghua) in Beijing during four months (January, April, July and October) in 2001. The simulation is based on WRF/Chem with 12-bin and COMB. The observations are taken from Tsinghua University. The values over each bar indicate the mass concentrations of each species.

3.3.2.2 Model Evaluation Using Satellite Data

Figure 3.15 compares simulated and observed column O_3, NO_2, and CO concentrations. Figure 3.16 compares simulated and observed aerosol and cloud variables. Table 3.8 summarizes the corresponding performance statistics for those variables. As shown in Figure 3.15 and Table 3.8a, except for column O_3 in January, and CO column mass abundance in January and October that show a poor agreement in terms of spatial distribution, all of those column variables in nearly all months are simulated reasonably well with NMBs of -19% to 30% and R values of 0.31 to 0.79. As shown in Figure 3.15 and Table 3.8b, AOD is reasonably well predicted with NMBs of -40% to 34% and R values of of 0.53 to 0.72. CF, COT, and CWP are significantly underpredicted, with NMBs of -73% to -38% and R values of 0.16 to 0.74 in the four months, especially in the northern part of East Asia, which may be due to the poor performance on simulating ice-clouds by the current model (Zhang et al., 2013) and the underestimations of the subgrid convective clouds and the related aerosol effects (Yu et al., 2013).

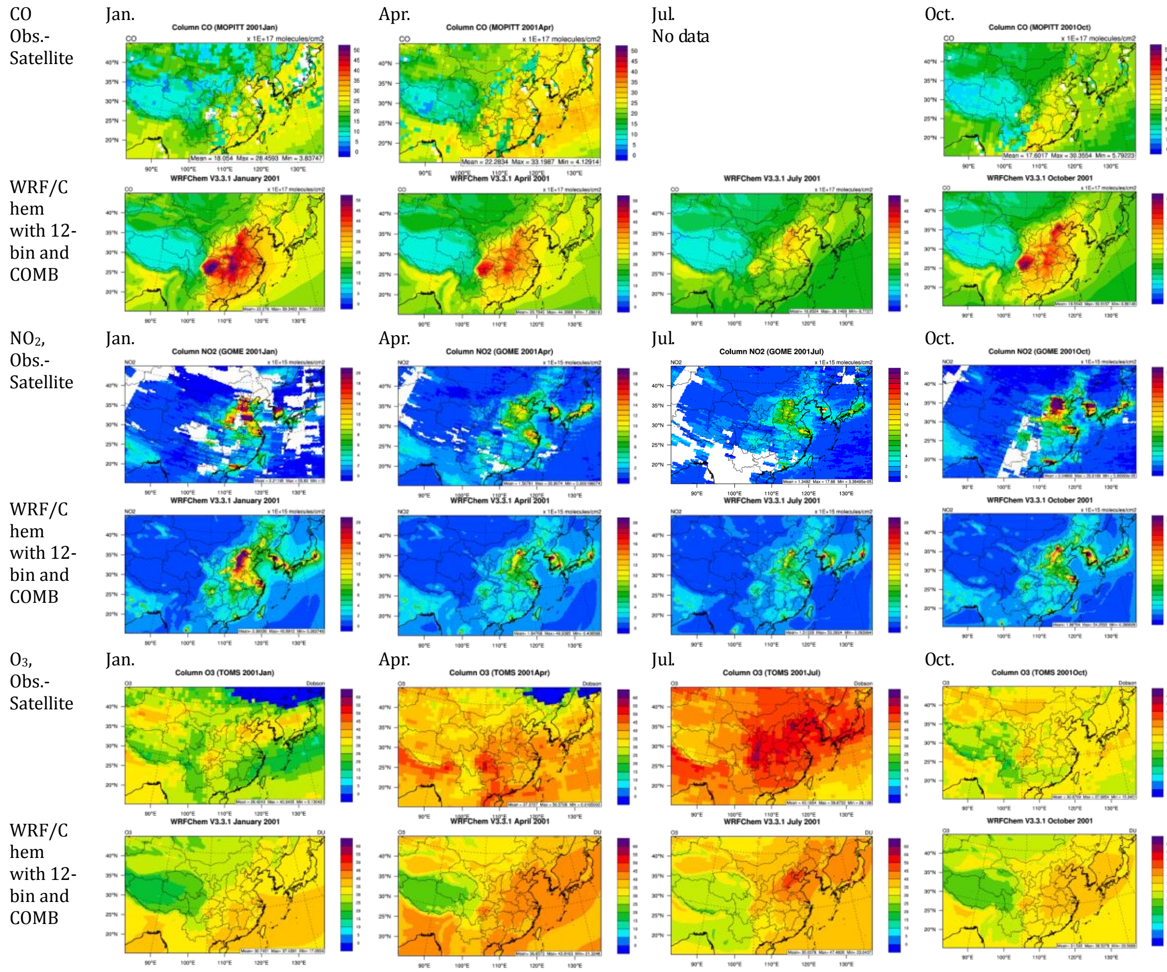

Figure 3.15 Observed and simulated spatial distributions of column mass concentrations of CO, O_3 and NO_2 during four months (January, April, July and October) in 2008. The simulation is based on WRF/Chem with 12-bin and COMB.

Figure 3.16 Observed and simulated spatial distributions of AOD, CCN5, CF, COT, and CWP in four months (January, April, July and October) of 2001. The simulation is based on WRF/Chem with 12-bin and COMB. The observations are taken from MODIS Terra data for all other variables.

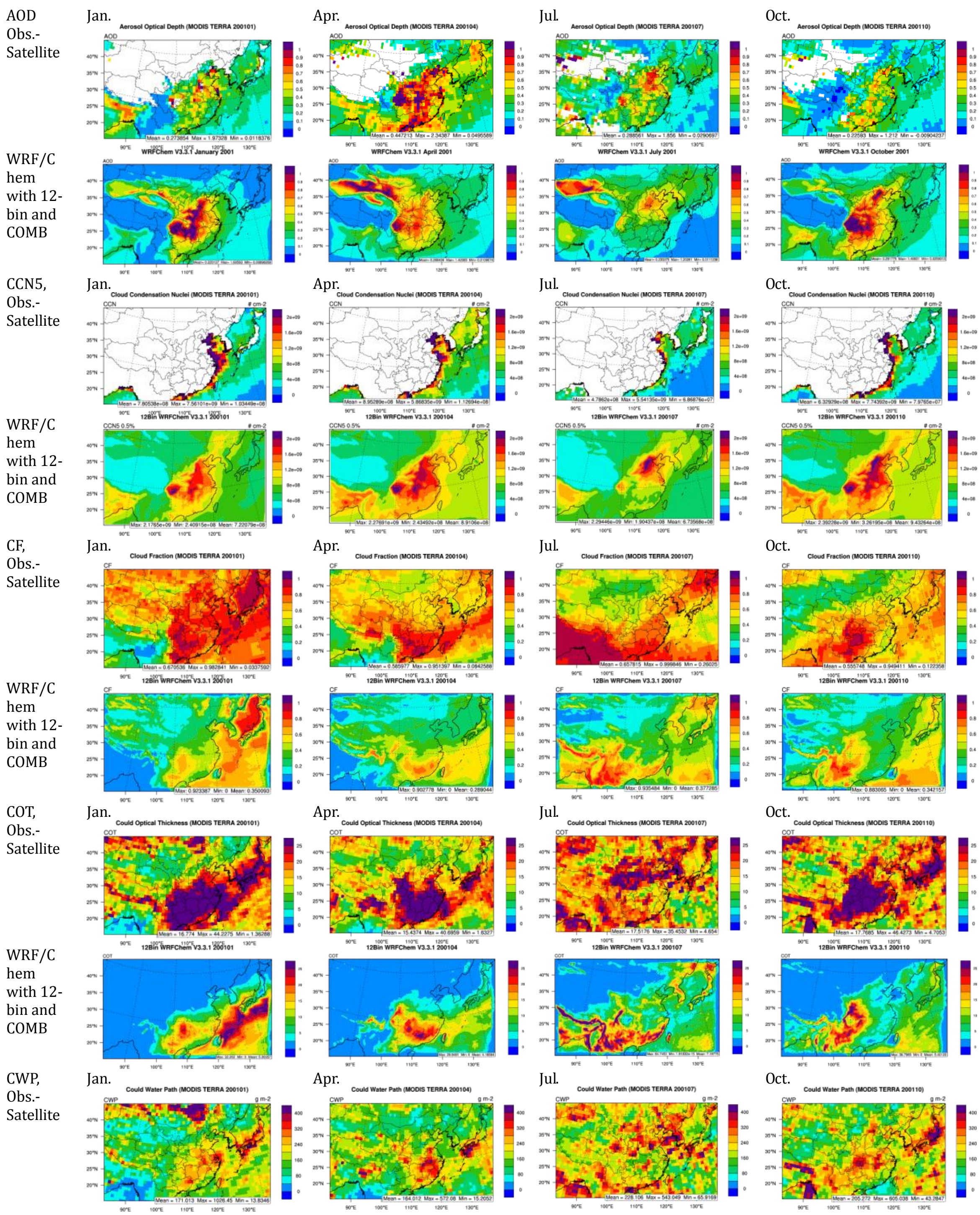
AOD
Obs.-
Satellite
Jan.
Aerosol Optical Depth (MODIS TERRA 200101)
Apr.
Aerosol Optical Depth (MODIS TERRA 200104)
Jul.
Aerosol Optical Depth (MODIS TERRA 200107)
Oct.
Aerosol Optical Depth (MODIS TERRA 200110)
WRF/C
hem
with 12-
bin and
COMB
WRFChem V3.3.1 January 2001
WRFChem V3.3.1 April 2001
WRFChem V3.3.1 July 2001
WRFChem V3.3.1 October 2001
CCN5,
Obs.-
Satellite
Jan.
Cloud Condensation Nuclei (MODIS TERRA 200101)
Apr.
Cloud Condensation Nuclei (MODIS TERRA 200104)
Jul.
Cloud Condensation Nuclei (MODIS TERRA 200107)
Oct.
Cloud Condensation Nuclei (MODIS TERRA 200110)
WRF/C
hem
with 12-
bin and
COMB
12Bin WRFChem V3.3.1 200101
12Bin WRFChem V3.3.1 200104
12Bin WRFChem V3.3.1 200107
12Bin WRFChem V3.3.1 200110
CF,
Obs.-
Satellite
Jan.
Cloud Fraction (MODIS TERRA 200101)
Apr.
Cloud Fraction (MODIS TERRA 200104)
Jul.
Cloud Fraction (MODIS TERRA 200107)
Oct.
Cloud Fraction (MODIS TERRA 200110)
WRF/C
hem
with 12-
bin and
COMB
12Bin WRFChem V3.3.1 200101
12Bin WRFChem V3.3.1 200104
12Bin WRFChem V3.3.1 200107
12Bin WRFChem V3.3.1 200110
COT,
Obs.-
Satellite
Jan.
Could Optical Thickness (MODIS TERRA 200101)
Apr.
Could Optical Thickness (MODIS TERRA 200104)
Jul.
Could Optical Thickness (MODIS TERRA 200107)
Oct.
Could Optical Thickness (MODIS TERRA 200110)
WRF/C
hem
with 12-
bin and
COMB
12Bin WRFChem V3.3.1 200101
12Bin WRFChem V3.3.1 200104
12Bin WRFChem V3.3.1 200107
12Bin WRFChem V3.3.1 200110
CWP,
Obs.-
Satellite
Jan.
Could Water Path (MODIS TERRA 200101)
Apr.
Could Water Path (MODIS TERRA 200104)
Jul.
Could Water Path (MODIS TERRA 200107)
Oct.
Could Water Path (MODIS TERRA 200110)

WRF/
Chem
with
12-bin
and
COMB

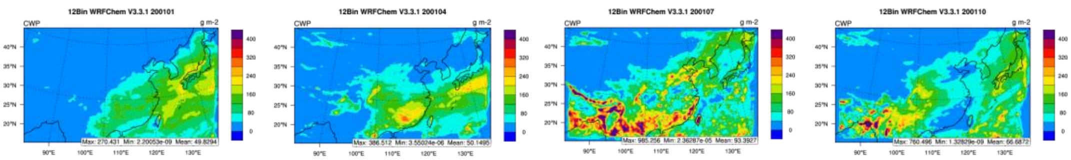

Table 3.8 Evaluation of column variables predicted with WRF/Chem model (12-bin) with COMB in 2001.

(a) Gases

Variable	Month	Mean Obs	Mean Mod	Data #	MB	RMSE	NMB, %	NME, %	R
CO, $\times 10^{17}$ molecules cm^{-2}	Jan.	18.1	22.5	15854	4.2	7.8	24.6	27.5	0.59
	Apr.	22.3	20.8	15908	-1.5	5.0	-6.7	18.5	0.70
	Jul.	No data							
	Oct.	17.6	19.6	15908	2.0	5.2	11.1	18.1	0.74
NO_2, $\times 10^{15}$ molecules cm^{-2}	Jan.	2.2	2.8	9845	0.6	2.8	25.1	64.1	0.74
	Apr.	1.6	1.9	14677	0.3	1.3	22.3	51.3	0.78
	Jul.	1.3	1.6	12671	0.3	1.4	19.8	54.0	0.69
	Oct.	2.0	2.2	12551	0.1	2.2	2.7	53.6	0.79
O_3, DU	Jan.	26.4	30.8	14850	4.4	8.4	16.6	25.0	0.02
	Apr.	37.4	36.8	15329	-0.5	6.1	-0.8	12.3	0.31
	Jul.	43.2	35.0	15908	-8.1	9.9	-18.9	20.3	0.40
	Oct.	30.7	31.5	15908	5.9	7.2	2.3	20.2	0.52

(b) Aerosol and cloud properties

Variable	Month	Mean Obs.	Mean Mod.	Data #	MB,	RMSE,	NMB, %	NME, %	R
AOD	Jan.	0.27	0.25	10735	-0.02	0.19	-9.1	48.4	0.63
	Apr.	0.45	0.27	13152	-0.18	0.25	-39.8	44.0	0.72
	Jul.	0.29	0.22	14907	-0.07	0.17	-23.5	40.9	0.66
	Oct.	0.22	0.30	14544	0.08	0.21	33.9	60.3	0.53
CCN5, $\times 10^{8}$ # cm^{-2}	Jan.	7.8	7.5	5871	-0.3	8.8	-6.6	62.3	0.72
	Apr.	9.0	9.8	5836	0.8	5.9	7.9	41.5	0.76
	Jul.	4.8	7.1	5718	2.3	4.7	45.2	71.8	0.79

Table 3.8 Continued.

	Oct.	6.3	9.8	6143	3.5	7.6	54.5	97.4	0.63
CF (%)	Jan.	0.67	0.35	15908	-0.32	0.36	-47.8	48.0	0.71
	Apr.	0.59	0.29	15908	-0.30	0.32	-50.7	50.8	0.73
	Jul.	0.66	0.38	15908	-0.28	0.32	-42.6	42.9	0.64
	Oct.	0.56	0.34	15908	-0.21	0.26	-38.4	40.4	0.62
COT	Jan.	16.8	5.2	15908	-11.6	13.7	-69.0	71.0	0.58
	Apr.	15.4	4.2	15908	-11.3	12.1	-72.9	73.1	0.72
	Jul.	17.5	7.2	15908	-10.3	13.0	-58.9	64.6	0.18
	Oct.	17.8	5.4	15908	-12.4	13.7	-61.1	65.5	0.48
CWP, g m^{-2}	Jan.	171.0	49.8	15908	-121.2	151.5	-70.9	71.3	0.34
	Apr.	164.0	50.1	15908	-113.9	127.7	-69.4	70.1	0.54
	Jul.	228.1	93.4	15908	-134.7	171.3	-59.1	66.7	0.23
	Oct.	205.3	66.7	15908	-138.6	156.4	-67.5	69.3	0.48

3.4 Feedbacks of Anthropogenic Aerosols to Meteorology

East Asia has been experiencing high economic development, industrialization and urbanization accompanied with heavy air pollution. To study the climatic effects of anthropogenic aerosols in East Asia, Figure 3.17 shows spatial distributions predicted from the 2001 baseline simulations with 12-bin WRF/Chem and absolute differences of PM number concentrations, AOD, CDNC, COT, LWP, and total precipitation (TP, which includes convective and non-convective precipitation) between the baseline simulations and those without anthropogenic aerosols. As shown in Figure 3.17a, the spatial distribution of total aerosol number concentrations over all size bins over East Asia are about 12 times higher compared with those simulated over the U.S. by Zhang et al. (2010d) in January and July, 2001, although Zhang et al. (2010d) studied the feedbacks of total aerosols, instead of anthropogenic aerosols only. Due to the increase of anthropogenic aerosols, AOD increases by about 0.09 to 0.20 (or by 73%-228%) during the four months in 2001 (see Figure 3.17b). Figures 3.17c, d, e and f show the direct and semi-direct effects of anthropogenic aerosols, suggesting that they can increase column CDNC (from 4.3×10^5 to 9.6×10^5 cm^{-2}, or from 40.2% to 76.4%), COT (from 0.52 to 1.36, or from 14.3% to 25.3%), and LWP (from 1.1 to 11.2 g cm^{-2}, or from 5.4% to 44.8%) during the four months in 2001. The total precipitation decreases from 0.02 to 0.11 mm day^{-1} (or by 0.7% to 2.7%).

Figure 3.17 Spatial distributions and absolute differences for (a) total PM number concentrations, (b) AOD, (c) CDNC, (d) COT, (e) LWP, and (f) total precipitation due to anthropogenic aerosols during the four months (January, April, July and October) in 2001. Spatial distributions are based on WRF/Chem with 12-bin and COMB, and the absolute differences are taken between simulations with and without anthropogenic aerosols.

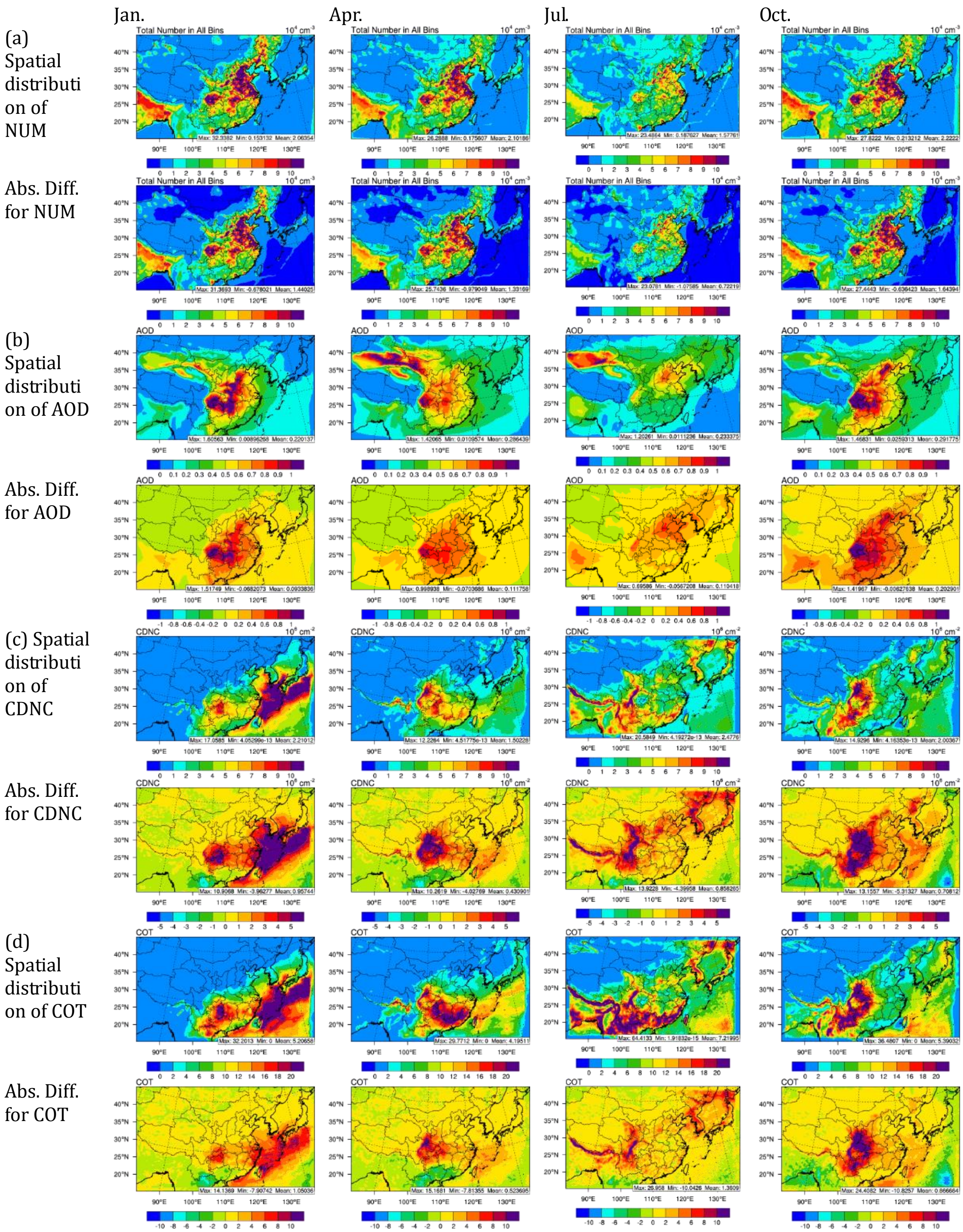
Jan.
Apr.
Jul.
Oct.
(a) Spatial distribution of NUM
Abs. Diff. for NUM
(b) Spatial distribution of AOD
Abs. Diff. for AOD
(c) Spatial distribution of CDNC
Abs. Diff. for CDNC
(d) Spatial distribution of COT
Abs. Diff. for COT
Total Number in All Bins
10^4 cm^-3
AOD
CDNC
10^8 cm^-2
COT

(e)
Spatial
distributi
on of
LWP

Abs. Diff.
for LWP

(f)
Spatial
distributi
on of TP

Abs. Diff.
for TP

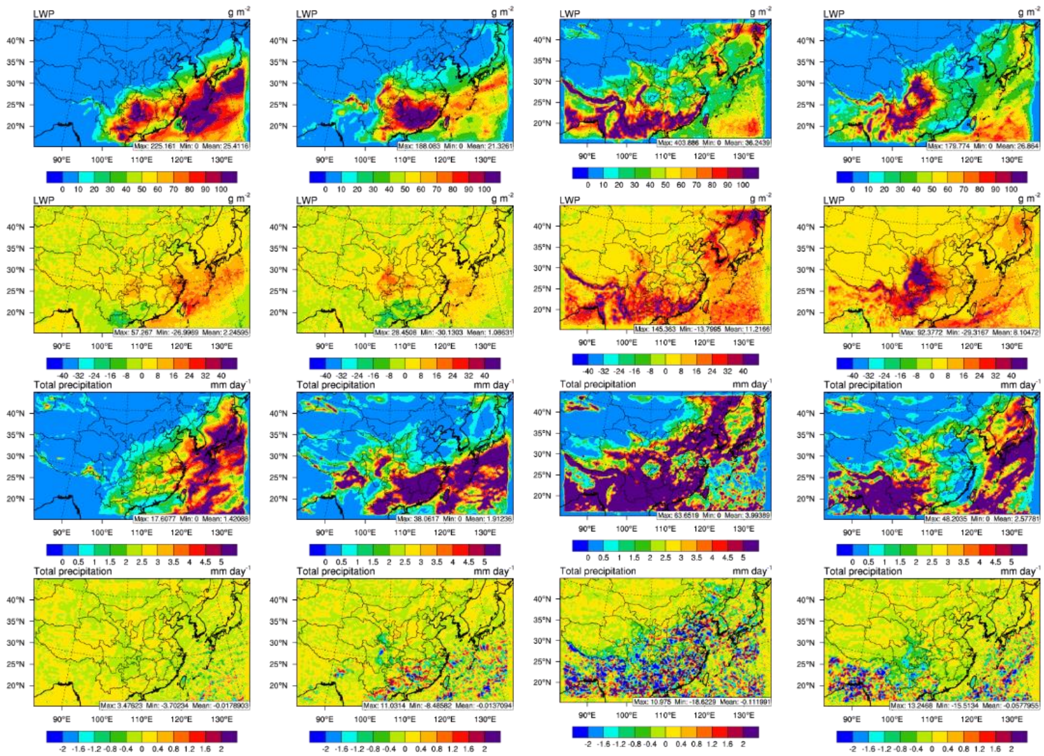

Figure 3.18 shows the direct and semi-direct feedbacks of anthropogenic aerosols on radiation, LH, 2-m temperature, and PBLH. Anthropogenic aerosols over East Asia can reduce surface net shortwave radiation (SNSR) by up to 42.5 W m^{-2} in January, 52.8 W m^{-2} in April, 48.2 W m^{-2} in July, and 51.1 W m^{-2} in October (or by 36.6%, 24.1%, 24.4%, and 33.2% respectively), 2 meter (2-m) temperature by up to 0.74 ºC in January, 0.54 ºC in April, 0.34 ºC in July, and 0.83 ºC in October and PBLH by up to 86.5 m in January, 108.4 m in April, 76.8 m in July, and 125.9 m in October (or by 20.3%, 16.6%, 11.2%, and 22.9% respectively) over the Asian continent. Table 3.9 summarizes the comparisons of indirect, direct, and semi-direct effects of aerosols between East Asia and continental U.S. (CONUS) (Zhang et al., 2010). Although Zhang et al. (2010d) studied the feedbacks of total aerosols, instead of anthropogenic aerosols only in this study, the indirect, direct and semi-direct effects of anthropogenic aerosols in East Asia are much more significant than total aerosol (including both of anthropogenic and natural aerosols) effects in CONUS due to high PM concentrations resulted from its severe pollution.

Figure 3.18 Spatial distribution and absolute differences for SNSR, LH, T2, and PBLH due to anthropogenic aerosols during the four months (January, April, July and October) in 2001. Spatial distributions are based on WRF/Chem with 12-bin and COMB, and the absolute differences are taken between simulations with and without anthropogenic aerosols.

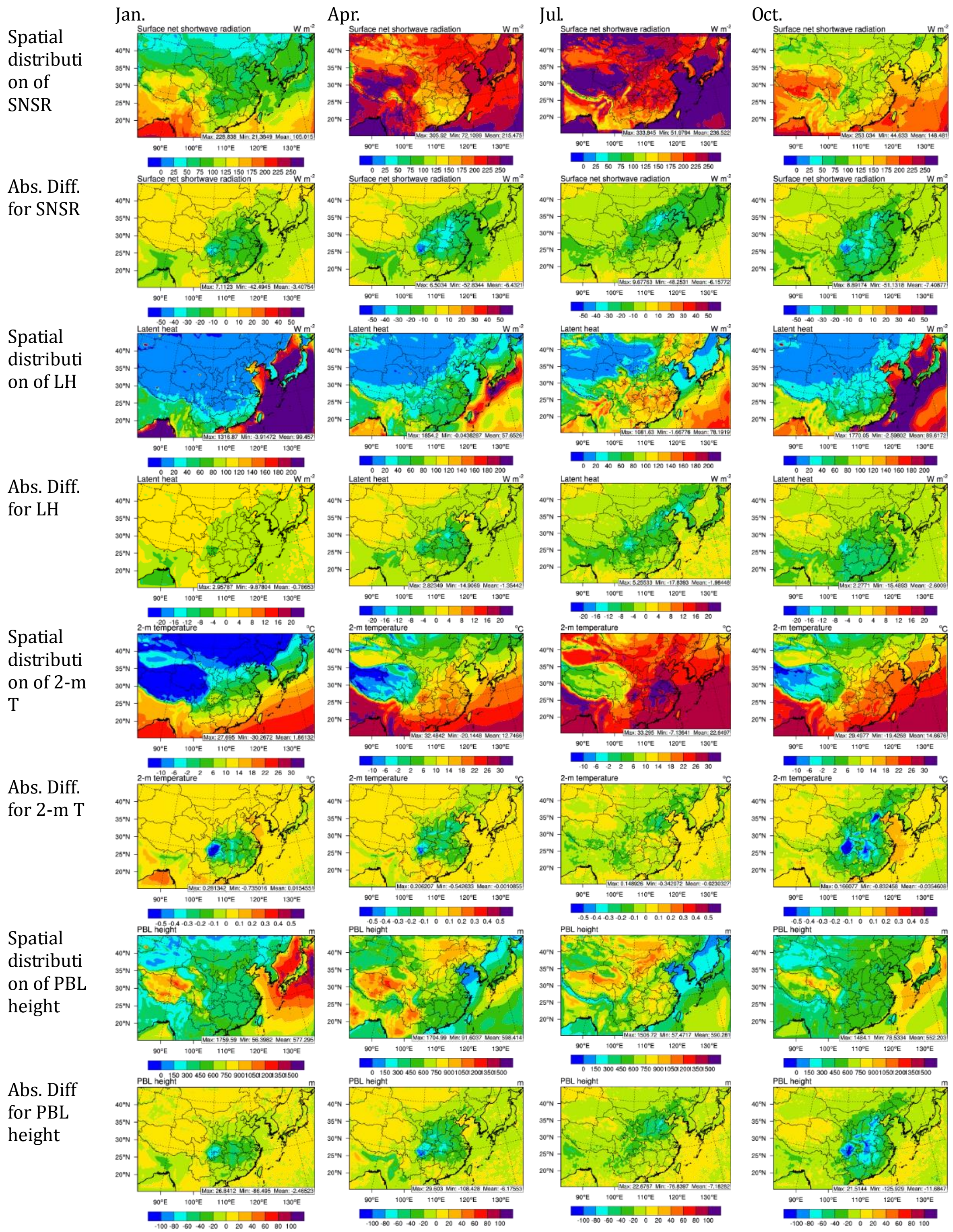
Jan.
Apr.
Jul.
Oct.
Spatial distribution of SNSR
Abs. Diff. for SNSR
Spatial distribution of LH
Abs. Diff. for LH
Spatial distribution of 2-m T
Abs. Diff. for 2-m T
Spatial distribution of PBL height
Abs. Diff for PBL height
Surface net shortwave radiation
Latent heat
2-m temperature
PBL height

Table 3.9 Comparisons of the effects of aerosols between East Asia and continental U.S. (CONUS) in 2001 (Note: only anthropogenic aerosols for East Asia, but both of anthropogenic and natural aerosols for CONUS).

Variables	Month	East Asia (This study)	CONUM (Zhang et al., 2010)
		Up to value	Up to value
SNSR[a], W m^{-2}	January	-42.5	-11.4
	July	-48.3	-39.5
T2[b], ^{o}C	January	-0.74	-0.16
	July	-0.34	-0.37
PBLH[c], m	January	-85.5	-22.4
	July	-76.8	-92.4
COT[d]	January	14.1	2.1
	July	27.0	10.3

[a]SNSR – Shortwave net surface radiation
[b]T2 – Temperature at 2 meter
[c]PBLH – Planetary boundary layer height
[d]COT – Cloud optical thickness

4. APPLICATION AND EVALUATION OF WRF-CAM5

4.1 Model Setup and Inputs

In this section, the WRF-CAM5 with default nucleation and without any nucleation are applied to East Asia at a horizontal resolution of 36-km. The vertical resolution is 23 layers from the surface to ~50 mbar. Three months (July, August, and September) in 2008 are selected for testing the model performance. The meteorological and chemical initial and boundary conditions are the same as WRF/Chem. One of the main differences in aerosol treatments between WRF/Chem and WRF-CAM5 lies in the size distribution. Unlike the sectional size bins used in MOSAIC in WRF/Chem, the modal aerosol module (MAM) in WRF-CAM5 uses a modal size representation with three log-normally-distributed modes (i.e., Aitken, accumulation, and coarse modes). Table 4.1 shows the details of the mode information used in MAM3. In addition, as mentioned in section 3.3.1, WS10 has been greatly overpredicted by WRF, which might be due to either too much mixing vertically or not enough drag in low-level (Mass et al., 2010). Thus, during the WRF-CAM5 test, the friction velocity is multiplied by a factor of 1.5 in PBL module, to increase the low-level drag as recommended by Mass et al. (2010).

Table 4.1 Geometric standard deviations (σ_g)and geometric number mean diameter (d_{pg}, μm).

Mode	σ_g	d_{pg} (μm)
MAM3[a]		
Aitken	1.6	2.82×10^{-2}
Accumulation	1.8	1.25×10^{-1}
Coarse	1.8	1.71

[a]MAM3 – Modal aerosol module with three lognormal modes

4.2 Evaluation for Summer 2008

Tables 4.2a, b, and c summarize the performance statistics for default nucleation of WRF-CAM5 using NCDC data and satellite data, respectively. The evaluation suggests that the wind speed has been greatly improved (with an NMB of -5.6%) compared with WRF/Chem (with an NMB of 49.1%, see Table 3.2) in July 2008. However, both AOD and PM_{10} have been largely underestimated, which may be due to the decrease of wind speed, and no dust and emissions for Aitken mode particles. This is because the dust module used here is DEAD, which is very sensitive to wind speed (Zender et al., 2003; K. Wang et al., 2012). As a result of decreased WS10, the dust concentrations decreased, which in turn decrease AOD. Figure 4.1 shows the zonal mean values of particle number concentrations for three modes, indicating that no emissions are allocated to the Aitken mode in the simulations and nearly all particles in Aitken mode are generated from nucleation. T2, Q2 and P are simulated reasonably well (with NMBs of -6.9% to 3.0%) and R values of 0.57 to 0.94. However, the precipitation is poorly simulated with a NMB of -16% and a R value of 0.05. PM_{10} concentrations are underpredicted due in part to underestimate in dust emissions and $PM_{2.5}$ concentrations. All those column variables (CO, NO_2, O_3, and SO_2) are simulated reasonably well with NMBs of -37.8% to 13.8% and R values of 0.54 to 0.72. Cloud fraction is reasonably well predicted, but the aerosol optical depth, cloud condensation nuclei, and cloud optical thickness are significantly underpredicted with NMBs of -74.8% to -65.9%. In addition, the simulation with the COMB nucleation generates more Aitken mode particles compared with the default one used in WRF-CAM5. Overall, WRF-CAM5 demonstrates reasonably good skills in capturing most meteorological variables and chemical concentrations in East Asia.

Table 4.2 Performance statistics using default WRF-CAM5.

(a) for meteorological variables using NCDC data

Variable	Dataset	Mean Obs	Mean Mod	Data #	MB	RMSE	NMB, %	NME, %	R
T2, °C	NCDC	25.0	23.3	317415	-1.7	25.7	-6.9	15.2	0.57
P, mb	NCDC	956.7	942.8	188655	-13.9	1324.7	-1.5	23.1	0.94
Q2, g kg^{-1}	NCDC	14.6	15.1	188514	0.5	4.5	3.0	11.1	0.89
WS10, m s^{-1}	NCDC	2.5	2.4	316653	-0.1	4.5	-5.6	65.0	0.33
WD10,	NCDC	183.2	178.2	283878	-4.9	13392.1	-2.7	47.3	0.15
24-h rain, mm	NCDC	4.9	4.1	22321	-0.8	244.6	-16	1.4	0.05

(b) for chemical, aerosol and cloud variables using satellite data

Variable	Dataset	Mean Obs	Mean Mod	Data #	MB	RMSE	NMB, %	NME, %	R
CO, $\times 10^{17}$ molecules cm^{-2}	MOPITT[c]	17.5	18.0	15606	1.2	5.4	6.7	22.4	0.54
NO_2, $\times 10^{15}$ molecules cm^{-2}	SCIAMACHY[a]	1.8	1.1	12649	-0.7	2.8	-37.8	57.3	0.67
O_3, DU	OMI[b]	39.6	33.0	15898	-6.6	8.9	-16.8	18.7	0.72
SO_2, DU	SCIAMACHY	0.14	0.16	10392	0.02	0.20	13.8	82.0	0.58
AOD	MODIS[d]	0.31	0.11	15047	-0.21	0.29	-65.9	67.0	0.55
CCN5[e], $\times 10^{8}$ # cm^{-2}	MODIS	6.4	2.2	5771	-4.3	9.8	-66.2	66.3	0.65
CF[f] (%)	MODIS	0.68	0.74	15908	0.06	0.2	8.6	0.19	0.77
COT[g]	MODIS	17.4	4.4	15908	-13.0	13.7	-74.8	75.0	0.40
CWP[h], g m^{-2}	MODIS	219.0	324.9	15908	105.9	309.3	48.4	93.2	0.31

Table 4.2 Continued

(c) for chemical variables using surface measurement data

Variable	Dataset	Mean Obs	Mean Mod	Data #	MB	RMSE	NMB, %	NME, %	R
Mainland China									
PM_{10}, µg cm^{-3}	API	87.6	36.0	888	-51.7	62.5	-59.0	64.6	0.28
SO_2, ppb	API	27.5	19.2	117	-8.3	17.3	-30.2	50.5	0.59
NO_2, ppb	API	35.2	19.5	117	-15.7	30.9	-44.5	75.5	0.40
Hong Kong									
PM_{10}, µg m^{-3}	EPD	28.2	17.4	744	-10.8	21.2	-38.3	44.9	0.61
$PM_{2.5}$, µg m^{-3}	EPD	20.7	17.1	744	-3.6	15.3	-17.6	36.8	0.64
SO_2, µg m^{-3}	EPD	24.9	6.3	744	-18.6	24.3	-74.7	74.8	0.50
NO_2, µg m^{-3}	EPD	37.8	11.1	744	-26.7	31.7	-70.7	70.7	0.25
NO, µg m^{-3}	EPD	49.8	0.8	744	-48.9	57.6	-98.4	98.4	0.32
CO, µg m^{-3}	EPD	572.7	276.7	744	-296.0	315.2	-51.7	51.7	0.57
O_3, µg m^{-3}	EPD	24.9	6.3	744	-18.6	24.3	-74.7	74.8	0.50

[a]SCIAMACHY – Scanning Imaging Absorption spectrometer
[b]OMI – Ozone Monitoring Instrument
[c]MOPITT – Measurements Of Pollution In The Troposphere
[d]MODIS – Terra moderate-resolution imaging
[e]CCN5 – Cloud condensation nuclei at 0.5% super-saturation
[f]CF – Cloud fraction
[g]COT – Cloud optical thickness
[h]CWP – Cloud water path; AOD – Aerosol optical depth

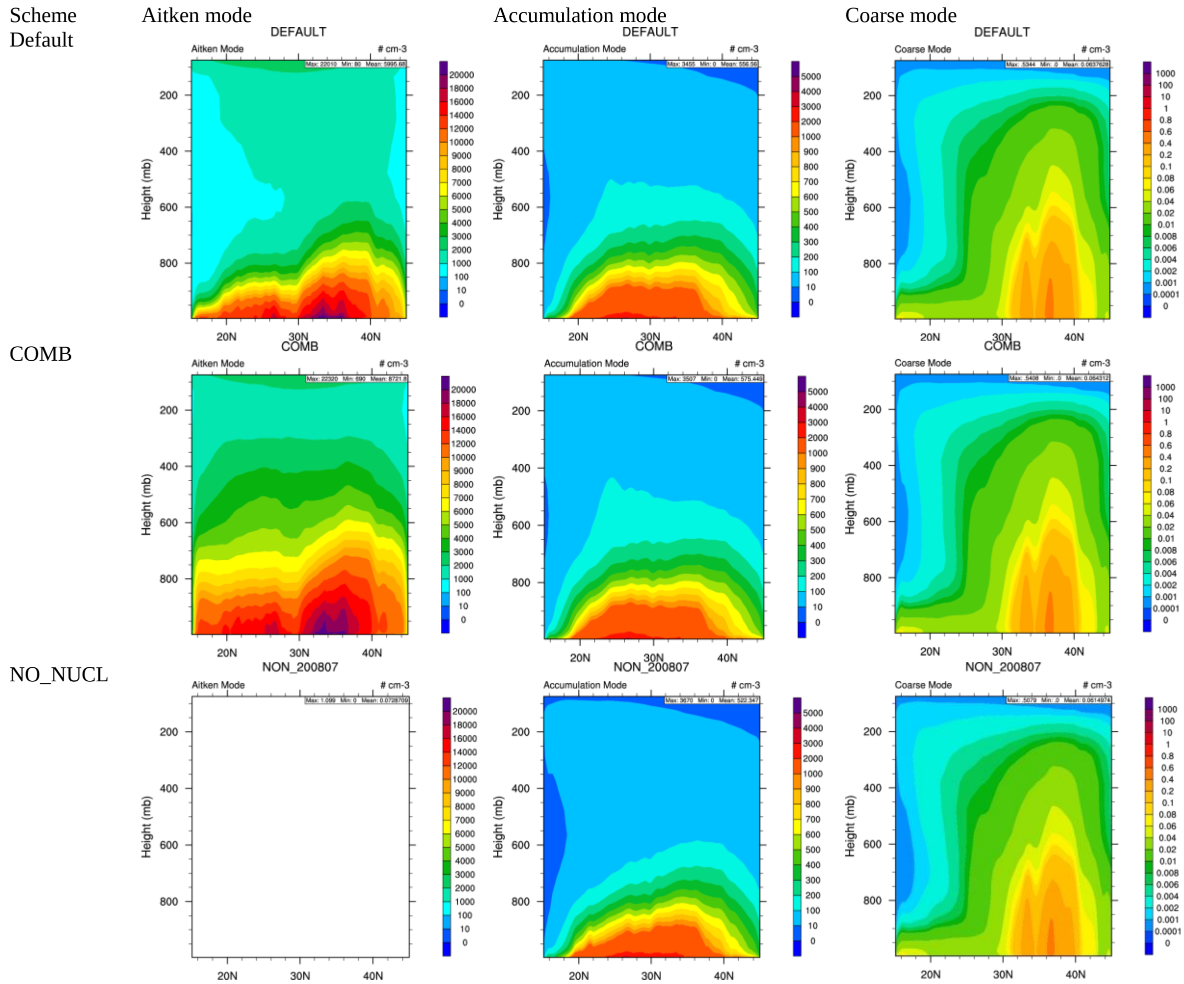

Figure 4.1 Zonal mean values of number concentrations for three modes from WRF-CAM5 with default and COMB nucleation schemes, and without nucleation scheme during July – September, 2008.

5. SUMMARY AND FUTURE WORK

5.1 Summary and Major Findings of WRF/Chem Modeling

East Asia has been selected for studying the new particle formation (NPF) events, testing various nucleation parameterizations, and examining the sensitivity of model performance to nucleation parameterizations. To explicitly track the formation and growth of new particles, the default 8-bin structure used in MOSAIC in WRF/Chem is modified first and then extended to 12-bin. Several nucleation schemes (BO08, WA11, YU10, and COMB) and one particle early growth scheme (LE07) have been incorporated into WRF/Chem with 12-bin. Different nucleation parameterizations are used over urban and non-urban areas and within and above PBLH. WRF/Chem simulations are conducted for July 2008 during which NPF events occurred in Beijing and observational data of relevant variables are available during the CAREBeijing2008 campaign. The simulated N-PSD can be improved using WRF/Chem with12-bin as oppose to the modified 8-bin structure. The simulations with individual nucleation parameterizations including WA11_ACTI, BO08_ACTI, YU10, and a combination of them identify the optimal nucleation parameterization (i.e., COMB), in which WA11_ACTI is used for urban areas and BO08_ACTI for non-urban areas in the PBL, and YU10 is applied above the PBL. Among all WRF/Chem simulations, the simulation with COMB and 12-bin gives the best overall performance in reproducing the reported NPF events in Beijing and the whole atmosphere. However, there remain some uncertainties. For example, the model overpredicts the concentrations of key precursor (H_2SO_4) of NPF, but underpredicts the condensation sink, growth rate, and PM concentrations. Those uncertainties can be explained to a large extent to the uncertainties in model predictions of four key variables in accurately simulating NPF events including the atmospheric oxidation capability, precipitation, background PM concentrations and particle early growth. The modeling results also show that low RH, high H_2SO_4 concentration, low background particle concentration, and low CS are four favorable conditions for NPF events in Beijing, which are consistent with their impacts on NPF events based on observational data analyses.

To study aerosol-cloud-precipitation interactions and their seasonal variations, WRF/Chem with COMB is futher applied to simulate four months (January, April, July and October) in 2001 during which heavy pollution occurred. The comprehensive model evaluation shows that the model can well predicts the near surface temperature, water vapor, and pressure, but larger biases exist in the predictions of the daily precipitation and wind speeds. Comparing with the satellite data, the model predicts AOD and column mass concentrations of CO, NO_2, O_3, and SO_2 reasonably well (except for the column O_3 in January, and CO in January and October 2001). However, comparing with the surface measurement data, the model underpredicts the concentrations of PM_{10}, NO_x, CO, SO_2, and VOCs. The dust storms from northwestern China, northern China and southern Mongolian are well captured with the newly-implemented online dust emission module. Due to high concentrations of anthropogenic aerosols over East Asia, the effects of anthropogenic aerosols are significant. The simulation results indicate that the anthropogenic aerosols can increase AOD by 64.0 - 228.3%, CDNC by 40.2 - 76.4%, COT by 14.3 - 25.3%, and LWP by 5.4 - 44.8% during the four months in 2001. In addition, they can reduce surface net shortwave radiation by up to 42.5 – 52.8 W m^{-2} (or by 24.1 - 36.6%), 2-m temperature by up to 0.34 - 0.83 ^{o}C and PBL height by up to 76.8 – 125.9 m (or by 11.2 - 22.9%) over the Asian continent.

5.2 Summary and Major Findings of WRF-CAM5 Modeling

For WRF-CAM5, the wind speed has been greatly improved (with NMBs changing from 49.1% to -5.6%) by increasing the low-level drag. Mass et al. (2010) indicated that the overprediction of wind speeds by WRF may be due to either too much mixing vertically or not enough drag in low-level. Some meteorological variables (T2, Q2 and P) are simulated reasonably well (with NMBs of -6.9% to 3.0%) and R of 0.57 to 0.94. However, the precipitation is poorly estimated with R of 0.05, which might be due to the large uncertainties in cloud formation and aerosol-cloud-precipitation interactions. PM_{10} concentrations are underpredicted due in part to underestimate in dust emissions and $PM_{2.5}$ concentrations. All those column variables (CO, NO_2, O_3, and SO_2) are simulated reasonably well with NMBs of -37.8% to 13.8% and R values of 0.54 to 0.72. Cloud fraction is reasonably well predicted, but the aerosol optical depth, cloud condensation nuclei, and cloud optical thickness are significantly underpredicted with NMBs of -74.8% to -65.9%. In addition, the simulation with the COMB nucleation generates more Aitken mode particles compared with the default one used in WRF-CAM5. Overall, WRF-CAM5 demonstrates reasonably good skills in capturing most meteorological variables and chemical concentrations in East Asia.

5.3 Limitations of Current Work

The July 2008 case study in Beijing indicates the importance of accurate predictions of the atmospheric oxidation capability, precipitation, background PM concentrations, and particle early growth in accurately reproducing the NPF events. In addition, large uncertainties still exist in nucleation mechanisms in the real atmosphere. A coarse resolution of 36-km is used in all simulations in this work, which may explain in part the biases in model predictions, e.g., the fraction of urban areas is small compared with other land cover, so only the fraction in each grid can be used in the coarse resolution, which result in that the model might not be able to reproduce the NPF event at a specific site. For example, two different representive sites (such as urban and rural) might be located in the same grid due to the coarse resolution. However, the NPF may be exactly the same in each grid in the modeling results, which is not true in the real atmosphere. Using a finer grid resolution with nesting methods will likely improve the model predictions of relevant variables during the NPF events. In addition, only two different types (urban and non-urban) of land covers are considered in this study. A total of 24 types of land covers are classified in model. Different land covers indicate different ambient conditions under which the nucleation mechanisms may be quite different due to different emissions of gaseous precursors (such as SO_2), thus affecting new particle formation.

5.4 Future Work

Based on the limitations mentioned above, several future work can be identified to improve the model performances in nucleation. First, the predictions of the atmospheric oxidation capability, precipitation, background PM concentrations, and particle early growth should be improved. Second, nesting simulations should be performed using finer resolutions. Third, more accurate nucleation schemes should be investigated and used in the model. Finally, sensitivity simulations using more reactive SO_2 emissions should be performed.

REFERENCES

Abdul-Razzak, H., and S. J. (1998), Ghan, A parameterization of aerosol activation 1. Single aerosol type, *J. Geophys. Res., 103*, 6123-6131.

Abdul-Razzak, H., and S. J., Ghan (2000), A parameterization of aerosol activation 2. Multiple aerosol types, *J. Geophys. Res., 105,* D5, 6837-6844.

Abdul-Razzak, H., and S. J., Ghan (2002), A parameterization of aerosol activation 3. Sectional representation, *J. Geophys. Res., 107,* D34026, doi:10.1029/2001JD000483.

Aitken, J. A. (1987), On some nuclei of cloudy condensation, *Trans. Roy. Soc. XXXIX*, 15-25.

Akimoto, H. (2003), Global air quality and pollution, *Science*, *302,* 1716-1719.

Albrecht, B. A. (1989), Aerosols, cloud microphysics, and fractional cloudiness, *Science, 245,* 1227-1230.

Andreae, M.O., D., Rosenfeld, P., Artaxo, A.A., Costa, G.P., Frank, K.M., Longo, and M.A.F., Silva-Dias (2004), Smoking rain clouds over the Amazon, *Science, 303,* 1337-1342.

Asmi, E., A., Frey, A., Virkkula, M., Ehn, H. E., Manninen, H., Timonen, O., Tolonen-Kivimaki, M., Aurela, R., Hillamo, and M., Kulmala (2010), Hygroscopicity and chemical composition of Antarctic sub-micrometre aerosol particles and observations of new particle formation, *Atmos. Chem. Phys.*, 10, 4253-4271.

Binkowski, F. S., and S. J. Roselle, Models-3 Community Multiscale Air Quality (CMAQ) model aerosol component, 1, Model description, *J. Geophys. Res., 108*, 4183, doi:10.1029/2001JD001409, 2003.

Birmili, W. and A. Wiedensohler (2000), New particle formation in the continental boundary layer: Meteorological and gas phase parameter influence. *Geophys. Res. Lett. 27(20),* 3325-3328.

Birmili, W., H. Berresheim, C. Plass-Dulmer, T. Elste, S. Gilge, A. Wiedensohler and U. Uhrner (2003), The Hohenpeissenberg aerosol formation experiment (HAFEX): a long-term study including size-resolved aerosol, H2SO4, OH, and monoterpenes measurements. *Atmos. Chem. Phys. 3,* 361-376.

Boy, M., J., Kazil, R. L., Turnipseed, R. L., Mauldin, E., Kosciuch, J., Greenberg, J., Rathbone, J., Smith, A., Held, K., Barsanti, B., Wehner, S., Bauer, A., Wiedensohler, B., Bonn, M., Kulmala, and A., Guenther (2008), New particle formation in the front range of the Colorado rocky mountains, *Atmos. Chem. Phys., 8,* 1577-1590.

Brennan, J.I., Y.J., Kaufman, H., Koren, and R.R., Li (2005), Aerosol-cloud interaction-misclassification of MODIS Clouds in heavy aerosol, *IEEE Trans. Geosci. Remote Sens., 43,* 911-915.

Bretherton, C.S., S., Park, (2009), A new moist turbulence parameterization in the community atmosphere model, *J. Climate, 22*, 3422-3448.

Cai, C., F., Geng, X., Tie, Q., Yu, and J., An (2010a), Characteristics and source apportionment of VOCs measured in Shanghai, China, *Atmos. Environ., 44*, 5005-5014.

Cai, C., F., Geng, X., Tie, Q., Yu, L., Peng, and G., Zhou (2010b), Characteristics of ambient volatile organic compounds (VOCs) measured in Shanghai, China, *Sensors, 10,* 7843-7862.

Carmichael, G.R., Y., Tang, G., Kurata, I., Uno, D.G., Streets, N., Thongboonchoo, J.-H., Woo, S., Guttikunda, A., White, T., Wang, D.R., Blake, E., Atlas, A., Fried, B., Potter, M.A., Avery, G.W., Sachse, S.T., Sandholm, Y., Kondo, R.W., Talbot, A., Bandy, D., Thorton, and A.D., Clarke (2003), Evaluating regional emission estimates using the TRACE-P observations, *J. Geophys. Res.*, 108, NO. D21, 8810, doiL:10.1029/2002JD00.

Charlson, R.J., S.E., Schwartz, J.M., Hales, R.D., Cess, J.A., Coakley, J.E., Hansen, and D.J., Hofmann (1992), Climate forcing by anthropogenic aerosols. *Science, 255,* 423-430.

Chapman, E. G., Jr., W. I., Gustafson, R. C., Easter, J. C., Barnard, S. J., Ghan, M. S., Pekour, and J. D., Fast (2009), Coupling aerosol-cloud-radiative processes in the WRF-Chem model: Investigating the radiative impact of elevated point sources, *Atmos. Chem. Phys., 9,* 945-964.

Cheng, W.Y.Y., and W.J., Steenburgh (2005), Evaluation of surface sensible weather forecasts by the WRF and the Eta Models over the Western United States, Weather and Forecasting, 20, 812-821.

Chou, M. D., and J. S., Max (1994), An efficient thermal infrared radiation parameterization for use in general circulation models. *NASA Tech. Memo.,* 84.

Clarke, A. D., V. Kapustin, S. Howell, K. Moore, B. Lienert, S. Masonis, T. Anderson, and D. Covert (2003), Sea-salt size distributions from breaking waves: Implications for marine aerosol production and optical extinction measurements during SEAS, *J. Atmos. Ocean. Technol., 20,* 1362-1374.

Cuitius, J. (2006), Nucleation of atmospheric aerosol particles, *C. R. Physique, 7,* 1027-1045.

Dal Maso, M., Kulmala, M., Riipinen, I., Wagner, T., Hussein, P. P., Aalto, and K. E. J., Lehtinen (2005), Formation and growth of fresh atmospheric aerosols: eight years of aerosol size distribution data from SMEAR II, Hyytiala, Finland, *Boreal Environ. Res.*, *10*, 323-336.

Duan, J., J., Tan, L., Yang, S., Wu, and J., Hao (2008), Concentration, sources and ozone formation potential of volatile organic compounds (VOCs) during ozone episode in Beijing, *Atmos. Res., 88,* 25-35.

Enghoff, M. B., J. O. P., Pedersen, U. I., Uggerhoj, S. M., Paling, and H., Svensmark (2011), Aerosol nucleation induced by a high energy particle beam, *Geophys. Res. Lett., 38,* L09805, doi:10.1029/2011GL047036.

Fahey, K.M., and S.N., Pandis (2001), Optimizing model performance: variable size resolution in cloud chemistry modeling, *Atmos. Environ.*, 35, 4471-4478.

Fast, J. D., Jr., W. I., Gustafson, R. C., Easter, R. A., Zaveri, J. C., Barnard, E. G., Chapman, and G. A., Grell (2006), Evolution of ozone, particulates, and aerosol direct forcing in an urban area using a new fully-coupled meteorology, chemistry, and aerosol model. *J. Geophys. Res., 111,* D21305. Doi:10.1029/2005JD006721.

Field, P.R., R.J., Hogan, P.R.A., Brown, A., Illingworth, T.W., Choularton, and R.J., Cotton (2005), Parameterization of ice-particle size distributions for mid-latitude stratiform cloud, *Q. J. Roy. Meteor. Soc., 131*, 1997-2017.

Gao, J., T., Wang, X., Zhou, W., Wu, and W., Wang (2009), Measurement of aerosol number size distributions in the Yangtze River Delta in China: Formation and growth of particles under polluted conditions, *Atmos. Environ.*, 43, 829-836.

Gao, J., F., Chai, T., Wang, and W., Wang (2011), Particle number size distribution and new particle formation (NPF) in Lanzhou, *Particuology*, 9, 611-618.

Gattett, T.J., and P.V., Hobbs (1995), Long-range transport of continental aerosols over the Atlantic Ocean and their effects on cloud droplet size distributions, *J. Atmos. Sci., 52,* 2977-2984.

Ginous, P., M., Chin, I., Tegen, J., Prospero, B. N., Holben, O., Dubovik, and S.J., Lin (2001), Sources and distributions of dust aerosols simulated with the GOCART model, *J. Geophys. Res., 106*, 20225-20274, 2001.

Gong, S.L. (2003), A parameterization of sea-salt aerosol source function for sub- and super-micron particles, *Global Biogeochem. Cycles, 17,* 1097, doi:10.1029/2003GB002079.

Gong, S. L., X. Y., Zhang, T. L., Zhao, I. G., McKendry, D. A., Jaffe, and M., Lu (2003), Characterization of soil dust aerosol in China and its transport and distribution during 2001 ACE-Asia, *J. Geophys. Res.*, 108, D9, 4262, doi:10.1029/2002JD002633.

Grell, G. A., S. E., Peckham, R., Schmitz, S. A., Mckeen, G., Frost, W. C., Skamarock, and B., Eder (2005), Fully coupled "online" chemistry within the WRF model, *Atmos. Environ.*, 39, 6957-6975.

Grell, G. A., and D., Devenyi (2002), A generalized approach to parameterizing convection combining ensemble and data assimilation techniques, *Geophys. Res. Lett.*, 29(14), 1963.

Guenther, A., T., Karl, P., Harley, C., Wiedinmyer, P.I., Palmer, and C., Geron (2006), Estimates of global terrestrial isoprene emissions using MEGAN (Model of Emissions of Gases and Aerosols from Nature), *Atmos. Chem. Phys., 6*, 3181-3210.

Gultepe, I., G.A., Isaac, and S.G., Cober (2001), Ice crystal number concentration versus temperature for climate studies, Internat, *J. Climatol., 21*, 1281-1302.

Guo, H., D. W., Wang, K., Cheung, Z. H., Ling, C. K., Chan, and X. H., Yao (2012), Observation of aerosol size distribution and new particle formation at a mountain site in subtropical Hong Kong, *Atmos. Chem. Phys.*, *12,* 9923-9939.

Gustafson, W. I., E. G., Chapman, S. J., Ghan, R. C., Easter, and J. D., Fast (2007), Impact on modeled cloud characteristics due to simplified treatment of uniform cloud condensation nuclei during NEAQS 2004, *Geophys. Res. Lett.*, 34, L19809, doi:10.1029/2007GL0300321.

Gunn, R., and B.B., Phillips (1957), An experimental investigation of the effect of air pollution on the initiation of rain, *J. Meteor., 14,* 272-280, 1957.

Hamed, A., J., Joutsensaari, S., Mikkonen, L., Sogacheva, M. D., Maso, M., Kulmala, F., Cavalli, S., Fuzzi, M. C., Facchini, S., Decesari, M., Mircea, K. E. J., Lehtinen, and A., Laaksonen (2007), Nucleation and growth of new particles in Po Valley, Italy, *Atmos. Chem. Phys.*, 7, 355-376.

Haywood, J. M., and O. Boucher (2000), Estimates of the direct and indirect radiative forcing due to tropospheric aerosols: a review, *Rev. Geophys., 38,* 513-543.

He, S.Z., Z.M., Chen, X., Zhang, Y., Zhao, D.M., Huang, J.N., Zhao, T., Zhu, M., Hu, and L.M., Zeng (2010), Measurement of atmospheric hydrogen peroxide and organic peroxides in Beijing before and during the 2008 Olympic Games: Chemical and physical factors influencing their concentrations, *J. Geophys. Res., 115*, D17307, doi:10.1029/2009JD013544.

Herrmann, E., A. J., Ding, T., Petaja, X. Q., Yang, J. N., Sun, X. M., Qi, H., Manninen, J., Hakala, T., Nieminen, P. P., Aalto, V.-M., Kerminen, M., Kulmala, and C. B., Fu (2013), New particle formation in the western Yangtze River Delta: fist data from SORPES-station, *Atmos. Chem. Phys. Discuss., 13,* 1455-1488.

Hinds, W. C. (1999), Aerosol Technology: Properties, Behavior, and Measurement of Airborne Particles (Second Edition). New York, John Wiley & Sons.

Hirsikko, A., L., Laakso, U., Horrak, P. P., Aalto, V. M., Kerminen, and M., Kulmala (2005), Annual and size dependent variation of growth rates and ion concentrations in boreal forest, *Boreal Environ. Res.*, 10, 357-369.

Hong, S. Y., Y., Noh, and J., Duhhia (2006), A new vertical diffusion package with an explicit treatment of entrainment processes, *Mon. Wea. Rev.*, *134,* 2318-2341.

Hussein, T., M. Dal Maso, T. Petaja, I. K. Koponen, P. Paatero, P. P. Aalto, K. Hameri and M. Kulmala (2005), Evaluation of an automatic algorithm for fitting the particle number size distributions. *Boreal Environ. Res. 10(5)*, 337-355.

Hussein, T., J., Martikainen, H., Junninen, L., Sogacheva, R., Wagner, M. D., Maso, I., Riipinen, P. P., Aalto, and M., Kulmala (2008), Observation of regional new particle formation in the urban atmosphere, *Tellus*, 60B, 509-521.

Iacono, M. J., J. S. Delamere, E. J. Mlawer, M. W. Shephard, S. A. Clough, and W. D. Collins (2008), Radiative forcing by long-lived greenhouse gases: Calculations with the AER radiative transfer models, *J. Geophys. Res.*, *113,* D13103, doi:10.1029/2008JD009944.

Iida, K., M. R., Stolzenburg, P. H., McMurry, and J. N., Smith (2008), Estimating nanoparticle growth rates from size-dependent charged fractions: Analysis of new particle formation events in Mexico City, *J. Geophys. Res.*, 113, D05207, doi:10.1029/2007JD009260.

Ito, A., and J. E., Penner (2005), Historical emissions of carbonaceous aerosols from biomass and fossil fuel burning for the period 1870-2000, *Global Biogeochem. Cycles*, GB2028, doi:10.1029/2004GB002374.

IPCC (The Intergovernmental Panel on Climate Change) (2007): IPCC Fourth Assessment Report: Climate change 2007: the physical science basis, edited by: Solomon, S., Qin, D., Manning, M., Chen, Z., Marquis, M., Averyt, K. B., Tignor, M., and Miller, H. L., Cambridge Univ. Press, United Kingdom and New York.

Jacob, D.J., J.H., Crawford, M.M., Kleb, V.S., Connors, R.J., Bendura, J.L., Raper, G.W., Sachse, J.C., Gille, L., Emmons, and C.L., Heald (2003), Transport and Chemical Evolution over the Pacific (TRACE-P) aircraft mission: Design, execution, and first results, *J. Geophys. Res.*, 108, NO. D20, 9000, doi:10.1029/2002jd003276.

Jacobson, M.Z., R.P., Turco, E.J., Jensen, and O.B., Toon (1994), Modeling coagulation among paricles of different composition and size, *Atmos. Environ., 28,* 1327-1338.

Jacobson, M.Z. (1998), Studying the effects of aerosols on vertical photolysis rate coefficient and temperature profiles over an urban airshed, *J. Geophys. Res.*, 103, 10,593-10604.

Jacobson, M.Z., Y.J., Kaufman, and Y., Rudich (2007), Examining feedbacks of aerosols to urban climate with a model that treats 3-D clouds with aerosol inclusions, *J. Geophys. Res.*, *112,* D24205, doi:10.1029/2007JD008922.

Jaffe, D., T., Anderson, D., Covert, R., Kotchenruther, B., Trost, J., Danielson, W., Simpson, T., Berntsen, S., Karlsdottir, D., Blake, J., Harris, G., Carmichael, and I., Uno (1999), Transport of Asian air pollution to North America, *Geophys. Res. Lett.*, *26*, 711-714.

Janjic, Z. I. (2002), Nonsingular implementation of the Mellor-Yamada level 2.5 scheme in the NCEP Meso model, NCEP Off. *Note, 437,* 61pp., Natl. Cent. for Environ. Predict., College Park, Md.

Jimenez, J. L., R., Bahreini, D. R., Cocker III, H., Zhuang, V., Varutbangkul, R. C., Flagan, J. H., Seinfeld, C. D., O’Dowd, and T., Hoffmann (2003), New particle formation from photooxidation of diiodomethane (CH_2I_2), *J. Geophys. Res., 108,* NO. D10, 4318, doi:10.1029/2002JD002452.

Karcher, B., and B., Spichtinger (2009), Cloud-controlling Factors of Cirrus From the Strungmann Forum Report, Clouds in the Perturbed Climate System: The Relationship to Energy Balance, *Atmospheric Dynamics*, 235-268.

Kaufman, Y.J., D., Tanre, and O., Boucher (2002), A satellite view of aerosols in the climate system, *nature, 419*, 215-223.

Kazil, J., P., Stier, K., Zhang, J., Quaas, S., Kinne, D., O'Donnell, S., Rast, M., Esch, S., Ferrachat, U., Lohmann, and J., Feichter (2010), Aerosol nucleation and its role for clouds and Earth's radiative forcing in the aerosol-climate model ECHAM5-HAM, *Atmos. Chem. Phys., 10*, 10733-10752.

Kerminen, V., and M., Kulmala (2002), Analytical formulae connecting the "real" and the "apparent" nucleation rate and the nuclei number concentration for atmospheric nucleation events, *J. Aero. Sci.*, *33*, 609-622.

King, M.D., W.P., Menzel, Y.J., Kaufman, D. Tanre, B.-C., Gao, S., Platnick, S.A., Ackerman, L.A., Remer, R., Pincus, and P.A., Hubanks (2003), Cloud and aerosol properties, precipitable water, and profiles of temperature and water vapor from MODIS, *IEEE Trans. Geosci. Remote Sens., 41*, 442-458.

Kirkby, J., J., Curtius, J., Almeida, E., Dunne, J., Duplissy, S., Ehrhart, A., Franchin, S., Gagne, L., Ickes, A., Kuerten, A., Kupc, A., Metzger, R., Riccobono, L., Rondo, S., Schobesberger, G., Tsagkogeorgas, D., Wimmer, A., Amorim, F., Bianchi, M., Breitenlechner, A., David, J., Dommen, A., Downard, M., Ehn, R. C., Flagan, S., Haider, A., Hansel, D., Hauser, W., Jud, H., Junninen, F., Kreissl, A., Kvashin, A., Laaksonen, K., Lehtipalo, J., Lima, E.R., Lovejoy, V., Makhmutov, S., Mathot, J., Mikkila, P., Minginette, S., Mogo, T., Nieminen, A., Onnela, P., Pereira, T., Petaja, R., Schnitzhofer, J. H., Seinfeld, M., Sipila, Y., Stozhkov, F., Stratmann, A., Tome, J., Vanhanen, Y., Viisanen, A., Vrtala, P. E., Wagner, H., Walther, E., Weingartner, H., Wex, P. M., Winkler, K. S., Carslaw, D. R., Worsnop, U., Baltensperger, and M., Kulmala (2011), Role of sulphuric acid, ammonia and galactic cosmic rays in atmospheric aerosol nucleation, *Nature*, 476, 429-433.

Korolev, A.V., G.A., Issac, S.G., Coper, J.W., Strapp, and J., Hallet (2003), Microphysical characterization of mixed-phase clouds, *Q. J. Roy. Meteor. Soc., 129*, 39-65.

Kulmala, M., A., Laaksonen, and L., Pirjola (1998), Parameterizations for sulfuric acid/water nucleation rates, *J. Geophys. Res.*, *103*, 8301-8307.

Kulmala, M. (2003), How particles nucleate and grow. *Science 302(5647),* 1000-1001.

Kulmala, M., H., Vehkamaki, T., Petaja, M. D., Maso, A., Lauri, V.-M., Kerminen, W., Birmili, and P. H. McMurry (2004), Formation and growth rates of ultrafine atmospheric particles: a review, *J. Aero. Sci.*, 35, 143-176.

Kulmala, M., I. Riipinen, M. Sipila, H. E. Manninen, T. Petaja, H. Junninen, M. Dal Maso, G. Mordas, A. Mirme, M. Vana, A. Hirsikko, L. Laakso, R. M. Harrison, I. Hanson, C. Leung, K. E. J. Lehtinen and V. M. Kerminen (2007), Toward direct measurement of atmospheric nucleation. *Science 318(5847),* 89-92.

Kulmala, M., T., Petaja, T., Nieminen, M., Sipila, H.E., Manninen, K., Lehtipalo, M.D., Maso, P.P., Aalto, H., Junninen, P., Paasonen, I., Riipinen, K.E.J., Lehtinen, A., Laaksonen, and V.-M., Kerminen (2012), Measurement of the nucleation of atmospheric aerosol particles, *Nature, 7,* 1651-1667.

Kulmala, M., J., Kontkanen, H., Junninen, K., Lehtipalo, H. E., Manninen, T., Nieminen, T., Petaja, M., Sipila, S., Schobesberger, P., Rantala, A., Franchin, T., Jokinen, E., Jarvinen, M., Aijala, J., Kangasluoma, J., Hakala, P. P., Aalto, P., Passonen, J., Mikkila, J., Vanhanen, J., Aalto, H., Hakola, Ulla, Makkonen, T., Ruuskanen, R. L., Mauldin III, J., Duplissy, H., Vehkamaki, J., Back, A., Kortelainen, I., Riipinen, T., Kurten, M. V., Johnston, J. N., Smith, M., Ehn, T. F., Mentel, K. E. J., Lehtinen, A., Laaksonen, V.-M., Kerminen, and D. R., Worsnop (2013), Direct observations of atmospheric aerosol nucleation, *Science, 339,* 943-946.

Lamb, D. and J. Verlinde (2011), Physics and chemistry of clouds, Cambridge University Press, Cambridge.

Lehtinen, K. E. J. and M., Kulmala (2003), A model for particle formation and growth in the atmosphere with molecular resolution in size, *Atmos. Chem. Phys.*, 3, 251-257, doi:10.5194/acp-3-251-2003.

Lehtinen, K. E. J., M. D., Maso, M., Kulmala, and V.-M., Kerminen (2007), Estimating nucleation rates from apparent particle formation rates and vice versa: Revised formulation of the Kerminen-Kulmala equation, *J. Aero. Sci., 38*, 988-994.

Levin, Z., E., Ganor, and V., Gladstein (1996), The effects of desert particles coated with sulfate on rain formation in the eastern Mediterranean, *J. Appl. Meteor., 35*, 1511-1523.

Lihavainen, H., V.M., Kerminen, M., Komppula, J., Hatakka, V., Aaltonen, M., Kulmala, and Y., Viisanen (2003), Production of “potential” cloud condensation nuclei associated with atmospheric new-particle formation in northern Finland, *J. Geophys. Res., 108*, 4782, doi:10.1029/2003JD003887.

Lin, Y. L., R. D., Farley, and H. D., Orville (1983), Bulk parameterization of the snow field in a cloud model. *Journal of Climate and Applied Meteorology, 22,* 1065-1092.

Liu, S., M., Hu, S., Slanina, L.-Y., He, Y.-W., Niu, E., Bruegemann, T., Gnauk, and H., Herrmann (2008a), Size distribution and source analysis of ionic compositions of aerosols in polluted periods at Xinken in Pearl River Delta (PRD) of China, *Atmos. Environ., 42*, 6284-6295.

Liu, S., M., Hu, Z., Wu, B., Wehner, A., Wiedensohler, and Y. Cheng (2008b), Aerosol number size distribution and new particle formation at a rural/coastal site in Pearl River Delta (PRD) of China, *Atmos. Environ.*, 42, 6275-6283.

Liu, X.-H., Y., Zhang, S.-H., Cheng, J., Xing, Q., Zhang, D.G., Street, C., Jang, W.-X., Wang, and J.-M., Hao (2010), Understanding of regional air pollution over China using CMAQ, part I performance evaluation and seasonal variation, *Atmos. Environ.*, 44, 2415-2426.

Liu, X., R.C., Easter, S.J., Ghan, R., Zaveri, P., Rasch, X., Shi, J.-F., Lamarque, A., Gettelman, H., Morrison, F., Vitt, A., Conley, S., Park, R., Neale, C., Hannay, A.M.L., Ekman, P., Hess, N., Mahowald, W., Collins, M.J., Iacono, C.S., Bretherton, M.G., Flanner, and D., Mitchell (2012), Toward a minimal representation of aerosols in climate models: description and evaluation in the Community Atmosphere Model (CAM5) *Geosci. Model Dev., 5*, 709-739.

Lushnikov, A. A., and M., Kulmala (1998), Dimers in nucleating vapors, *Phys. Rev. E., 58,* 3157-3167.

Lohmann, U., and J. Feichter (2005), Global indirect aerosol effects: a review, *Atmos. Chem. Phys., 5*, 715-737.

Madronich, S. (1987), Photodissociation in the atmosphere: 1. Actinic flux and the effect of ground reflections and clouds, J. Geophys. Res., 92, 9740– 9752.

Manninen, H. E., T., Nieminen, E., Asmi, S., Gagne, S., Hakkinen, K., Lehtipalo, P., Aalto, M., Vanna, A., Mirme, S., Mirme, U., Horrak, C., Plass-Dulmer, G., Stange, G., Kiss, A., Hoffer, N., Toro, M., Moerman, B., Henzing, G. de, Leeuw, M., Brinkenberg, G. N., Kouvarakis, A., Bougiatioti, N., Mihalopoulos, C., O'Dowd, D., Ceburnis, A., Arneth, B., Svenningsson, E., Swietlicki, L., Tarozzi, S., Decesari, M. C., Facchini, W., Birmili, A., Sonntag, A., Wiedensohler, J., Boulon, K., Sellegri, P., Laj, M., Gysel, N., Bukowiecki, E., Weingartner, G., Wehrle, A., Laaksonen, A., Hamed, J., Joutsensaari, T., Petaja, V.-M., Kerminen, and M., Kulmala (2010), EUCAARI ion spectrometer measurements at 12 European sites – analysis of new particle formation events, *Atmos. Chem. Phys.*, *10*, 7907-7927.

Maso, M. D., M., Kulmala, I., Riipinen, R., Wagner, T., Hussein, P. P., Aalto. and E. J., Lehtinen (2005), Formation and growth of fresh atmospheric aerosols: eight years of aerosol size distribution data from SMEAR II, Hyytiala, Finland, *Boreal Env. Res., 10,* 323-336.

Mass, C., D., Ovens, J., Baars, M., Albright, P., Regulski, and D., Carey (2010), Update on the northwest regional modeling system, *Consortium Meeting*, University of Washington.

Matsui, H., M., Koike, Y., Kondo, N., Takegawa, A., Wiedensohler, J.D., Fast, and R.A., Zaveri (2011), Impact of new particle formation on the concentrations of aerosols and cloud condensation nuclei around Beijing, *J. Geophys. Res.*, *116,* D19208, doi:10.1029/2011JD016025.

McFiggans, G., P., Artaxo, U., Baltensperger, H., Coe, M.C., Facchini, G., Feingold, S., Fuzzi, M., Gysel, A., Laaksonen, U., Lohmann, T.F., Mentel, D.M., Murphy, C.D., O’Dowd, J.R., Snider, and E., Weingartner (2006), The effect of physical and chemical aerosol properties on warm cloud droplet activation, *Atmos. Chem. Phys., 6,* 2593-2649.

McMurry, P. H., M. Fink, H. Sakurai, M. R. Stolzenburg, R. L. Mauldin, J. Smith, F. Eisele, K. Moore, S. Sjostedt, D. Tanner, L. G. Huey, J. B. Nowak, E. Edgerton and D. Voisin. (2005), A criterion for new particle formation in the sulfur-rich Atlanta atmosphere. *J. Geophys. Res. 110(D22),* D22S02.

McNaughton, C.S., A.D., Clarke, S.G., Howell, K.G.M. II, V., Brekhovskikh, R.J., Weber, D.A., Orsini, D.S., Covert, G., Buzorius, F.J., Brechtel, G.R., Carmichael, Y., Tang, F.L., Eisele, R.L., Mauldin, A.R., Bandy, D.C., Thornton, and B., Blomquist (2004), Spatial distribution and size evolution of particles in Asian outflow: Significance of primary and secondary aerosols during ACE-Asia and TRACE-P, *J. Geophys. Res., 109,* D19S06, doi:10.1029/2003JD003528.

Merikanto, J., I., Napari, H., Vehkamaki, T., Anttila, and M., Kulmala (2007), New parameterization of sulfuric acid-ammonia-water ternary nucleation rates at tropospheric conditions, *J. Geophys. Res.*, *112*, D15207, doi:10.1029/2006JD007977.

Merikanto, J., D. V., Spracklen, G. W., Mann, S. J., Pickering, and K. S., Garslaw (2009), Impact of nucleation on global CCN, *Atmos. Chem. Phys., 9*, 8601-8616, doi:10.5194/acp-9-8601-2009a.

Merikanto, J., I., Napari, H., Vehkamaki, T., Anttila, and M., Kulmala, (2009b), Correction to “New parameterization of sulfuric acid-ammonia-water ternary nucleation rates at tropospheric conditions", *J. Geophys. Res.*, 114, D09206, doi:10.1029/2009JD012136.

Mlawer, E. J., S. J., Taubman, P. D., Brown, M. J., Iacono, and S. A., Clough (1997), Radiative transfer for inhomogeneous atmospheres: RRTM, a validated correlated-k model for the longwave. *J. Geophys. Res., 102,* D14, 16663-16682.

Monin, A. S., and A. M. Obukhov (1954), Basic laws of turbulent mixing in the surface layer of the atmosphere [in Russian], Contrib. Geophys. *Inst. Acad. Sci. USSR, 151,* 163–187.

Morrison, H., and A., Gettelman, (2008), A new two-moment bulk stratiform cloud microphysics scheme in the community atmosphere model, Version 3 (CAM3). Part I: Description and Numerical Tests, *J. Climate*, *21*, 3642–3659.

O'Dowd, C. D., J. Makela, M. Vakeva, P. Aalto, G. de Leeuw, G. J. Kunz, E. Becker, H. C. Hansson, A. G. Allen, R. M. Harrison, H. Berresheim, M. Geever, S. G. Jennings and M. Kulmala (2002). Coastal new particle formation: Environmental conditions and aerosol physicochemical characteristics during nucleation bursts. *J. Geophys. Res. 107(D19),* 8107.

Paasonen, P., T., Nieminen, E., Asmi, H. E., Manninen, T., Petaja, C., Plass-Dulmer, H., Flentje, W., Birmili, A., Wiedensohler, U., Horrak, A., Metzger, A., Hamed, A., Laaksonen, M. C., Facchini, V.-M., Kerminen, and M., Kulmala (2010), On the roles of sulphuric acid and low-volatility organic vapours in the initial steps of atmospheric new particle formation, *Atmos. Chem. Phys., 10*, 11223-11242.

Petters, M.D., and S.M., Kreidenweis (2007), A single parameter representation of hygroscopic growth and cloud condensation nucleus activity, *Atmos. Chem. Phys., 7,* 1961-1971.

Prenni, A.J., P.J., DeMott, C., Twohy, M.R., Poellot, S.M., Kreidenweis, D.C., Rogers, S.D., Brooks, M.S., Richardson, and A.J., Heymsfield, Examinations of ice formation processes in Florida cumuli using ice nuclei measurements of anvil ice crystal particle residues, *J. Geophys. Res., 112*, 10221, doi:10.1029/2006JD007549.

Qian, S., H., Sakurai, and P. H., McMurry (2007), Characteristics of regional nucleation events in urban East St. Louis, *Atmos. Environ., 41,* 4119-4127.

Radke, L.G., and P.V., Hobbs (1976), Cloud condensation nuclei on the Atlantic seaboard of the United States, *Science, 193,* 99-1002.

Ramanathan, V., P., Crutzen, J., Kiehl, and D., Rosenfeld (2001), Aerosols, climate, and the hydrological cycle, *Science, 294*, 2119-2124.

Ran, L., C., Zhao, F., Geng, X., Tie, X., Tang, L., Peng, G., Zhou, Q., Yu, J., Xu, and A., Guenther (2009), Ozone photochemical production in urban Shanghai, China: Analysis based on ground level observations, J. Geophys. Res., 114, D15301, doi:10.1029/2008JD010752.

Riipinen, I., S.-L., Sihto, M., Kulmala, F., Arnold, M. D., Maso, W., Birmili, K., Saarnio, K., Teinila, Y.-M., Kerminen, A., Laaksonen, and K. E. J., Lehtinen (2007), Connections between atmospheric sulphuric acid and new particle formation during QUEST III-IV campaigns in Heidelberg and Hyytiala, *Atoms. Chem. Phys., 7,* 1899-1914.

Rosenfeld, D. (2006), Aerosols, clouds, and climate, *Science*, *312*, 1323-1324.

Rosenfeld, D., U., Lohmann, G.B., Raga, C.D., O'Dowd, M., Kulmala, S., Fuzzi, A., Reissell, and M.O., Andreae (2008), Flood or drought: how do aerosols affect precipitation? *Science, 321,* 1309-1313.

Rutledge, S. A. and P. V., Hobbs (1994), The mesoscale and microscale structure and organization of clouds and precipitation in midlatitude cyclones. XII: a diagnostic modeling study of precipitation development in narrow cold-frontal rainbands, *Journal of the Atmospheric Sciences, 41(20),* 2949-2972.

Saha, L. (2010), Tropical circulation systems and monsoons, *Springer*, 123-153.

Salma, I., T., Borsos, T., Weidinger, P., Aalto, T., Hussein, M. D., Maso, and M., Kulmala (2011), Production, growth and properties of ultrafine atmospheric aerosol particles in an urban environment, *Atoms. Chem. Phys.*, 11, 1339-1353.

Scott, W. D., and F. C. R., Cattell (1979), Vapor pressure of ammonium sulfates, *Atmos. Environ.*, *13*, 307-317.

Seinfeld, J. H. and S. N., Pandis (2006), Atmospheric chemistry and physics: from air pollution to climate change, Wiley, New York.

Shaw, W.J., K.J., Allwine, B.G., Fritz, F.C., Rutz, J.P., Rishel, and E.G., Chapman (2008), An evaluation of the wind erosion module in DUSTRAN, *Atmos. Environ.*, 42, 1907-1921.

Shen, X. J., J. Y., Sun, Y. M., Zhang, B., Wehner, A., Nowak, T., Tuch, X. C., Zhang, T. T., Wang, H. G., Zhou, X. L., Zhang, F., Dong, W., Birmili, and A., Wiedensohler (2011), First long-term study of particle number size distributions and new particle formation events of regional aerosol in the North China Plain, *Atoms. Chem. Phys.*, 11, 1565-1580.

Shi, J. P., D. E., Evans, A. A., Khan, and R. M., Harrison (2001), Sources and concentration of nanoparticles (<10 nm diameter) in the urban atmosphere, *Atmos. Environ.*, 35, 1193-1202.

Sihto, S.-L., M., Kulmala, V.-M., Kerminen, M., Dal Maso, T., Petaja, I., Riipinen, H., Korhonen, F., Arnold, R., Janson, M., Boy, A., Laaksonen, and K.E.J., Lehtinen (2006), Atmospheric sulphuric acid and aerosol formation: implications from atmospheric measurements for nucleation and early growth mechanisms, *Atmos. Chem. Phys.*, 6, 4079-4091.

Smith, J. N., M. J., Dunn, T. M., VanReken, K., Iida, M. R., Stolzeburg, P. H., McMurry, and L. G., Huey, (2008), Chemical composition of atmospheric nanoparticles formed from nucleation in Tecamac, Mexico: Evidence for an important role for organic species in nanoparticle growth, *Geophys. Res. Lett., 35,* L04808.

Song, X., G.J., Zhang, (2011), Microphysics parameterization for convective clouds in a global climate model: description and single-column model tests, *J. Geophys. Res., 116,* D02201, doi:10.1029/2010JD014833.

Spichtinger, P., and K.M., Gierens, Modeling of cirrus clouds – Part 2: Competition of different nucleation mechanisms, *Atmos. Chem. Phys., 9,* 2319-2334.

Spracklen, D. V., K. S., Carslaw, M., Kulmala, V. M., Kerminen, G. W., Mann, and S. L., Sihto (2006), The contribution of boundary layer nucleation events to total particle concentrations on regional and global scales, *Atoms. Chem. Phys., 6,* 5631-5648.

Spracklen, D. V., K. S., Carslaw, M., Kulmala, V. M., Kerminen, S. L., Sihto, I., Riipinen, J., Merikanto, G. W., Mann, M. P., Chipperfield, A., Wiedensohler, W., Birmili, and H., Lihavainen (2008), Contribution of particle formation to global cloud condensation nuclei concentrations, *Geophys. Res. Lett., 35,* L06808, doi:10.1029/2007g1033038.

Squires, P. (1958), The microstructure and colloidal stability of warm clouds. I. The relation between structure and stability, Tellus, 10, 256-271.

Stier, P., J. H., Seinfeld, S., Kinne, and O., Boucher (2007), Aerosol absorption and radiative forcing, *Atoms. Chem. Phys., 7,* 5237-5261.

Strader, R., F., Lurmann, and S. N., Pandis (1999), Evaluation of secondary organic aerosol formation in winter, *Atmos. Environ., 33,* 4849-4863.

Taina, Y., I., Riipinen, P., Aalto, T., Nieminen, W., Maenhaut, I. A., Janssens, M., Claeys, I., Salma, R., Ocskay, A., Hoffer, K., Imre, and M., Kulmala (2009), Characteristics of new particle formation events and cluster ions at K-puszta, Hungary, *Boreal Env. Res., 14,* 683-698.

Tewari, M., F., Chen, W., Wang, J., Dudhia, M. A., LeMone, K., Mitchell, M., Ek, G., Gayno, J., Wegiel, and R. H., Cuenca (2004), Implementation and verification of the unified NOAH land surface model in the WRF model. *20th conference on weather analysis and forecasting/16th conference on numerical weather prediction*, 11-15.

Tie, X., S. Madronich, S. Walters, R. Zhang, P. Racsh, and W. Collins (2003), Effect of clouds on photolysis and oxidants in the troposphere, *J. Geophys. Res., 108*, 4642, doi:10.1029/2003JD003659.

Trochkine, D., Y., Iwasaka, A., Matsuki, M., Yamada, Y.S., Kim, T., Nagatani, D., Zhang, G.Y., Shi, and Z., Shen (2003), Mineral aerosol particles collected in Dunhuang, China, and their comparison with chemically modified particles collected over Japan, *J. Geophys. Res., 108,* 8642, doi:10.1029/2002JD003268.

Twomey, S. (1977), The influence of pollution on the shortwave albedo of clouds. *J. Atmos. Sci., 34*, 1149-1152.

Twomey, S., K.A., Davidson, and K.J., Seton (1978), Results of five years' observations of cloud nucleus concentration at Roberson, New South Wales', *J. Atmos. Sci., 35,* 650-656.

Vakkari, V., H., Laako, M., Kulmala, A., Laaksonen, D., Mabaso, M., Molefe, N., Kgabi, and L., Laakso (2011), New particle formation events in semi-clean South African savannah, *Atmos. Chem. Phys., 11,* 3333-3346.

Venzac, H., K., Sellegri, P., Laj, P., Villani, P., Bonasoni, A., Marinoni, P., Cristofanelli, F., Calzolari, S., Fuzzi, S., Decesari, M.-C., Facchini, E., Vuillermoz, and G. P., Verza (2008), High frequency new particle formation in the Himalayas, PNAS, 15666-15671.

Wang, T., A., Ding, J., Gao, and W.S., Wu (2006), Strong ozone production in urban plumes from Beijing, China, *Geophys. Res. Lett., 33*, L21806, doi:10.1029/2006GL027689.

Wang, M., J.E., Penner, and X., Liu (2009), Coupled IMPACT aerosol and NCAR CAM3 model: Evaluation of predicted aerosol number and size distribution, *J. Geophys. Res. 114*, D06302, doi:10.1029/2008JD010459.

Wang, M., and J. E., Penner (2009), Aerosol indirect forcing in a global model with particle nucleation, *Atoms. Chem. Phys.*, *9*, 239-260.

Wang, K., Y., Zhang, C., Jang, S., Phillips, and B., Wang (2009), Modeling intercontinental air pollution transport over the trans-Pacific region in 2001 using the Community Multiscale Air Quality modeling system, *J. Geophy. Res.*, *114*, D04307, doi:10.1029/2008JD010807.

Wang, K., and Y., Zhang (2012), Application, evaluation, and process analysis of the US EAP's 2002 multiple-pollutant air quality modeling platform, *Atmospheric and Climate Sci*, *2*, 254-289

Wang, B., M., Shao, S.H., Lu, B., Yuan, Y., Zhao, M., Wang, S.Q., Zhang, and D., Wu (2010), Variation of ambient non-methane hydrocarbons in Beijing city in summer 2008, Atmos. Chem. Phys., 10, 5911-5923.

Wang, L., C., Jang, Y., Zhang, K., Wang, K., Wang, Q., Zhang, D., Streets, J., Fu, Y., Lei, J., Schreifels, K., He., J., Hao, Y.-F., Lam., J., Lin, N., Meskhidze, S., Voorhees, D., Evarts, and S., Phillips (2010), Assessment of air quality benefits from national air pollution control policies in China. Part II: Evaluation of air quality predictions and air quality benefits assessment, Atmos. Environ., 44, 3449-3457.

Wang, Z. B., M., Hu, D. L., Yue, J., Zheng, R. Y., Zhang, A., Wiedensohler, Z. J., Wu, T., Nieminen, and M., Boy (2011), Evaluation on the role of sulfuric acid in the mechanisms of new particle formation for Beijing case, *Atmos. Chem. Phys.*, 11, 12663-12671.

Wang, Z. (2012), Research on new particle formation and growth properties in the urban atmosphere. *PhD thesis*, Peking University, China.

Weber, R. J., J. J. Marti, P. H. McMurry, F. L. Eisele, D. J. Tanner and A. Jefferson (1997), Measurements of new particle formation and ultrafine particle growth rates at a clean continental site. *J. Geophys. Res. 102(D4)*, 4375-4385.

Weber, R. J., P. H. McMurry, R. L. Mauldin, D. J. Tanner, F. L. Eisele, A. D. Clarke and V. N. Kapustin (1999), New particle formation in the remote troposphere: A comparison of observations at various sites. *Geophys. Res. Lett. 26(3):* 307-310.

Weber, R.J., S., Lee, G., Chen, B., Wang, V., Kapustin, K., Moore, A.D., Clarke, L., Mauldin, E., Kosciuch, C., Cantrell, F., Eisele, D.C., Thornton, A.R., Bandy, G.W., Sachse, and H.E., Fuelberg (2003), New particle formation in anthropogenic plumes advecting from Asia observed during TRACE-P, *J. Geophys. Res.*, *108*, NO.D21, 8814, doi:10.1029/2002JD003112.

Weiss-Penzias, P., D. A., Jaffe, P., Swartzendruber, J. B., Dennison, D., Chand, W., Hafner, and E., Prestbo (2006), Observations of Asian air pollution in the free troposphere at Mount Bachelor Observatory during the spring of 2004, *J. Geophys. Res.*, *111*, D10304, doi:10.1029/2005JD006522.

Wexler, A. S., F. W., Lurmann, and J. H., Seinfeld (1994), Modelling urban and regional aerosols-I. Model development, *Atmos. Environ.*, *28*, 531-546.

Whitby, K. T. (1987), The physical characteristics of sulfur aerosols. *Atmos. Environ. 12(1-3)*, 135-159.

Wild, O., X., Zhu, and M. J., Prather (2000), Fast-J: accurate simulation of in- and below cloud photolysis in tropospheric chemical models, *J. Atmos. Chem.*, *37*, 245-282.

Wu, Z., M., Hu, S., Liu, B., Wehner, S., Bauer, A. M., Bling, A., Wiedensohler, T., Petaja, M. D., Maso, and M., Kulmala (2007), New particle formation in Beijing, China: Statistical analysis of a 1-year data set, *J. Geophys. Res.*, *112*, D09209, doi:10.1029/2006JD007406.

Wu, Z., M., Hu, D.L., Yue, B., Wehner, and A., Wiedensohler (2011), Evolution of particle number size distribution in an urban atmosphere during episode of heavy pollution and new particle formation, Sci. China Earth Sci., 54, doi:10.1007/s11430-011-4227-9.

Yin, Y., Z., Levin, T.G., Reisin, and S., Tzivion (2000), The effects of giant condensation nuclei on the development of precipitation in convective clouds – A numerical study, *Atmos. Res.*, *53*, 91-116.

Young, L. H., D. R. Benson, F. R. Kameel, J. R. Pierce, H. Junninen, M. Kulmala and S. H. Lee (2008), Laboratory studies of H_2SO_4/H_2O binary homogeneous nucleation from the SO_2+OH reaction: evaluation of the experimental setup and preliminary results. *Atmos. Chem. Phys. 8(16)*, 4997-5016.

Yu, F., R. P., Turco (2000b), Ultrafine aerosol formation via ion-mediated nucleation, *Geophys. Res. Lett.*, *27*, 883-886.

Yu, F., Z., Wang, G., Luo, and R., Turco (2008), Ion-mediated nucleation as an important global source of tropospheric aerosols. *Atmos. Chem. Phys., 8,* 2537-2554.

Yu, F. (2010), Ion-mediated nucleation in the atmosphere: Key controlling parameters, implications, and look-up table, *J. Geophys. Res., 115,* D03206, doi:10.1029/2009JD012630.

Yu, F. and R. P., Turco (2011), The size-dependent charge fraction of sub-3-nm particles as a key diagnostic of comprehensive nucleation mechanisms under atmospheric conditions, *Atmos. Chem. Phys.*, 11, 9451-9463.

Yu, F., G., Luo, X., Liu, R. C., Easter, X., Ma, and S. J., Ghan (2012), Indirect radiative forcing by ion-mediated nucleation of aerosol, *Atmos. Chem. Phys.*, 12, 11451-11463.

Yu, S. (2000a), Role of organic acids (formic, acetic, pyruvic and oxalic) in the formation of cloud condensation nuclei (CCN): a review, *Atmos. Res., 53*, 185-217.

Yu, S., B., Eder, R., Dennis, S.-H., Chu, and S.E., Schwartz (2006), New unbiased symmetric metrics for evaluation of air quality models, *Atmos. Sci. Lett., 7,* 27-34.

Yu, S., R., Mathur, J., Pleim, D., Wong, R., Gilliam, K., Alapaty, C., Zhao, and X., Liu (2013), Aerosol indirect effect on the grid-scale clouds in the two-way coupled WRF-CMAQ: model description, development, evaluation and regional analysis, *Atmos. Chem. Phys. Discuss., 13,* 25649-25739.

Yue, D., M., Hu, Z., Wu, Z., Wang, S., Guo, B., Wehner, A., Nowak, P., Achtert, A., Wiedensohler, J., Jung, Y. J., Kim, and S., Liu (2009), Characteristics of aerosol size distributions and new particle formation in the summer in Beijing, *J. Geophys. Res., 114,* D00G12, doi:10.1029/2008jd010894.

Yue, D., M., Hu, R. Y., Zhang, Z. B., Wang, J., Zheng, Z. J., Wu, A., Wiedensohler, L. Y., He, X. F., Huang, and T., Zhu (2010), The roles of sulfuric acid in new particle formation and growth in the mega-city of Beijing, *Atmos. Chem. Phys., 10,* 4953-4960.

Zaveri, R. A., and L. K., Peters (1999), A new lumped structure photochemical mechanism for large-scale applications. *J. Geophys. Res., 104,* 30387-30415.

Zaveri, R. A., R. C., Easter, J. D., Fast, and L. K., Peters (2008), Model for simulating aerosol interactions and chemistry (MOSAIC), *J. Geophys. Res., 113*, D13204, doi:10.1029/2007JD008782, 2008.

Zender, C. S., H., Bian, and D., Newman (2003), Mineral dust entrainment and deposition (DEAD) model: Description and 1990s dust climatology, *J. Geophys. Res.*, 108, D14, 4416, doi:10.1029/2002JD002775.

Zhang, G. J., and N. A. McFarlane (1995), Sensitivity of climate simulations to the parameterization of cumulus convection in the Canadian Climate Centre general circulation model, Atmos. Ocean, 33, 407–446.

Zhang, K., X., Liu, M., Wang, J.M., Comstock, D.L., Mitchell, S., Mishra, and G.G., Mace (2013), Evaluating and constraining ice cloud parameterizations in CAM5 using aircraft measurement from the SPARTICUS campaign, *Atmos. Chem. Phys.*, *13,* 4963-4982.

Zhang, Q., D.G., Streets, G.R., Carmichael, K.B., He, H., Huo, A., Kannari, Z., Klimont, I.S., Park, S., Reddy, J.S., Fu, D., Chen, L., Duan, Y., Lei, L.T., Wang, and Z.L., Yao (2009), Asian emissions in 2006 for the NASA INTEX-B mission, *Atmos. Chem. Phys. 9, 5131-5153.*

Zhang, R., I., Suh, J., Zhao, D., Zhang, E. C., Fortner, X., Tie, L. T., Molina, and M. J., Molina (2004), Atmospheric new particle formation enhanced by organic acids, *Science*, *304,* 1487-1490.

Zhang, R. (2010), Getting to the Critical Nucleus of Aerosol Formation. *Science 328(5984),* 1366-1367.

Zhang, R., A. F., Khalizov, L., Wang, M., Hu, and X., Wen (2012), Nucleation and growth of nanoparticles in the atmosphere, *Chem. Rev.*, 112, 1957-2011, doi:10.1021/cr2001756.

Zhang, X. (2013), Examining aerosol indirect effects using a regional climate-aerosol model with improved aerosol activation and cloud parameterizations. *Master thesis*, North Carolina State University, USA.

Zhang, X. Y., S. L., Gong, Z. X., Shen, F. M., Mei, X. X., Xi, L. C., Liu, Z. J., Zhou, D., Wang, Y. Q., Wang, and Y., Cheng (2003), Characterization of soil dust aerosol in China and its transport and distribution during 2001 ACE-Asia, *J. Geophys. Res.*, 108, D9, 4261, doi:10.1029/2002JD002632.

Zhang, Y., P. H., McMurry, F., Yu, and Z., Jacobson (2010a), A comparative study of nucleation parameterizations: 1. Examination and evaluation of the formulations, *J. Geophys. Res., 115,* D20212, doi:10.1029/2010JD014150.

Zhang, Y., P., Liu, X.-H., Liu, M. Z., Jacobson, P. H., McMurry, F., Yu, S., Yu, and K. L., Schere (2010b), A comparative study of nucleation parameterizations: 2. Three-dimensional model application and evaluation, *J. Geophys. Res.*, *115*, D20213, doi:10.1029/2010JD014151.

Zhang, Y., X. Y., Wen, and C. J., Jang (2010c), Simulating chemistry-aerosol-cloud-radiation-climate feedbacks over the continental U.S. using the online-coupled Weather Research Forecasting Model with chemistry (WRF/Chem), *Atmos. Environ., 44,* 3568-3582.

Zhang, Y., P., Karamchandani, T., Glotfelty, D. G., Streets, G., Grell, A., Nenes, F., Yu, and R., Bennartz (2012), Development and initial application of the global-through-urban weather research and forecasting model with chemistry (GU-WRF/Chem), *J. Geophys. Res.*, *117*, D20206, doi:10.1029/2012JD017966.

Zhang, Y., K., Sartelet, S.-Y., Wu, and C. Seigneur (2013), Application of WRF/Chem-MADRID and WRF/Polyphemus in Europe – Part 1: Model description, evaluation of meteorological predictions, and aerosol-meteorology interactions, *Atmos. Chem. Phys. 13*, 6807-6843.

Zheng, J., M. Hu, R. Zhang, D. Yue, Z. Wang, S. Guo, X. Li, B. Bohn, M. Shao, L. He, X. Huang, A. Wiedensohler and T. Zhu (2011), Measurements of gaseous H2SO4 by AP-ID-CIMS during CAREBeijing 2008 Campaign. *Atmos. Chem. Phys. 11(15),* 7755-7765.